

POLITECNICO DI TORINO

Collegio di Ingegneria Meccanica, Aerospaziale, dell'Autoveicolo e della
Produzione

**Master of Science Course
in Automotive Engineering**

Master of Science Thesis

Rear-Wheel Steering: State of the Art Control Creation



Academic Tutor
prof. Andrea Tonoli

Company Tutor
ing. Salvatore Calanna

Candidate
Xilong He

October 2022

Contents

- Abstract iii
- List of figures v
- List of tables ix
- Acknowledgments xi
- 1. Introduction 1
 - 1.1 Background and Motivation 1
 - 1.2 About Danisi Engineering S.r.l 2
 - 1.3 Thesis Layout 3
- 2. Literature Review 5
 - 2.1 Rear-Wheel Steering (RWS) Introduction 5
 - 2.2 State-of-the-Art 6
 - 2.2.1 History Outline of Vehicles with RWS 6
 - 2.2.2 Recent Vehicles with RWS 9
 - 2.2.3 RWS System Types 11
 - 2.2.4 RWS Control Review 14
 - 2.3 Pros and Cons of RWS 17
 - 2.4 Safety Aspect of RWS 17
- 3. Lateral Vehicle Dynamics 19
 - 3.1 Single-Track Model 19
 - 3.2 Steady-State Handling Parameters 22
 - 3.2.1 Understeer Gradient 22
 - 3.2.2 Characteristic Speed 23
 - 3.2.3 Critical Speed 23
 - 3.2.4 Static Margin 24
- 4. 14 DOF Model Vehicle Dynamics 27
 - 4.1 Ride Model 28
 - 4.2 Handling Model 29
 - 4.3 Tire Dynamics 32
 - 4.4 Handling Diagrams 37
- 5. RWS Control Design 41

5.1	Vehicle Plant Model Realization	42
5.2	Reference Model Realization	45
5.3	RWS Controller Design	49
5.3.1	PI Controller	49
5.3.2	LQI Controller	50
5.3.3	MPC Controller	52
5.4	Control Implementation in MATLAB/Simulink.....	54
5.4.1	Vehicle Plant Model.....	54
5.4.2	Reference Model	56
5.4.3	RWS Controllers	58
6.	Offline Simulation and Results	60
6.1	Maneuvers Definition.....	60
6.1.1	Ramp Steer	60
6.1.2	Step Steer.....	61
6.1.3	Sine Sweep Steer	62
6.2	Controller Parameters Tuning	63
6.2.1	PI Controller	63
6.2.2	LQI Controller	64
6.2.3	MPC Controller	65
6.3	Simulation Results	66
6.3.1	Ramp Steer: PI Control	66
6.3.2	Ramp Steer: LQI Control	68
6.3.3	Step Steer: PI Control.....	70
6.3.4	Step Steer: LQI Control.....	71
6.3.5	Sine Sweep Steer: PI Control	72
6.3.6	Sine Sweep Steer: LQI Control	73
7.	Conclusion	77
7.1	Future Work	78
	Bibliography.....	79

Abstract

Nowadays, the integration of various electronic systems in the chassis of vehicles for active safety purposes is widespread and ever increasing in the automotive industry. Motivated by the potential benefits of electronic systems in terms of handling and safety, this master thesis aims at investigating and developing an active rear-wheel steering (RWS) controller which incorporates a control logic with the best performance when deployed on a virtual vehicle model. The identified control logic is integrated on a vehicle model based on the know-how of Danisi Engineering company, headquartered in Nichelino (TO). For the controller's creation, various classical and optimal control methods are explored and realized.

An initial review displays the growing interests from major car manufacturers and researchers since the eighties regarding RWS systems' realization and their control design. Benefits in terms of maneuverability and stability are obtained from proposals of RWS control based on different theories for various typologies of RWS systems.

The vehicle of the subject is modelled as a linearized single-track model with nonlinear axle lateral force characteristics, essentially capturing the vehicle's lateral dynamic behaviors. Starting from setting the desired control goals in terms of desired yaw rate and understeering characteristics, multiple controllers based on different control theories are created in *MATLAB/Simulink*, among them PI, LQI and MPC control. They all improve the vehicle's lateral dynamic responses by exerting an active RWS angle from an input of yaw rate tracking error.

The effectiveness of proposed control structures is verified from simulations of several typical steady-state and transient maneuvers in *MATLAB/Simulink*: ramp steer, step steer and sine sweep steer are considered. The controllers are subsequently tuned to have appropriate parameters able to achieve desired performance goals. Then, comparisons between the passive and controlled vehicle's responses are made for every maneuver with each controller configuration. Simulation results show that the proposed RWS controllers effectively enhance the vehicle's cornering responses and achieve their design goals.

List of figures

Figure 1.1 Advanced Vehicle Dynamics (AVD) department of Danisi Engineering [2].	3
Figure 2.1 Basic scheme of RWS [4].	5
Figure 2.2 Nissan R31 Skyline [9].	7
Figure 2.3 Honda Prelude 3rd Generation [12].	7
Figure 2.4 Mitsubishi Galant VR-4 [13].	8
Figure 2.5 BMW 840 Ci [15].	8
Figure 2.6 BMW 7 Series [18].	9
Figure 2.7 Scheme of Renault 4Control [19].	10
Figure 2.8 Ferrari GTC4 Lusso [21].	10
Figure 2.9 Lamborghini Urus [23].	10
Figure 2.10 Porsche 991 GT3 [25].	11
Figure 2.11 Mercedes S500 W223 [27].	11
Figure 2.12 Rear steering gearbox in Honda's 4WS [10].	12
Figure 2.13 “HICAS” four-wheel steering system [29].	12
Figure 2.14 Mitsubishi “Active Four” [8].	13
Figure 2.15 BMW's AHK [8].	13
Figure 2.16 Porsche Rear-axle Steering [24].	14
Figure 2.17 ASILs for some automotive systems and components [42].	18
Figure 3.1 Kinematic steering with the required steering angle (adapted from [43]). (a) vehicle with nominal wheelbase; (b) vehicle with longer wheelbase.	20
Figure 3.2 Dynamic steering (adapted from [44]).	20
Figure 3.3 Tire cornering force properties [44].	21
Figure 3.4 Change of front wheel steer angle with speed (adapted from [44]). Here the number 57.3 represents the unit conversion from <i>radians</i> to <i>degrees</i> .	24
Figure 3.5 Definition of Neutral Steer Point and Neutral Steer Line [44]. The letter <i>e</i> represents the longitudinal distance between the vehicle’s CG and its Neutral Steer Point.	24
Figure 4.1 Schematic of the DOF considered in the 14 DOF model [46].	27
Figure 4.2 7 DOF vehicle ride model [45].	28
Figure 4.3 7 DOF vehicle handling model [45].	29
Figure 4.4 Pitch motion due to longitudinal acceleration a_x (adapted from [45]).	31
Figure 4.5 Roll motion due to lateral acceleration (adapted from [45]).	31
Figure 4.6 Free body diagram of a single wheel [48].	32
Figure 4.7 Tire rolling on a flat road; Peripheral speed on contact area [49].	33

Figure 4.8 Curves $F_x - \sigma$ for a 195/65 R 15 tire obtained for different values of vertical load F_z [49].	34
Figure 4.9 Curves $F_y - \alpha$ and $M_z - \alpha$ for a 205/60 R 15 V tire obtained for different values of vertical load F_z [49].	35
Figure 4.10 Scheme of camber force [49].	36
Figure 4.11 Interaction between F_x and F_y . (a) Experimental diagrams; (b) Elliptic approximation [49].	36
Figure 4.12 Curve produced by the original sine version of Magic Formula [50].	37
Figure 4.13 Example of steady-state understeer characteristics [43].	38
Figure 4.14 Example of steady-state vehicle sideslip angle characteristics [43].	38
Figure 4.15 Example of steady-state vehicle roll angle characteristics [43].	39
Figure 5.1 RWS overall control scheme.	41
Figure 5.2 Single-track model of a vehicle with RWS [51].	42
Figure 5.3 $C_f - a_y$ and $C_r - a_y$ relationships.	45
Figure 5.4 Elastic $K_{US,des} - V$.	47
Figure 5.5 $r_{des} - \delta_{sw}$ for different V during ramp steer maneuver.	48
Figure 5.6 $\delta_{sw} - a_{y,des}$ for different V during ramp steer maneuver.	48
Figure 5.7 General structure of PI control.	50
Figure 5.8 General structure of LQI control.	50
Figure 5.9 RHC logic for MPC [56].	53
Figure 5.10 General structure of MPC control.	54
Figure 5.11 RWS control implementation in <i>Simulink</i> .	55
Figure 5.12 Vehicle plant model in <i>Simulink</i> .	56
Figure 5.13 Details of vehicle plant model.	56
Figure 5.14 Reference model in <i>Simulink</i> .	57
Figure 5.15 Details of reference model.	57
Figure 5.16 RWS controllers in <i>Simulink</i> .	58
Figure 5.17 Details of PI controller.	59
Figure 5.18 Details of LQI controller.	59
Figure 6.1 Ramp steer maneuver.	61
Figure 6.2 Step steer maneuver.	62
Figure 6.3 Sine sweep steer maneuver.	63
Figure 6.4 PI ramp steer: time history of r and e . The line with green color results “hidden” because the controlled vehicle yaw rate overlaps the desired yaw rate.	66
Figure 6.5 PI ramp steer: handling diagrams of $\delta_{sw} - a_y$ and $\beta - a_y$.	67
Figure 6.6 PI ramp steer: time history of δ_r and vehicle trajectory comparison.	68

Figure 6.7 LQI ramp steer: time history of r and e	68
Figure 6.8 LQI ramp steer: handling diagram of $\delta_{sw} - a_y$	69
Figure 6.9 LQI ramp steer: understeer gradient K_{US}	69
Figure 6.10 LQI ramp steer: time history of δ_r and vehicle trajectory comparison.	70
Figure 6.11 PI step steer: time history of r and e	70
Figure 6.12 PI step steer: time history of δ_r	71
Figure 6.13 LQI step steer: time history of r and e	71
Figure 6.14 LQI step steer: time history of δ_r	72
Figure 6.15 PI sine sweep steer: time history of r and e	72
Figure 6.16 PI sine sweep steer: time history of δ_r	73
Figure 6.17 PI sine sweep: time history of a_y	73
Figure 6.18 LQI sine sweep steer: time history of r and e	74
Figure 6.19 LQI sine sweep steer: time history of δ_r	74
Figure 6.20 LQI sine sweep steer: time history of a_y	75

List of tables

Table 1 Vehicle model parameters	44
Table 2 Data of C_f and C_r	44
Table 3 Design parameters of the reference model	47
Table 4 Ramp steer maneuver parameters.....	61
Table 5 Step steer maneuver parameters	62
Table 6 Sine sweep steer maneuver parameters	62
Table 7 PI controller parameters	64
Table 8 LQI controller parameters	65
Table 9 MPC controller parameters.....	66

Acknowledgments

First and foremost, I would like to thank Politecnico di Torino and Danisi Engineering for giving me the opportunity to develop my master thesis on such an interesting topic. I would like to express my sincere gratitude to Ms. Nicoletta Travaglini and ing. Claudio Ricci, who first welcomed me with open arms into the company. A special thanks to ing. Salvatore Calanna, my company tutor and ing. Federico Ravera who followed me throughout the project providing guidance, support, and outstanding advice. I am sure that they will benefit me throughout my life. I would like to extend my thanks to the engineers and interns in the Advanced Vehicle Dynamics (AVD) group, especially Javier, Andrea, and Marco for being a great bunch of people in and out of the office. Long hours in the office did feel as if they were much shorter with them.

In addition, I would like to give my warmest gratitude to my academic tutor in Politecnico di Torino, prof. Andrea Tonoli and his Ph.D. student Eugenio Tramacere, for their availability and invaluable advice offered throughout the thesis project. I would like to also thank prof. Carlo Novara, for his availability and willingness to reply to my doubts and offer me helpful hints regarding the different controls.

I am forever grateful to my friends for all sorts of memories along the way. Life in Italy would definitely not have been this wonderful without them. Among them I would like to highlight my exceptional friend Chen Hang, with whom I shared most of my academic journey. It has been a hell of a ride from our high school days till this moment. I wish him all the best for his future life in China and I look forward to our reunion wherever it may be.

I would like to give special thanks to my girlfriend Valeria for all her love and support, for having always been there with me through ups and downs. Finally, but the most importantly, I would like to express my greatest gratitude to my parents and my grandparents for their unconditional love and support at every step of the way. I left home to pursue my career in Italy as a teenage boy and arrived at this point as a man. Their beliefs in me have truly made the journey possible.

1. Introduction

This thesis project aims at exploring the state-of-the-art of active Rear-Wheel Steering (RWS) systems and developing an active rear-wheel steering controller in *MATLAB/Simulink*, investigating various design methods to create the one with the best performance when implemented on a virtual vehicle model. Simulations of standard vehicle lateral dynamics maneuvers are carried out to validate the effectiveness of the design choices. This chapter is first dedicated to providing the readers with some background information and motivation for the thesis work. Then a short introduction of Danisi Engineering S.r.l., the company in which the thesis project is carried out, is given. Finally, the thesis layout is described in detail.

1.1 Background and Motivation

In the recent years, the automotive industry has witnessed a technology advancement in terms of vehicle chassis active systems. Their developments have been driven by different factors that all played an important role: the ever-increasing vehicle on-board computational power due to technology innovation; the pursuit of a vehicle with ever higher handling and comfort performance; the growing need for vehicle handling stability and safety etc. They lead to the development of more sophisticated electric and electronic systems. Some examples of these systems are Torque Vectoring (TV), Anti-lock Braking System (ABS), Traction Control System (TCS), Electronic Stability Program (ESP) etc. They are capable of altering the vehicle's longitudinal and/or lateral dynamics in various ways, such as: by avoiding wheel spin in ABS and TCS; by independently managing wheel torques in TV etc.

The steering system is also fundamental to the handling and stability of a vehicle. Ever since the invention of the first automobiles, Front-Wheel Steering (FWS) has always been the prevailing type of steering systems. It transforms the driver's steering wheel angle demand to the actuation of front wheels' steering angle through different mechanisms such as rack-and-pinion, recirculating ball steering etc. However, there are some inherent performance limitations. In conventional FWS vehicles, only the front tires are involved in controlling the sideslip angle needed for cornering. The rear tires generate cornering force only by the resulting side slip angle from the front steering angle input [1]. Since the rear tires respond to the front steering action and generate cornering forces with a delay, a non-negligible vehicle sideslip angle will always be generated that degrades the vehicle handling stability. This leads to the fact that a traditional FWS vehicle tends to show limited maneuverability during low-speed maneuvers and reduced stability when the vehicle is approaching its cornering limit.

The idea of Rear-Wheel Steering (RWS) was conceived to counteract the inefficiency addressed above: additional actuators are added on the rear axle. By actively steering the rear wheels together with the front wheels, the delay in generating cornering forces as well as the eventual vehicle sideslip angle can be greatly reduced. By setting different objectives and

strategies to control the active rear steering angle, advantages such as increased maneuverability and handling stability can be achieved.

RWS systems and their applications on vehicles have been subjects of research and development since the 1980s, a period when the leading Japanese car manufacturers started to conceive relatively simple RWS control methods and bring them on production cars such as Nissan Skyline, Honda Prelude, Mitsubishi Galant etc. The systems proposed at that time were mainly hydraulic and mechanical which show limited actuating power and reaction speed. This aspect, coupled with the Japanese economic collapse in 1990s, and a shift of focus towards environmental and engine efficiency problems resulted a decline in interest towards new RWS systems' developments.

The first decades of the 21st century witnessed a resurgence of more powerful RWS systems and their applications on vehicles with increasing dimensions. Nowadays, almost all major car manufacturers have realized their own RWS systems on some commercial products: BMW 7 Series, Ferrari GTC4Lusso, Porsche 911 GT3, Lamborghini Aventador, Mercedes S500 V223, just to name a few. Moreover, various control methods based on different principles, including both classical and optimal controls have been successfully applied on RWS systems to realize a robust control and improve system performance under all situations.

Motivated by the current developments in RWS systems, this thesis focuses on the creation of an RWS controller and its integration with a virtual vehicle model. During the controller's creation, various control strategies proposed in literature are explored, and standard lateral dynamics test maneuvers are subsequently carried out on a virtual vehicle. Simulation results of the control method with the best performance are shown and commented on. In particular, the adopted control logic can effectively change the vehicle's cornering response according to the vehicle's longitudinal speed, i.e., change the vehicle's understeering characteristics according to vehicle longitudinal speed, thus improve the handling and stability performance in the considered speed range.

1.2 About Danisi Engineering S.r.l.

Founded in 1995 by Giacomo Danisi, Danisi Engineering S.r.l. is a company specialized in providing vehicle engineering and prototyping solutions for the automotive industry. The company is a key partner of world-renowned industry leaders, car manufacturers as well as OEMs and leading Tier-1 suppliers [2].

Danisi Engineering S.r.l. provides engineering solutions from single components to full vehicle engineering, from one-off designs to prototypes for mass production, from electric and hybrid traction, ADAS controls to Autonomous Driving development and tuning. The company is also actively involved in racing motorsport, developing complete racing cars, rolling chassis, sub-systems, and components for the racing departments of leading manufacturers [2].

The company is headquartered in Nichelino (TO), while it is also branched in Modena (MO), Florence (FI) and Shanghai (China). This thesis work is carried out in the company's headquarter with the support of Advanced Vehicle Dynamics (AVD) group (**Figure 1.1**).



Figure 1.1 Advanced Vehicle Dynamics (AVD) department of Danisi Engineering [2].

1.3 Thesis Layout

The layout of this thesis is shown below:

- **Chapter 2** is the result of an extensive literature review which presents a history outline of RWS vehicles, introducing the general concepts of RWS and the current state-of-the-art of RWS technologies. Moreover, technical findings of the bibliographic research regarding various RWS control proposals and the safety aspect of RWS are detailed.
- **Chapter 3** introduces lateral vehicle dynamics based on the famous single-track vehicle model, describing its low-speed and high-speed steering characteristics. Furthermore, several handling parameters capable of summarizing a vehicle's steady-state cornering behavior are introduced which establishes a foundation for the development of the RWS controller in subsequent chapters.
- **Chapter 4** details the theories of a 14 DOF vehicle model divided into a ride and handling model. Equations describing its dynamics relevant to ride, handling and tire dynamics are explained. A section is dedicated to several handling diagrams derived from experimental tests that are useful in helping to characterize a vehicle's handling behavior.
- **Chapter 5** concentrates on the design of the RWS controller exploring several control methods previously reviewed in literature. Starting from describing the general RWS control structure, the vehicle plant model, reference model and various controller blocks are subsequently implemented in *MATLAB/Simulink* based on the descriptions of their respective theories and equations. Then the integration of the various blocks to complete the control loop in *MATLAB/Simulink* is demonstrated.
- **Chapter 6** deals with controller offline tuning, simulation, and results validation. Some standard lateral dynamics maneuvers are explained and utilized to test the vehicle's steady-state and dynamic cornering responses. In particular, the results obtained by the controlled

vehicle model are compared with the baseline vehicle model (without RWS control) to show the effectiveness of the proposed control structures and validate the design choice.

- **Chapter 7** concludes the thesis by summarizing the work carried out in the thesis and proposes several potential improvements for future works.

2. Literature Review

It is important to first carry out some bibliographic research on RWS with the aim of getting familiar with its general concepts, the history and current state-of-the-art of RWS in the automotive industry and the state-of-the-art of various control methods proposed for RWS in literature. A brief review regarding the safety aspect of their deployment in vehicles is also conducted. The following sections report the results of the research on RWS.

2.1 Rear-Wheel Steering (RWS) Introduction

In a traditional FWS vehicle, only the front tires are actively involved in controlling the tire sideslip angles and generating the cornering forces needed for cornering. However, this traditional way suffers from a delay of cornering force generation since the rear tires' cornering force is generated only by the sideslip angle resulting from the vehicle motion [3]. As the requirements on vehicle performance are getting higher and higher, this shortcoming leads to the conception that if also the rear axle of a vehicle is made steerable even by a very small amount and in both directions, this delay in lateral force generation can be greatly reduced. In other words, the cornering response can be greatly improved in terms of maneuverability and stability.

Nowadays, RWS (or 4WS) is employed by many vehicles to improve the overall steering response by actively steering the rear wheels of a vehicle using some actuation devices, either mechanically or electronically, of an amount that depends on the dynamic response requirements imposed by the driver. At low speed it effectively decreases the vehicle turning radius and when maneuvering at high speed, on the contrary, it increases the turning radius thus increases its stability. **Figure 2.1** shows the basic scheme of RWS.

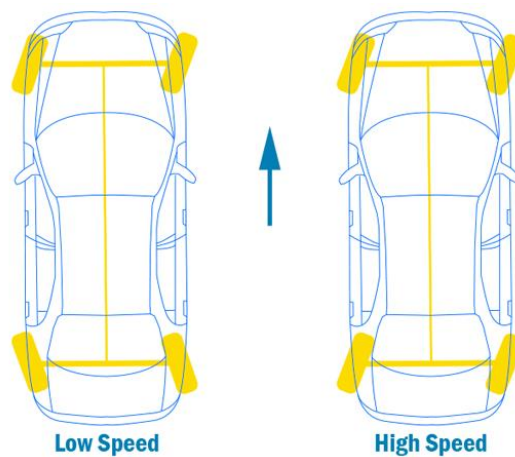


Figure 2.1 Basic scheme of RWS [4].

Usually when the vehicle maneuvers at relatively low speed, as happens in tight spaces such as alleyways and narrow streets, or a parking lot, the desired scenario is that the rear wheels are counter steered with respect to the front wheels, which is also called out-of-phase steering. This leads to higher maneuverability and a less understeering behavior that is advantageous in tight spaces at low speed.

On the contrary, when the vehicle maneuvers at high speed, such as running on a highway and the driver negotiates a lane change maneuver, it would be desirable to have the rear wheels steer towards the same direction of the front wheels, which is also called in-phase steering. When the speed is high, the vehicle is potentially closer to its cornering limit decided by the tire characteristics and road adhesion ability. This in-phase steering can effectively make the vehicle corner in a more stabilized way, leading to a more understeering behavior that in turn improves safety.

Apart from the active RWS, another scheme under investigation for electronically controlled steering system is 4-Wheels Active Steering (4WAS) [5] which incorporates RWS with Steer-By-Wire (SBW) technology to realize active steering on all the wheels. This adds an additional control freedom (active front wheels steering angle) and by controlling the steering angle of all four wheels, it helps to reduce the driver's steering effort at low speed and improve the stability and response at high speed.

2.2 State-of-the-Art

2.2.1 History Outline of Vehicles with RWS

The history of RWS can be dated back to the year **1938** when Mercedes-Benz built a military off-roader called 170VL. In this vehicle the rear wheels could be steered in opposite direction with respect to the front wheels to shorten the turning radius [6]. While being an inspiring idea, Mercedes-Benz did not apply this technology to its passenger vehicles and the 170VL also turned out to be a failure.

Research on the adoption of RWS concept on passenger cars started since the early 1980s, during which there was a surge of products and patents from the major Japanese car manufacturers. In **1985**, Nissan produced the world's first mass production passenger car **Nissan R31 Skyline (Figure 2.2)** that was equipped with an RWS system called 'HICAS'. Essentially it is hydraulic system which has speed sensors and uses the power steering pump to steer the rear wheels [7]. However, its function is limited to providing parallel RWS to improve stability at high speeds. It is deactivated at speeds below 30 *km/h*. The maximum rear steering angle is limited to 0.5 *degrees* [8].



Figure 2.2 Nissan R31 Skyline [9].

In 1987 Honda produced the 3rd generation of **Honda Prelude** (**Figure 2.3**), a sports car featuring the world's first steering angle sensing RWS [10]. All mechanical, a shaft is used to connect the steering rack at the front and rear tie rods. A planetary gearbox determines the rear steering angle so that when the steering wheel is around its neutral position (small steering wheel movements), the rear wheels are steered in the same direction (up to 1.5 *degrees*), while in the larger steering angle range, they are steered in the opposite direction (up to 5.3 *degrees*) [3, 11].



Figure 2.3 Honda Prelude 3rd Generation [12].

In the same year, **Mitsubishi** introduced on some Galant models, such as **Galant VR-4** (**Figure 2.4**) a fully hydraulic system called “**Active Four**”. This system presents no mechanical linkages between front and rear axles and features two pumps, one at each axle. The rear steering power is provided by the rear pump that pushes the suspension trailing arms. The magnitude of the steering angle applied to the rear wheels is determined by the wheel cut of the front wheels and the vehicle's velocity. The rear wheels steer up to 1.5 *degrees* in phase with the front wheels at speeds over 50 *km/h*; below this speed the RWS is deactivated [8].



Figure 2.4 Mitsubishi Galant VR-4 [13].

The early systems developed by major Japanese carmakers were similar, that is, most of them worked mechanically or hydraulically without electronic controls, and their excessive weight proved to be a disadvantage. Thus, by **1989**, Nissan developed the “**Super HICAS**” system that uses an electronically controlled hydraulic actuator to steer the rear wheels through the rear suspensions [6]. This system also uses its own computers instead of speed sensors to control the steering action. It also includes opposite RWS functionality for improved steering response and noticeable improvements in terms of stability. Also, the range of RWS angle adjustment increased to 1 *degree*. In the further generation of “Super HICAS” launched in **mid-1993**, Nissan replaced the hydraulic actuator used in previous generations with an electrical one. Around the same period Honda also shifted from using a steering shaft and planetary gearbox to using computer controls and an electric motor [11]. They were successfully implemented on Honda’s new vehicle models.

In **1992**, **BMW** began offering RWS as an option on 8-series coupe models, such as the **840 Ci (Figure 2.5)**. The system used is referred to as “**AHK**”, an abbreviation of its German name *Aktive Hinterachskinematik* (active rear-axle kinematics). It features a computer-controlled electro-hydraulic actuator unit at the center of chassis subframe which can actively steer the rear wheels plus or minus 2 *degrees*. Steering wheel angle and vehicle speed are used as input parameters, and the control unit uses these parameters to calculate the optimal steering angle of the rear wheels depending on the current driving situation [8, 14].



Figure 2.5 BMW 840 Ci [15].

Despite the booming development of RWS systems, the **1990s** witnessed a decline in interest towards RWS from major carmakers. This decline can be attributed to different factors. Firstly,

the decade-long depression hit hard and forced the Japanese carmakers to cut operating costs. In addition, the limited on-board computing capabilities and slow actuators hindered the power of RWS systems, which at that time possessed redundant weight, expensive cost, and potentially expensive repair bills that gradually turned off buyers. Meanwhile, the rise of ESP and TV means that RWS was no longer the only solution to influence a vehicle's cornering responses [6]. Finally, the automotive industry gradually shifted its attention towards other concerns, such as fuel consumption, emissions etc. Due to these reasons, by the early 2000s, RWS already seemed like a thing of the past.

The new millennium witnessed a resurgence of RWS. With the ever-growing dimensions and wheelbase length of luxury vehicles, it became more difficult to maintain a small turning radius. Steering the rear wheels opposite to the front wheels – even of only a small angle – can considerably reduce the turning radius and make parking or taking short corners easier for those vehicles [16]. The major carmakers showed new interests towards RWS, mainly due to the agility performance promised by RWS. The technological development of control engineering and less expensive actuators were also decisive for their resurgence. For example, starting from **2001**, **BMW** included **Integral Active Steering** on their **7 Series (Figure 2.6)** luxury sedan. At low speeds, it can steer the rear wheels up to *2.5 degrees* in the opposite direction, giving the effect of a shortened wheelbase for enhanced maneuverability. When changing lanes at speeds over *50 mph* (roughly *80 km/h*), both front and rear wheels turn in the same direction, giving the feel of an extended wheelbase [17].



Figure 2.6 BMW 7 Series [18].

2.2.2 Recent Vehicles with RWS

More recently, an increasing number of top-tier sportscar makers saw the benefits of RWS to handling and started to equip various RWS systems as standard, while more passenger cars started to adopt RWS as an optional system. A current trend is to integrate RWS systems with other chassis active systems so that more advantages in ride and handling can be achieved.

The **2017 Renault Megane RS** features **4Control (Figure 2.7)**, which has an electromagnetic actuator integrated on the rear axle. The onboard computer collects vehicle speed and steering wheel angle information, and the rear steering angle is decided upon those signals. At speeds lower than *60 km/h*, the rear wheels can be turned up to *2.7 degrees* out-

of-phase, which decreases the turning radius from 11.2 *m* to 10.4 *m*; while at speeds higher than 60 *km/h*, the rear wheels can be turned up to 1 *degree* in-phase [19].



Figure 2.7 Scheme of Renault 4Control [19].

The **2016 Ferrari GTC4 Lusso (Figure 2.8)** features a control system called **4RM-S** that incorporates 4-Wheel Drive (4WD) and 4-Wheel Steering (4WS). It was the first time anyone has packed 4WD and 4WS in the same car [20]. It is also equipped with a Side Slip Control system (SSC3) with an electronic differential and electronic suspension dampers to adjust the handling and ride dynamics.



Figure 2.8 Ferrari GTC4 Lusso [21].

The **2018 Lamborghini Urus (Figure 2.9)** integrates 4WD with TV and 4WS for perfect handling performance. Its RWS includes two separate electromechanical actuators, one on each side of the rear axle. The rear steering angle varies up to 3 *degrees* in-phase or out-of-phase, depending on vehicle speed and driving mode. It effectively decreases or increases the SUV's wheelbase up to 600 *mm* [22].



Figure 2.9 Lamborghini Urus [23].

Porsche offers RWS as **Rear-axle Steering (Figure 2.10)** on several of its sports GT models, including the **991 GT3**. It also features two electromechanical actuators bolted onto either side of the chassis. The actuators are connected to the car's ECU which measures vehicle speed and steering angle and then sends a signal that causes the electric motors to either 'push' or 'pull' the tie rods to realize RWS action. The turning radius can be effectively reduced by 0.5 m to 10.7 m [24].



Figure 2.10 Porsche 991 GT3 [25].

The **2021 Mercedes S500 W223 (Figure 2.11)** is by far the carmaker's most maneuverable luxury sedan thanks to the optional RWS. It provides up to 10 *degrees* of rear wheel steering angle which can reduce the car's turning radius by up to 2 m. An electric motor drives a rod from the rear axle with the help of a drive belt. Active telemetry from radar, cameras and ultrasonic sensors is fed into the system which adapts the steering angle to the relevant situation. Below the transition speed of 60 km/h, the rear wheels move to the opposite direction while above 60 km/h they move to the same direction as the front axle [26].



Figure 2.11 Mercedes S500 W223 [27].

2.2.3 RWS System Types

According to their construction methods, three basic types of RWS are distinguished [28]:

- **Mechanical systems:** A direct mechanical connection shaped like a shaft with step-up gear exists in these RWS systems which links the front axle and rear axle. The mechanism leads to a direct dependency of front and rear steering angles such that for each front wheel steering angle, a fixed rear wheel steering angle is defined. An example is **Honda's 4WS (Figure 2.12)** that was first applied to Honda Prelude 3rd generation.

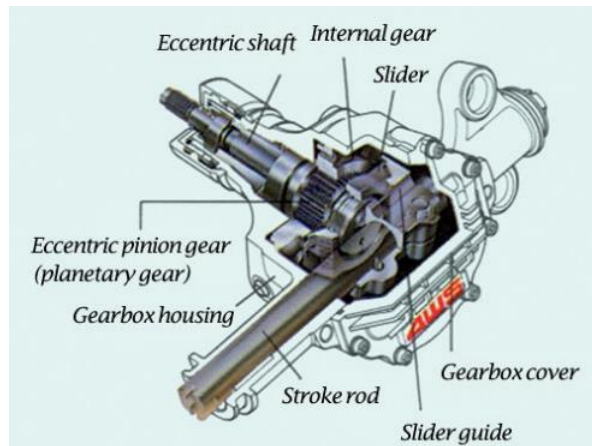


Figure 2.12 Rear steering gearbox in Honda's 4WS [10].

- Hydraulic systems:** In these systems there commonly exists an actuator in the form of a cylinder and a piston that can store hydraulic pressure. It can build up very high actuating forces, which is often necessary to move vehicles of heavy classes from at rest. Being a very complex system, it can be developed to be controlled purely hydraulically or electronically. Examples of use of purely hydraulic systems are Nissan's "HICAS" (Figure 2.13) and Mitsubishi's "Active Four" (Figure 2.14). An example of electronically controlled hydraulic system is BMW's "AHK" (Figure 2.15).

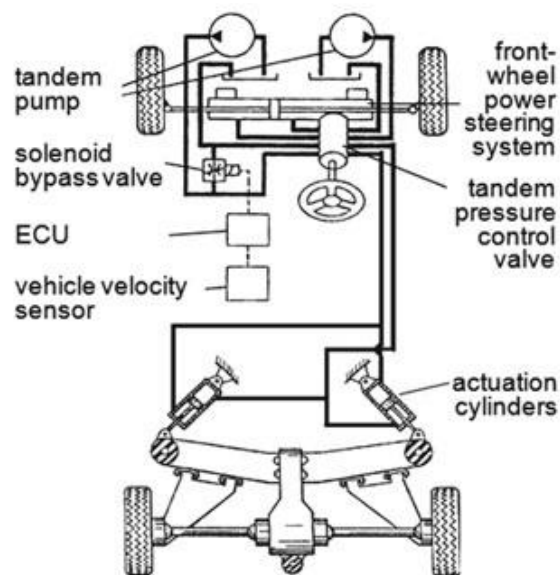


Figure 2.13 "HICAS" four-wheel steering system [29].

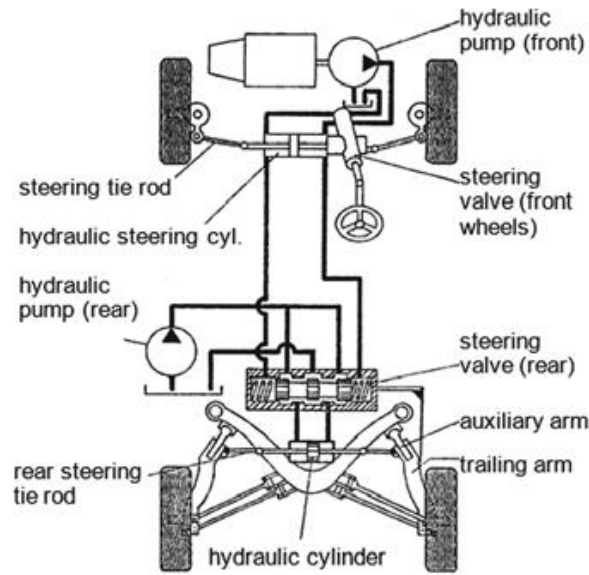


Figure 2.14 Mitsubishi “Active Four” [8].

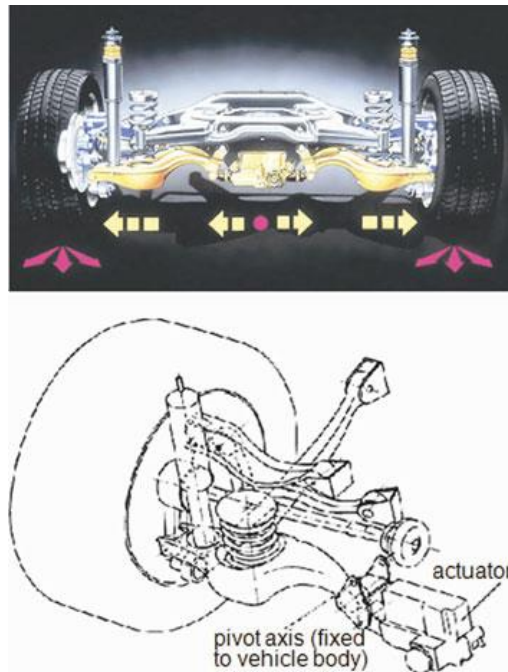


Figure 2.15 BMW's AHK [8].

- Electromechanical systems:** These systems proved to be the more powerful types in the course of RWS development in comparison with the hydraulic and the mechanical systems that show high complexity and limited functions [28]. In these systems the actuator is usually an electric motor which is actuated according to the ECU's calculation based on various input values. Then, the rotation of the motor is converted to a stroke movement by dedicated drives. They bring several benefits, for example, a range of inputs can be used such as vehicle speed, steering wheel angle, vehicle yaw rate and lateral acceleration etc. Furthermore, rear steering angles can be set independent of front steering angles. They also present a simpler construction with lighter weight compared

to other systems and are less susceptible to faults. Nowadays the majority of commercial RWS systems are electromechanical systems. **Figure 2.16** shows the scheme of Porsche's Rear-axle Steering.

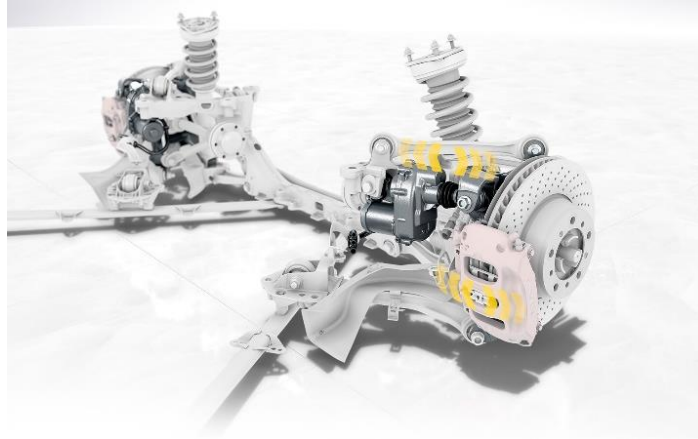


Figure 2.16 Porsche Rear-axle Steering [24].

2.2.4 RWS Control Review

The most important part of the whole RWS system is its control algorithm, which works as the brain of the system for control decision making. In modern RWS systems it is usually embedded in the form of a controller in the vehicle's ECU which receives as inputs the various real-time signals provided by various sensors. These usually come from driver inputs, for example, the steering wheel angle and/or steering wheel rotation velocity; or from information of vehicle responses such as current vehicle velocity, yaw rate, sideslip angle and the lateral acceleration. After processing the signal inputs using dedicated control algorithms, actuation signals are sent to the RWS actuators that carry out the RWS action.

In terms of how the RWS controller generates the rear steering angle, RWS systems can be categorized into three basic types [8], namely:

- **Steering Angle Proportional RWS**
- **Slip Angle Compensation RWS**
- **Active RWS**

The **Steering Angle Proportional RWS** system is made in a way that the effective RWS angle is always proportional to the imposed FWS angle as shown in the following relationship:

$$\delta_r = K_p \cdot \delta_f \quad (2.1)$$

In this equation, δ_r is the rear wheel steering angle, δ_f is the front wheel steering angle, and K_p is the coefficient of proportionality. The sign of K_p determines the direction of RWS:

- $K_p > 0$: parallel RWS
- $K_p = 0$: no RWS

- $K_p < 0$: opposite RWS

Note that production steering angle proportional RWS systems vary the value of K_p either with vehicle speed or with the steering angle depending upon the requirements.

The **Slip Angle Compensation RWS** system generally features open-loop control. The value of K_p is selected such that the vehicle's sideslip angle becomes zero. While using open-loop control only, the results depend on how well the assumed parameters match the measured ones. Furthermore, disturbances such as unknown dynamics or side winds are not considered in the control. These dictate that using open-loop control only cannot guarantee a satisfied control performance. Note that since inherently the vehicle's sideslip angle is hard to measure, closed-loop sideslip angle control is hard to be established.

The **Active RWS** tackles the aforementioned disadvantages by including a closed-loop system, usually in the form of closed-loop yaw rate feedback control. It first calculates desired (target) yaw rate by using the steering wheel angle and vehicle velocity as inputs. Then this value is compared with the actual yaw rate coming from the feedback portion to calculate the difference between the two values. Finally, a RWS angle proportional to the difference is applied to the rear wheels [8]. In this way the control is said to be robust, in the sense that it is designed to overcome the uncertainties and external disturbance problems.

In 1989, *Furukawa et al.* made a review of 4WS studies from the viewpoint of vehicle dynamics and control [3]. It is argued that the steering response of a vehicle can be represented by a rotation response (yaw response) and a translation response (lateral acceleration response) and 4WS can vary the degree of coupling of these two degrees of freedom (DOF). The control strategies can be divided into feedforward and feedback compensations. Moreover, a series of control objectives are envisaged:

- Shorter phase lags in lateral acceleration and yaw responses
- Reduction of vehicle body sideslip angle
- Stability augmentation by feedback or feedforward + feedback control
- Better vehicle maneuverability at low speed
- Achievement of desired steering responses by model-matching/following control
- Maintenance of desired responses against parameter variations by adaptive control
- Better responses near tire adhesion limits by considering tire nonlinearities

Recent research and development in RWS control has indicated that there is a continuous interest in the field of **Active RWS**. Most of these systems strive to improve the control robustness and efficiency by setting different control objectives and by utilizing various control theories and strategies. Their main passages include the generation of different vehicle states' references according to a wide range of necessities using different vehicle models ranging from very simple models to more complicated ones, and the adoption of various classical and modern control theories when creating the RWS controller.

Classical control theories using Laplace transform and frequency domain analysis techniques have been extensively explored and integrated into various RWS control proposals in literature. *Marino et al.* proposed a Proportional-Integral (PI) active rear steering control and an additional active front steering control [30, 31]. A desired yaw rate reference map is generated based on a first-order nonlinear equation that comes from the 2 DOF single-track model with nonlinear tire characteristics. This model is considered to capture the essential vehicle steering dynamics. Experimental validations carried out on a vehicle model with more DOF demonstrate improvements in low-speed maneuverability and high-speed safety with reduced driver control effort.

Vilaplana et al. also used classical techniques of PI according to Individual Channel Design (ICD) methodology to design the 4WAS controller, including an anti-windup scheme against actuator saturation [32]. This methodology basically restates a 2-by-2 Multiple-Input Multiple-Output (MIMO) problem as two Single-Input Single-Output (SISO) problems with two channels of yaw rate and sideslip angle, where each channel has its own performance specification and reference derived from the 2 DOF single-track model. Through simulation, the resulting controller is verified to satisfy robustness and disturbance rejection requirements.

Canale et al. applied Internal Model Control (IMC) based on H_∞ optimization techniques and designed a feedback RWS controller that is able to effectively handle robustness and saturation issues [33, 34]. The yaw rate reference maps are generated by properly modifying the established steering diagram based on the nonlinear 2 DOF single-track model. Furthermore, a feedforward path is added to improve the transient yaw rate response in face of driver input. Results of verification maneuvers on a 14 DOF full vehicle model certify the effectiveness of the proposed control.

Modern control theories and their adoption on RWS are explored by some more recent studies. These theories are usually based on state equations written in the state space. Moreover, optimal control, with the goal of achieving desired responses of the closed-loop system subjecting to some limiting conditions and objective functions are continuously being explored. They have proved to be more effective when dealing with MIMO systems and system nonlinearities. *Zhang et al.* designed an 4WAS controller based on the Linear Quadratic Control (LQC) strategy [35]. Desired responses are obtained from an ideal 2 DOF single-track vehicle model that mimics the steady-state response of a passive vehicle (without RWS) and to realize zero sideslip angle response. Vehicle actual states are set to track the desired states applying LQC strategy to minimize the tracking error. Compared to RWS using proportional control, improved vehicle response is obtained.

Du et al. [36], *Hamzah et al.* [37] all designed a 4WAS controller adopting Sliding Mode Control (SMC) technique. It consists of the use of a sliding surface in the state space that represents the target of system trajectories. The RWS control inputs are designed to lead the system to that surface by a constant reaching law, with the target trajectories derived from the 2 DOF linear single-track model. Robustness against parameter uncertainties and disturbances are verified by carrying out simulations on dedicated maneuvers using vehicle models of different complexities.

Lucchini et al. proposed a Model Predictive Control (MPC) based controller for active RWS with a focus on the maximization of performance in the context of sports cars [38]. It assumes an optimization-based robust control: given a defined time horizon, MPC solves an optimization problem at discrete time steps using a predictive plant model under some given constraints. A more accurate linear time varying (LTV) predictive model based on the linearization of a nonlinear 2 DOF vehicle model is proposed and MPC theory is used to minimize the vehicle states' tracking error. Step steer and ramp steer maneuvers are carried out in simulation environment and the controller's effectiveness on high-speed stability is verified. Following a similar approach, *Guo et al.* also proposed a Nonlinear Model Predictive Control (NMPC) scheme for the active RWS controller design for an electric vehicle. It can better deal with the nonlinearity and constraint in vehicle steering dynamics by directly using a nonlinear prediction model inside the MPC controller [39].

2.3 Pros and Cons of RWS

To sum up, a number of advantages over traditional FWS can be identified by adding a RWS system to a vehicle. They include:

- Improved steering response to driver steering inputs
- Improved vehicle maneuverability at low speeds, with increased yaw rate and smaller turning radius
- Improved vehicle stability at high speeds, with increased yaw damping and cornering stability

On the other hand, they also present some potential drawbacks:

- Cost: many more components are required for the RWS system construction compared to FWS only. Higher repair costs are also expected in face of malfunctions
- Unfamiliar steering feel: generally, inexperienced drivers could perceive some undesired steering and driving feel

2.4 Safety Aspect of RWS

RWS systems, as well as other active chassis control systems generally have high requirements on safety. These systems are constructed in a sophisticated way, involving various components such as sensors, actuators, signal transmissions, electronic hardware, and software etc. In fact, a failure or malfunction in any chassis or powertrain control system can lead to serious consequences for the driver, passengers, and other motorists [8]. Under malfunctioning circumstances, the whole system should be capable of entering a safe mode, also called fail safe or fail silent. As soon as a threshold of normal operating conditions is reached, the system should allow the rear wheels to quickly return to neutral through dedicated mechanisms.

As the number of electric and electronics systems is constantly increasing, there is the need to quantify the safety requirements on these systems related to the automotive field. In ISO

26262 – Functional Safety for Road Vehicle Standard it is defined an automotive-specific, risk-based approach for determining risk classes called “Automotive Safety Integrity Levels” (ASILs). It is defined to comply with the needs specific to the electronic systems within road vehicles [40]. In this scheme, five levels are established after executing risk analysis regarding Severity, Exposure and Controllability: Severity – when a system were to fail, how severe could be the potential consequences; Exposure – the probability of the hazardous situations to happen and Controllability – if the system were to fail, how much possible could the people involved react in a timely fashion to avoid a harm [41]. They range from ASIL-D level which represents the highest level of risk and safety requirements on the product to “Quality Measurement” (QM) level which does not require any safety measures due to the low accompanied level of automotive hazards. **Figure 2.17** is a scheme of the ASILs for automotive systems and components.

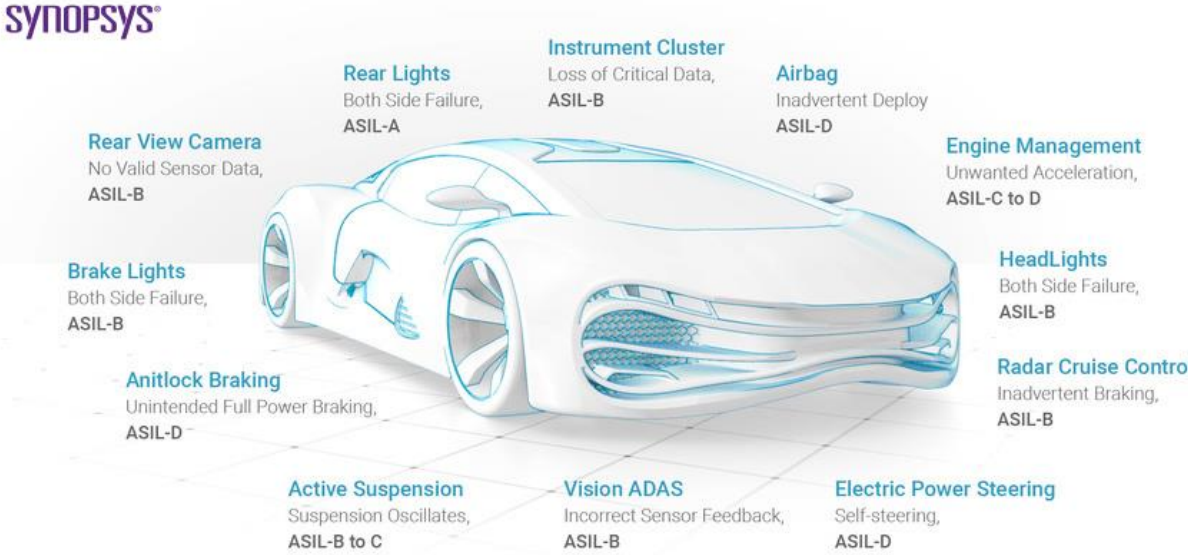


Figure 2.17 ASILs for some automotive systems and components [42].

For vehicle active steering systems, since a range of scenarios under different vehicle operating conditions need to be supported during the system’s intervention to improve the active safety of a vehicle, the need for these systems to be able to meet ASIL-D requirements are constantly increasing.

3. Lateral Vehicle Dynamics

RWS systems effectively improve the vehicle's low-speed maneuverability and high-speed stability by actively changing the rear steering angle. Thus, vehicle dynamics responses are changed to match the desired responses. In order to design an RWS controller, it is necessary to introduce and understand the relevant vehicle dynamics theories. In particular, the lateral vehicle dynamics are the most important regarding the vehicle steering response. Lateral vehicle motion equations based on the famous single-track model are detailed in the following passages, taking into account the simplifications made on the model. Some important handling parameters are described in detail, which are helpful in understanding a vehicle's cornering responses.

3.1 Single-Track Model

As evidenced from the RWS control literature review, the single-track model (or bicycle model) is the most adopted vehicle model for controller design purposes. It provides a foundation for controller reference values generation and can also be adopted to represent the controlled vehicle whenever its low level of modelling complexity is accepted. Lateral vehicle dynamics can be studied by analyzing the steering responses based on this model under different speeds ranges. This section is based on the single-track model of a passive vehicle (vehicle without RWS capability) and the equations are adapted from [43] and [44].

In the study and creation of the single-track model, a number of assumptions are made [43]:

- There is no lateral load transfer, i.e., the left and right wheel are combined in one at each axle
- No longitudinal load transfer is present
- Plane vehicle movements are considered, with the radius of curvature much larger than the vehicle's wheelbase
- The vehicle is moving at constant longitudinal speed, i.e., the longitudinal and lateral vehicle dynamics are totally decoupled
- Tire forces are considered in linear range, i.e., small tire sideslip angles are considered
- No rolling, pitch motion and aerodynamic effects are considered
- Small wheel steering angle and vehicle sideslip angle

First of all, **low-speed cornering** scenarios are considered. They are representatives of the typical parking lot maneuvers. In these cases, the wheel slip angles are zero and the front and rear wheels turn on concentric circles, as shown in **Figure 3.1**. This steering condition is named "**kinematic steering**" since no dynamic effects are involved and the wheels are in pure rolling condition.

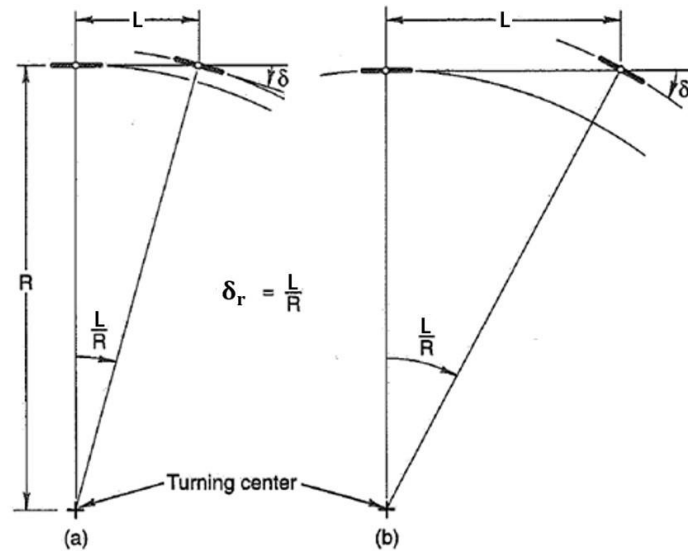


Figure 3.1 Kinematic steering with the required steering angle (adapted from [43]). (a) vehicle with nominal wheelbase; (b) vehicle with longer wheelbase

From **Figure 3.1** it can be noticed that during low-speed cornering with constant radius of turn R , the front wheels steering angle required for a vehicle with wheelbase L to negotiate the turn is:

$$\delta_r = \frac{L}{R} \quad (3.1)$$

This angle is usually referred to as *Ackermann angle* and is related to the geometry of the vehicle.

In **high-speed cornering** scenarios instead, non-negligible lateral acceleration are present. The tires must develop lateral forces to counteract the lateral acceleration effects and slip angles are present on each wheel. This steering condition is named “**dynamic steering**” as shown in **Figure 3.2**:

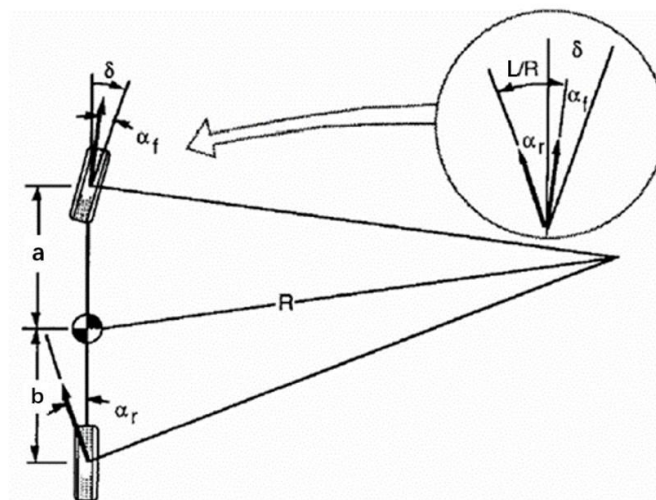


Figure 3.2 Dynamic steering (adapted from [44]).

If steady-state condition is considered and by applying Newton's Second Law, the following lateral force equilibrium is obtained:

$$\sum F_y = F_{yf} + F_{yr} = M \frac{V^2}{R} \quad (3.2)$$

Where F_{yf} and F_{yr} are the lateral forces at front and rear axle, M is the mass of vehicle and V is vehicle's longitudinal velocity.

The following moment equilibrium about the vehicle's center of gravity (CG) is also obtained by applying Newton's Second Law:

$$\sum M_z = F_{yf}a = F_{yr}b \quad (3.3)$$

$$F_{yf}a - F_{yr}b = 0 \quad (3.4)$$

Which leads to:

$$F_{yf} = F_{yr} \frac{b}{a} \quad (3.5)$$

Substituting (3.5) back in (3.2) gives the expressions of F_{yf} and F_{yr} :

$$\begin{cases} F_{yf} = M \frac{b V^2}{L R} \\ F_{yr} = M \frac{a V^2}{L R} \end{cases} \quad (3.6)$$

These forces must be generated by the tires. Considering small tire sideslip angles, the linear region of $F_y(\alpha)$ curve (**Figure 3.3**) is considered, which states that the lateral force is equal to the product of tire sideslip angles α and the gradient of the linear tract of the curve called *cornering stiffness*. Note that in this case no camber angle is considered, which substantially contributes to a small amount of lateral force if it is present:

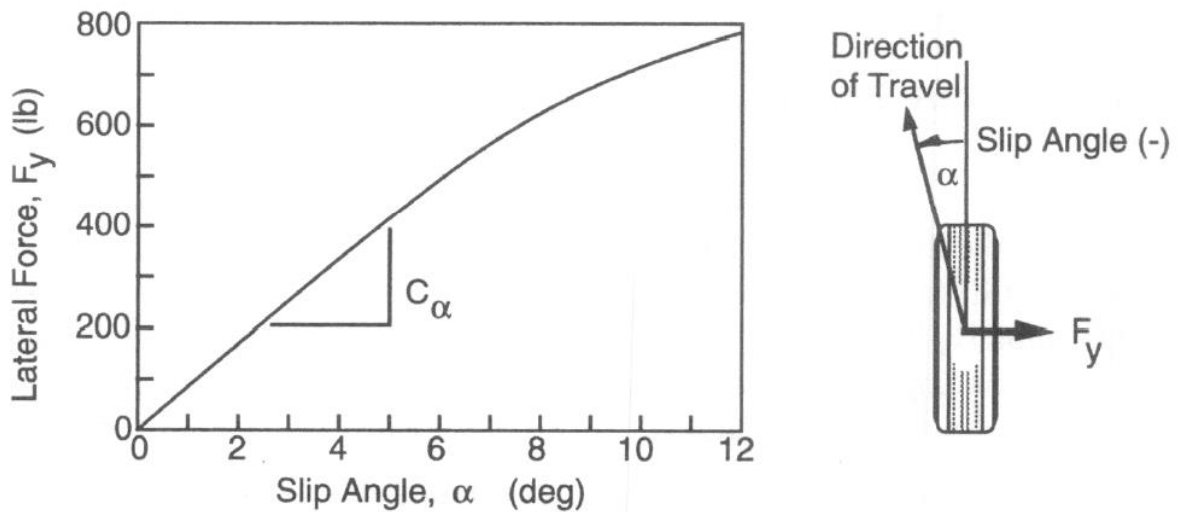


Figure 3.3 Tire cornering force properties [44].

$$\begin{cases} F_{yf} = C_{\alpha f} \alpha_f \\ F_{yr} = C_{\alpha r} \alpha_r \end{cases} \quad (3.7)$$

Where $C_{\alpha i}$ are the equivalent cornering stiffness for each axle. Substituting (3.7) back in (3.6) gives the expressions of front and rear tire sideslip angles:

$$\begin{cases} \alpha_f = M \frac{b}{L} \frac{V^2}{RC_{\alpha f}} \\ \alpha_r = M \frac{a}{L} \frac{V^2}{RC_{\alpha r}} \end{cases} \quad (3.8)$$

Looking at the geometry of the vehicle in turn (**Figure 3.2**), the following geometrical relationship is established:

$$\delta = \delta_r + \alpha_f - \alpha_r = \frac{L}{R} + \alpha_f - \alpha_r \quad (3.9)$$

Where δ is the steering angle at front wheels in *radians*. Considering $a_y = V^2/R$ and substituting (3.8) in (3.9):

$$\delta = \frac{L}{R} + \frac{M}{L} \left(\frac{b}{C_{\alpha f}} - \frac{a}{C_{\alpha r}} \right) a_y \quad (3.10)$$

Equation (3.10) is very important for the cornering response properties of the vehicle. It determines how the front wheel's steering angle needs to be changed with R or a_y . Several important vehicle handling parameters can be derived from the observations of this equation, as will be detailed in the following section.

3.2 Steady-State Handling Parameters

3.2.1 Understeer Gradient

The term $M/L \cdot (b/C_{\alpha f} - a/C_{\alpha r})$ in equation (3.10) is called **Understeer Gradient (UG)** and denoted by the symbol K_{US} which in this case has the units of *rad/g*. It is the most commonly used measure of vehicle open-loop response under steady-state or quasi steady-state conditions. It determines the magnitude and direction of the steering inputs required [44]:

$$K_{US} = \frac{M}{L} \left(\frac{b}{C_{\alpha f}} - \frac{a}{C_{\alpha r}} \right) \quad (3.11)$$

According to the value of K_{US} , three possibilities of vehicle behavior exist [44]:

- **Neutral steer:** $K_{US} = 0 \rightarrow \alpha_f = \alpha_r \rightarrow \delta = \delta_r$, no change in front wheel's steering angle is required as the lateral acceleration increases (by changing V with R constant or by changing R with V constant), so the steering angle necessary to make the turn is always equal to the *Ackermann angle* δ_r . In this case, the same amount of increase in slip angle can be noticed for front and rear wheels.

- **Understeer:** $K_{US} > 0 \rightarrow \alpha_f > \alpha_r \rightarrow \delta > \delta_r$, an increase in front wheel's steering angle is required as the lateral acceleration increases. Specifically, a linear increase with respect to increasing a_y or V^2 is expected. In this case, a higher increase in front wheel's slip angle than the rear slip angle is necessary to maintain the steering maneuver.
- **Oversteer:** $K_{US} < 0 \rightarrow \alpha_f < \alpha_r \rightarrow \delta < \delta_r$, a decrease in front wheel's steering angle is required as the lateral acceleration increases. Specifically, a linear decrease with respect to increasing a_y or V^2 is expected. In this case, a higher increase in rear wheel's slip angle than the front slip angle is necessary to maintain the steering maneuver.

3.2.2 Characteristic Speed

For an understeering vehicle, this parameter is used to quantify the understeering level. It represents the speed at which the steering angle required to negotiate any turn is twice the *Ackermann angle* [44]:

$$\delta = 2 \frac{L}{R} \quad (3.12)$$

Combining (3.12) with (3.10) and (3.11) leads to the expression:

$$K_{US} \frac{V_{char}^2}{R} = \frac{L}{R} \quad (3.13)$$

$$V_{char} = \sqrt{\frac{L}{K_{US}}} \quad (3.14)$$

It represents the speed at which the understeering vehicle is the most responsive in yaw direction.

3.2.3 Critical Speed

For an oversteering vehicle, this parameter establishes an upper bound of velocity above which the vehicle will develop directionally unstable behavior. It is given by the following expression:

$$V_{crit} = \sqrt{-\frac{L}{K_{US}}} \quad (3.15)$$

Note that in this case K_{US} is negative in value since it is the case with an oversteering vehicle. From equation (3.15) it is notable the dependence of critical speed on a vehicle's wheelbase. In general, vehicles with longer wheelbases tend to have higher critical speeds for the same oversteering level.

Figure 3.4 summarizes the three types of steering response behaviors mentioned, highlighting also the characteristic and critical speed.

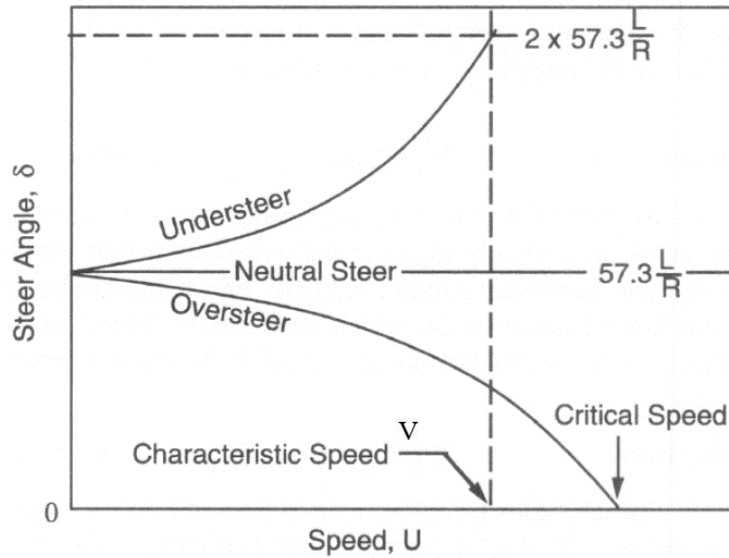


Figure 3.4 Change of front wheel steer angle with speed (adapted from [44]). Here the number 57.3 represents the unit conversion from *radians* to *degrees*.

3.2.4 Static Margin

Another term that characterizes the vehicle steady-state handling behavior is the **Static Margin**. It derives from the definition of **Neutral Steer Point**, which represents the point along the vehicle chassis at which an external lateral force can be applied which produces no steady-state yaw velocity [43]. This definition can be extended to **Neutral Steer Line** that is made up of points in the x-z plane along which external lateral force produces no steady-state yaw velocity, as shown in **Figure 3.5**.

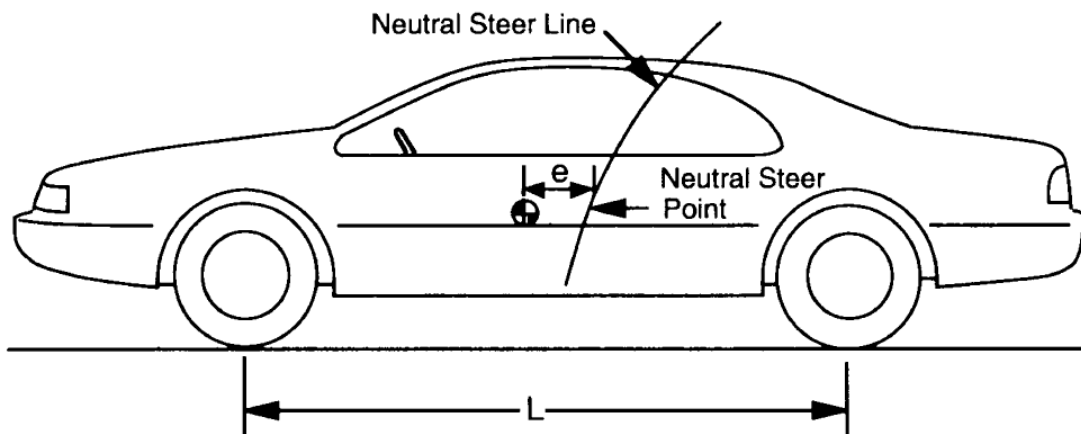


Figure 3.5 Definition of Neutral Steer Point and Neutral Steer Line [44]. The letter *e* represents the longitudinal distance between the vehicle's CG and its Neutral Steer Point.

Static Margin is defined as the distance *e* normalized by the vehicle's wheelbase [44]:

$$\text{Static Margin} = \frac{e}{L} \quad (3.16)$$

Combining the definition with the three types of vehicle cornering behaviors, it follows that: for a Neutral Steering vehicle, the Neutral Steer Point is at the vehicle's CG and *Static Margin* = 0; for an Understeering vehicle, the Neutral Steer Point is behind the vehicle's CG and *Static Margin* > 0; for an Oversteering vehicle, the Neutral Steer Point is ahead of the vehicle's CG and *Static Margin* < 0.

4. 14 DOF Model Vehicle Dynamics

The 2 DOF single-track model works well when representing the vehicle's directional response in the linear regions of tire behaviors. As a result, it is suitable both for the RWS controller design purposes and for tuning and simulations by representing the vehicle plant in order to validate the design choices. However, in order to achieve more faithful design validation results of a RWS system, a vehicle model with more DOF is oftentimes required since it can more accurately replicate a real vehicle due to the additional DOF considered.

In view of this, a 14 DOF full vehicle model and its vehicle dynamics theories are introduced. This model describes the vehicle behavior in longitudinal, lateral, and vertical directions consisting of a sprung mass of vehicle body and four unsprung masses of the wheels [45]. In particular, the DOF considered in the model (**Figure 4.1**) are:

- Sprung mass 6 DOF: vehicle body longitudinal, lateral, vertical, roll, pitch, and yaw motion
- Unsprung mass 8 DOF: vertical and spinning motion of each of the 4 wheels

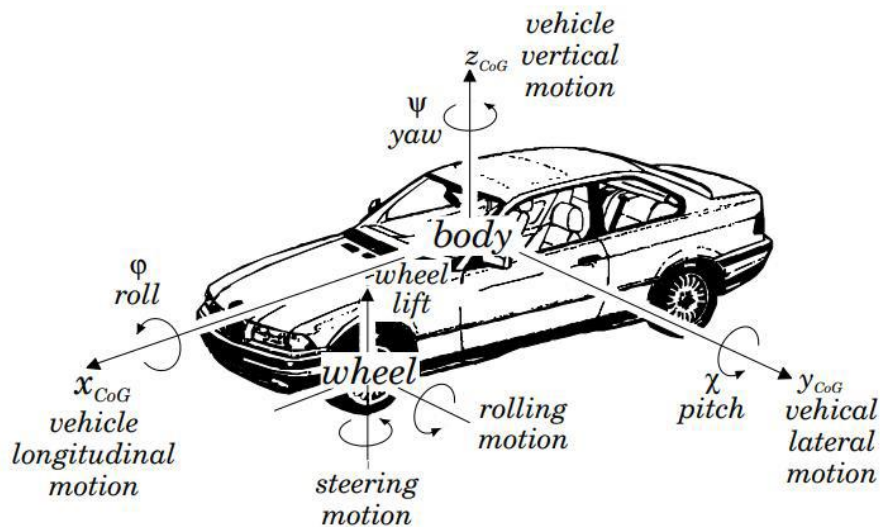


Figure 4.1 Schematic of the DOF considered in the 14 DOF model [46].

The DOF of the model can be further attributed according to two different dynamics theories: ride and handling model, each of which contains 7 DOF. The following sections detail the two theories and also provide a description of tire dynamics. Moreover, the concept of handling diagrams is introduced.

4.1 Ride Model

The ride model contains 7 DOF:

- Sprung mass 3 DOF: vehicle body vertical, roll and pitch motion
- Unsprung mass 4 DOF: vertical motion of each of the 4 wheels

In particular, spring, and damper elements are present in between the sprung and unsprung masses, as shown in **Figure 4.2**.

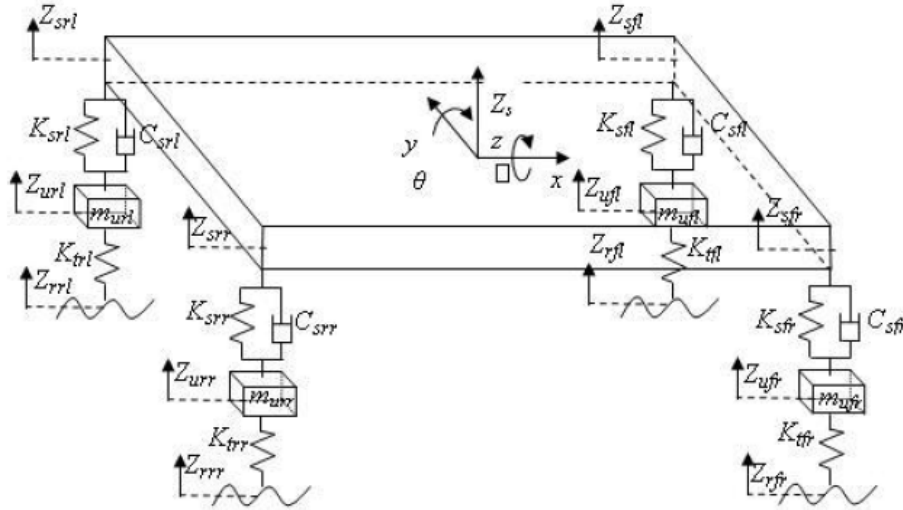


Figure 4.2 7 DOF vehicle ride model [45].

Several assumptions are made regarding the ride model [47]:

- Vehicle body is represented as a lumped mass, i.e., mass is concentrated at one point
- Aerodynamic drag forces, vehicle pitch and roll angles are neglected
- Constant damping coefficient, tire stiffness and spring stiffness are assumed
- The road is assumed to be level except for disturbances

By applying Newton's Second Law, the following force and moment balances regarding the 7 DOF can be obtained (all equations are adapted from [47], with modifications on subscripts). Starting with sprung mass vertical force equilibrium:

$$F_{sfl} + F_{dfl} + F_{sfr} + F_{dfr} + F_{srl} + F_{drl} + F_{srr} = m_s a_z \quad (4.1)$$

Where m_s is the sprung mass; a_z is the sprung mass vertical acceleration; F_{ijk} represents the various spring and damper force contributions due to spring stiffness K_{ijk} and damper coefficient C_{ijk} ; the subscripts s and d stand for spring and damper; fl , fr , rl and rr stand for front left, front right, rear left and rear right.

Sprung mass moment equilibrium around y axis:

$$(F_{srl} + F_{drl} + F_{srr} + F_{drr})l_r - (F_{sfl} + F_{dfl} + F_{sfr} + F_{dfr})l_f = I_p \ddot{\theta} \quad (4.2)$$

Sprung mass moment equilibrium around x axis:

$$(F_{sfl} + F_{dfl} + F_{srl} + F_{drl}) \frac{w}{2} - (F_{sfr} + F_{dfr} + F_{srr} + F_{drr}) \frac{w}{2} = I_r \ddot{\varphi} \quad (4.3)$$

Where l_f and l_r are the distance of vehicle's CG between front and rear axles; I_p is the vehicle's pitch moment of inertia about its y axis; $\ddot{\theta}$ is the pitch acceleration at vehicle's CG; w is wheel track length (front and rear wheel track length are assumed to be equal); I_r is the vehicle's roll moment of inertia about its x axis; $\ddot{\varphi}$ is the roll acceleration at vehicle's CG.

Unsprung mass vertical force equilibrium:

$$\begin{cases} F_{tfl} - F_{sfl} - F_{dfl} = m_{ufl} \ddot{z}_{ufl} \\ F_{tfr} - F_{sfr} - F_{dfr} = m_{ufr} \ddot{z}_{ufr} \\ F_{trl} - F_{srl} - F_{drl} = m_{url} \ddot{z}_{url} \\ F_{trr} - F_{srr} - F_{drr} = m_{urr} \ddot{z}_{urr} \end{cases} \quad (4.4)$$

Where F_{tij} are the tire vertical forces in each wheel due to tire stiffness k_{tij} ; m_{uij} are the mass of each of the four wheels; \ddot{z}_{uij} are the vertical acceleration of each wheel.

4.2 Handling Model

The handling model contains 7 DOF:

- Sprung mass 3 DOF: vehicle body longitudinal, lateral and yaw motions
- Unsprung mass 4 DOF: spinning motion of each of the 4 wheels

A schematic of the handling model is presented in **Figure 4.3**. Most assumptions made for the ride model are considered also for the handling model, except that instead of null pitch and roll angles, these are considered here and their magnitudes are assumed small. Additionally, the left and right front wheel steering angles are considered equal.

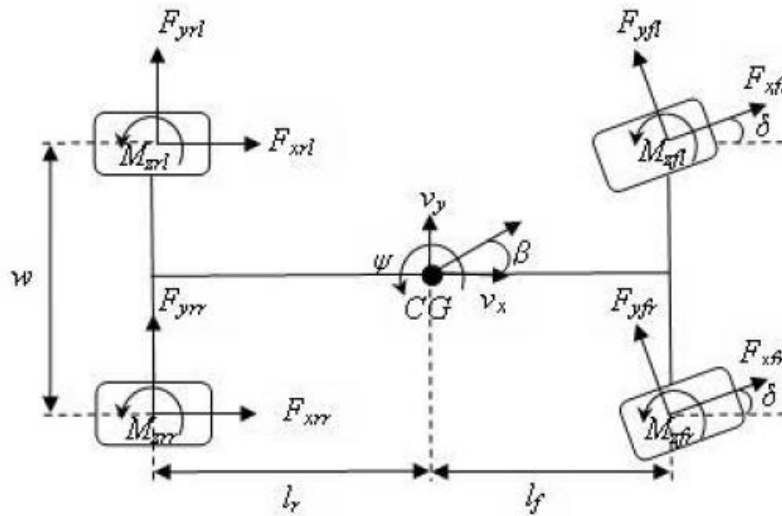


Figure 4.3 7 DOF vehicle handling model [45].

Following a similar approach as before by applying Newton's Second Law, the following force and moment balances can be obtained (all equations are adapted from [45], with modifications on subscripts). Starting with sprung mass longitudinal force equilibrium:

$$F_{xfl} \cos \delta - F_{yfl} \sin \delta + F_{xfr} \cos \delta - F_{yfr} \sin \delta + F_{xrl} + F_{xrr} = m_s a_x \quad (4.5)$$

Where δ is the front wheels steering angle; F_{ijk} represents the various tire longitudinal and lateral force contributions: the subscripts x and y stand for longitudinal and lateral direction; fl , fr , rl and rr stand for front left, front right, rear left and rear right; a_x is vehicle's longitudinal acceleration and is made up of the following terms:

$$a_x = \dot{v}_x - v_y \dot{\psi} \quad (4.6)$$

Where \dot{v}_x is the acceleration term due to the motion along x axis; $v_y \dot{\psi}$ is the acceleration term due to centripetal acceleration.

Sprung mass lateral force equilibrium:

$$F_{yfl} \cos \delta + F_{xfl} \sin \delta + F_{yfr} \cos \delta + F_{xfr} \sin \delta + F_{yrl} + F_{yrr} = m_s a_y \quad (4.7)$$

Where a_y is vehicle's lateral acceleration and is made up of the following terms:

$$a_y = \dot{v}_y + v_x \dot{\psi} \quad (4.8)$$

Where \dot{v}_y is the acceleration term due to the motion along y axis; $v_x \dot{\psi}$ is the acceleration term due to centripetal acceleration.

The longitudinal and lateral vehicle velocities v_x and v_y can be obtained by integrating the expressions of \dot{v}_x and \dot{v}_y :

$$\begin{cases} v_x = \int (a_x + v_y \dot{\psi}) dt \\ v_y = \int (a_y - v_x \dot{\psi}) dt \end{cases} \quad (4.9)$$

Then the overall velocity v of the vehicle is expressed as:

$$v = \sqrt{v_x^2 + v_y^2} \quad (4.10)$$

With the vehicle sideslip angle β denoted by:

$$\beta = \tan^{-1} \frac{v_y}{v_x} \quad (4.11)$$

Sprung mass moment equilibrium around z axis:

$$\begin{aligned} -\frac{W}{2} (F_{xfl} \cos \delta - F_{xfr} \cos \delta + F_{xrl} - F_{xrr} - F_{yfl} \sin \delta + F_{yfr} \sin \delta) \\ + l_f (F_{xfl} \sin \delta + F_{yfl} \cos \delta + F_{xfr} \sin \delta + F_{yfr} \cos \delta) \\ - l_r (F_{yrl} + F_{yrr}) + M_{zfl} + M_{zfr} + M_{zrl} + M_{zrr} = I_z \ddot{\psi} \end{aligned} \quad (4.12)$$

Where M_{zij} are the self-aligning moment of each of the four wheels.

An improvement of the 14 DOF model with respect to the 2 DOF model in handling is that load transfer effects due to sprung mass longitudinal and lateral accelerations are taken into account. Specifically, longitudinal acceleration a_x leads to pitch motion that is the rotation of the vehicle body of an angle θ with respect to the pitch center, as shown in **Figure 4.4**.

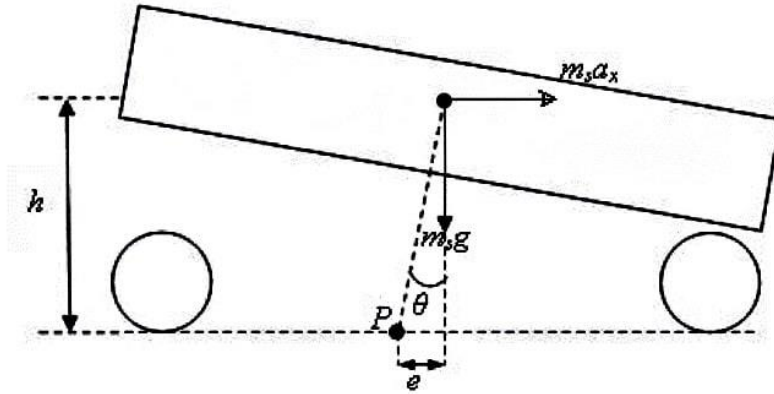


Figure 4.4 Pitch motion due to longitudinal acceleration a_x (adapted from [45]).

The pitch acceleration $\ddot{\theta}$ can be determined from the following sprung mass moment equilibrium around y axis:

$$m_s a_x h + m_s g h \theta - K_\theta \theta - C_\theta \dot{\theta} = I_p \ddot{\theta} \quad (4.13)$$

Where h is the height of the vehicle's CG; K_θ is suspension pitch stiffness; C_θ is damper pitch coefficient.

Due to longitudinal acceleration, a longitudinal load transfer takes place:

$$\Delta F_{z,long} = \frac{m_s a_x h}{l_f + l_r} \quad (4.14)$$

Similarly, lateral acceleration a_y leads to roll motion that is the rotation of the vehicle body of an angle φ with respect to the roll center, as shown in **Figure 4.5**.

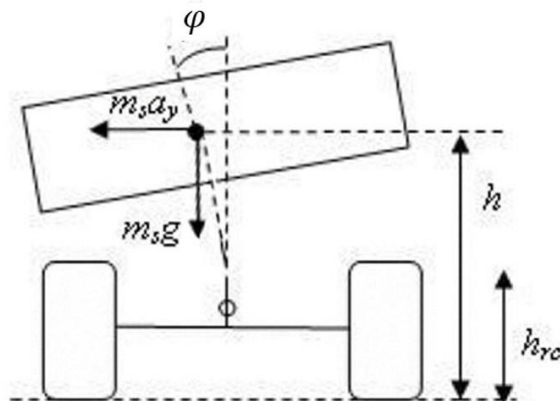


Figure 4.5 Roll motion due to lateral acceleration (adapted from [45]).

The roll acceleration $\ddot{\phi}$ can be determined from the following sprung mass moment equilibrium around x axis:

$$m_s a_y (h - h_{rc}) + m_s g (h - h_{rc}) \phi - K_\phi \phi - C_\phi \dot{\phi} = (I_r + m_s (h - h_{rc})^2) \ddot{\phi} \quad (4.15)$$

Where h_{rc} is vehicle's roll center height; K_ϕ is suspension total roll stiffness; C_ϕ is damper total roll coefficient considering both front and rear axle contribution.

The total lateral load transfer due to lateral acceleration is represented as:

$$\Delta F_{z,lat} = \frac{m_s a_y (h - h_{rc})}{w} + \frac{K_\phi \phi + C_\phi \dot{\phi}}{w} \quad (4.16)$$

The spinning motion of each wheel is determined from the wheel free body diagram with force and moments acting on the wheel, as shown in **Figure 4.6**. The spinning motions of the four wheels make up the last 4 DOF of the handling model.

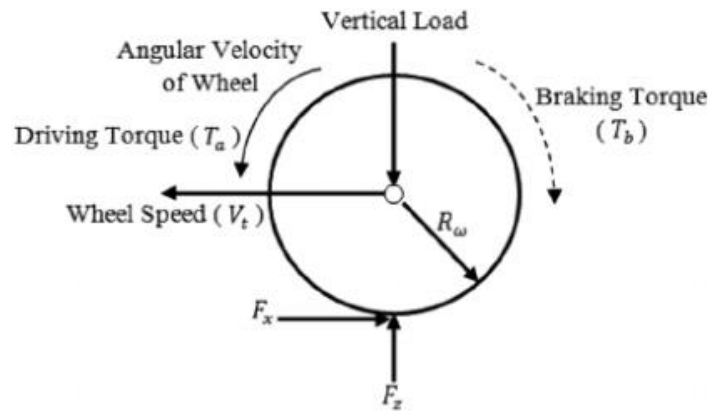


Figure 4.6 Free body diagram of a single wheel [48].

The wheel's angular acceleration $\dot{\omega}$ can be obtained from the following wheel moment equilibrium around its rotation axis:

$$T_a - T_b - F_x R_\omega = I_w \dot{\omega} \quad (4.17)$$

Where T_a is driving torque; T_b is braking torque; F_x is the total longitudinal force transmitted between wheel and ground; R_ω is the wheels' loaded radius; I_w is the wheel's rotational moment of inertia.

4.3 Tire Dynamics

Tires are of paramount importance in determining a vehicle's dynamic responses. In fact, a modern vehicle is able to exchange forces with the ground thanks to the tires. The forces exchanged between tires and ground can be differentiated into longitudinal, lateral, and vertical forces. The ability for a tire to carry weights (thus vertical forces) has always been a requisite since the beginning of automobiles, while along with the increasing speed of modern vehicles the bearing ability for longitudinal and lateral forces becomes more and more important [49].

When a wheel is rolling on a level road with its mean plane perpendicular to the road and without the application of tractive or braking torque, the wheel is said to be in pure rolling condition. An **effective rolling radius** R_e can be defined:

$$R_e = \frac{V}{\Omega} \quad (4.18)$$

With V the forward speed of wheel and Ω its angular velocity. This effective radius R_e is different from both the unloaded radius R and the loaded radius R_l due to the fact that the tread band is naturally compliant also in circumferential direction, as shown in **Figure 4.7**. The relationship between them is:

$$R_l < R_e < R \quad (4.19)$$

The effective rolling radius depends on different factors, such as the type of tires, the tread wear, the tire's working conditions, and the application of tractive or braking torques. In particular, when a braking torque is applied the new effective rolling radius is larger than the nominal case; when a tractive torque is applied the new effective rolling radius is smaller than the nominal case, owing to the tire's deformation.

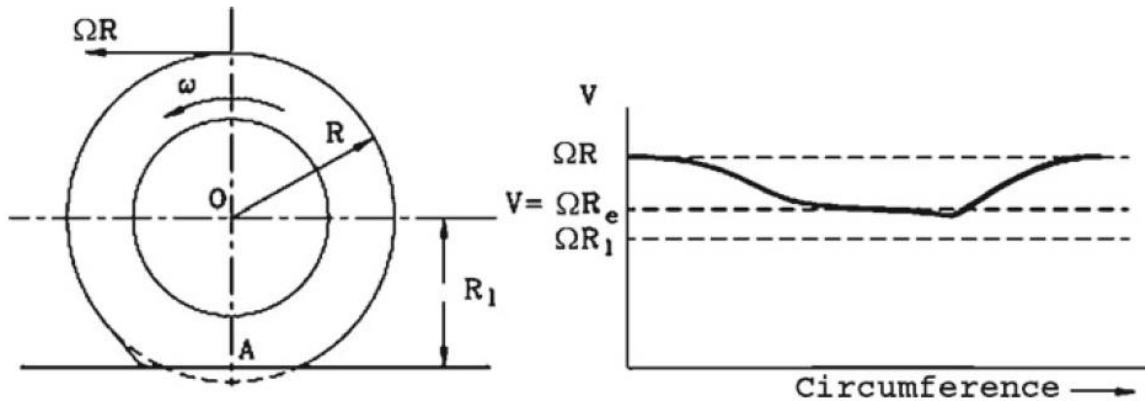


Figure 4.7 Tire rolling on a flat road; Peripheral speed on contact area [49].

Due to the deformation of pneumatic tires in the contact zone, some energy is dissipated in the process. They are the main contributions to the **rolling resistance** F_r that is generally expressed as:

$$F_r = -fF_z \quad (4.20)$$

Where f is the rolling resistance coefficient and is usually determined experimentally; F_z is the normal force on the wheel. The coefficient f depends on many factors, for example, the travelling speed, tire's inflation pressure, the normal force, the size of the tire and of the contact zone, the structure and material of the tire, the working temperature, the road conditions and, last but not least, the longitudinal and lateral forces exerted by the wheel [49].

When a braking or tractive moment is applied to a pure rolling wheel, the **longitudinal slip** σ is defined to characterize the change of wheel angular velocity Ω with respect to the free rolling condition $\Omega_0 = V/R_e$:

$$\sigma = \frac{\Omega - \Omega_0}{\Omega_0} = \frac{R_e(\Omega - \Omega_0)}{V} \quad (4.21)$$

- In braking: $\Omega < \Omega_0$, thus $-1 < \sigma < 0$
- In traction: $\Omega > \Omega_0$, thus $0 < \sigma < 1$

Due to longitudinal slip, different values of **longitudinal force** F_x are exchanged between the tire and the ground. Its value is 0 when there is no slip and it increases almost linearly with longitudinal slip for values of slip from about -0.25 to about 0.25 [49]:

$$F_x = C_\sigma \sigma \quad (4.22)$$

Where the constant C_σ is called the *longitudinal stiffness* of the tire. Outside of the linear range, the absolute value of F_x decreases up to the value $|\sigma| = 1$.

The value of F_x generally depends on the value of F_z at the same level of longitudinal slip, as shown in **Figure 4.8**, and on the operating conditions. To mention a few, higher F_x are obtained on roads with higher friction coefficient; and a reduced maximum F_x are obtained with increasing speed V .

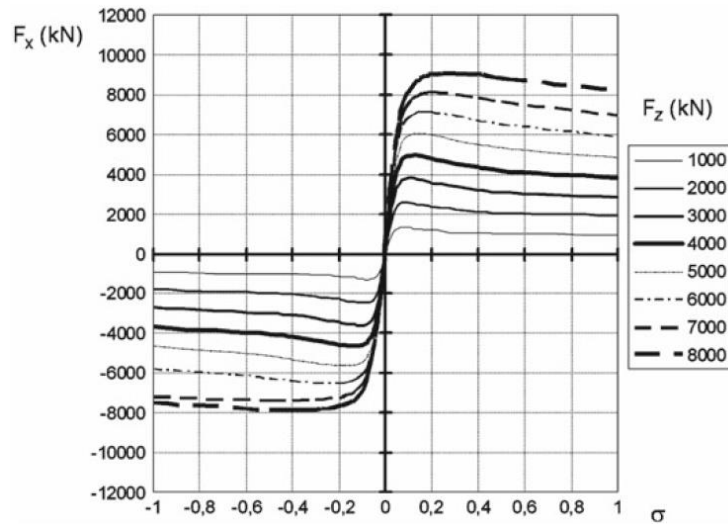


Figure 4.8 Curves $F_x(\sigma)$ for a 195/65 R 15 tire obtained for different values of vertical load F_z [49].

In a similar fashion due to the tire compliance, when the tire shows lateral deformation a **sideslip angle** α exists, which is the ratio between wheel lateral and longitudinal velocity as defined in the single-track model section. Following the results of the handling dynamic section it can also be expressed based on the knowledge of vehicle longitudinal and lateral velocity. Hence, for front and rear sideslip angles:

$$\begin{cases} \alpha_f = \tan^{-1} \left(\frac{v_y + l_f \dot{\psi}}{v_x} \right) - \delta \\ \alpha_r = \tan^{-1} \left(\frac{v_y - l_r \dot{\psi}}{v_x} \right) \end{cases} \quad (4.23)$$

The sideslip angle α leads to the generation of **lateral force** F_y whose value grows almost linearly at first as α increases:

$$F_y = C_\alpha \alpha \quad (4.24)$$

Where similarly the constant C_α is the *cornering stiffness* of the tire. Next, when the limit conditions of sliding are approached, F_y grows at a slower rate. Eventually it remains constant or decreases slightly when sliding conditions are reached [49].

Generally, the resultant lateral force is not applied at the center of tire-ground contact area but at a distance behind the center. This distance is defined as **pneumatic trail** t . Furthermore, an **aligning moment** M_z exists that tends to force the wheel midplane towards the direction of wheel velocity:

$$M_z = F_y t \quad (4.25)$$

Both the values of F_y and M_z again generally depends on the value of F_z at the same value of sideslip as shown in **Figure 4.9**, and on the operating conditions. They can reach high values on roads with high friction coefficient; and they tend to decrease as the speed V increases, especially in high sideslip angle ranges.

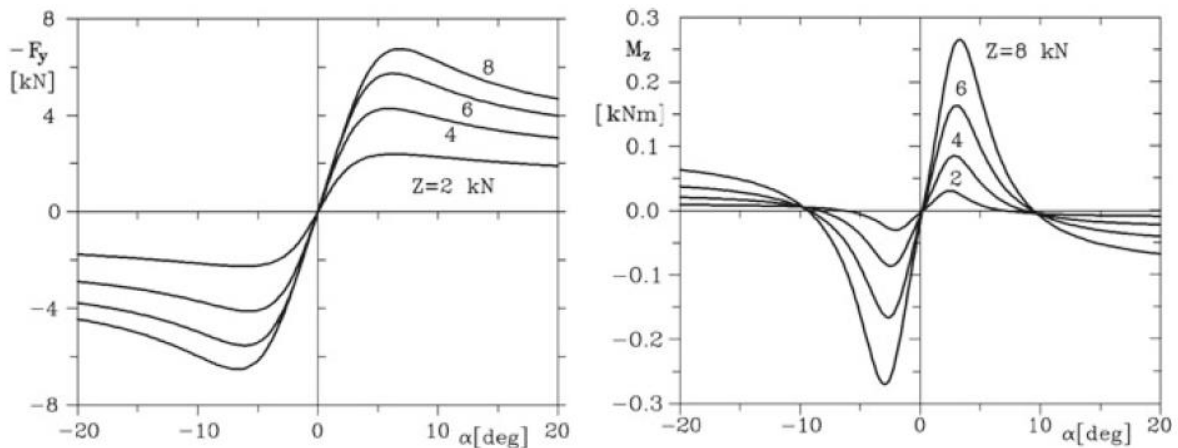


Figure 4.9 Curves $F_y(\alpha)$ and $M_z(\alpha)$ for a 205/60 R 15 V tire obtained for different values of vertical load F_z [49].

Additionally, a **camber angle** γ can also be present which has a very small contribution to lateral force, as shown in **Figure 4.10**. It usually coexists with sideslip angle. The lateral force generated by this angle shows a linear trend as camber angle increases and also depends on F_z .

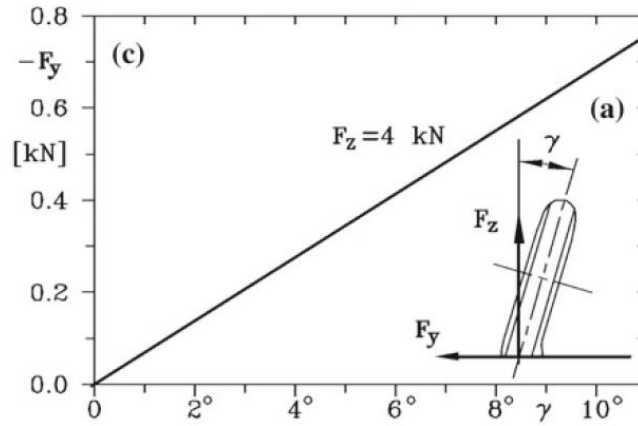


Figure 4.10 Scheme of camber force [49].

In vehicle actual working conditions, the tire is generally in **combined slip** condition. When a tractive or braking force is applied to a tire which has a certain sideslip angle, the lateral force reduces and the same applies to the longitudinal force a tire can exert if it is called to also exert a lateral force [49]. The phenomenon is represented by the *friction ellipse* (**Figure 4.11**) in which F_y are plotted against F_x for various constant tire sideslip angle α :

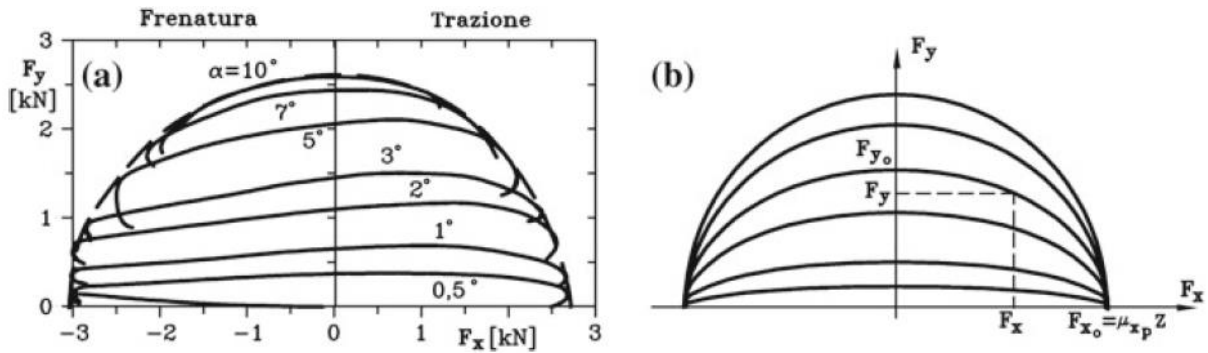


Figure 4.11 Interaction between F_x and F_y . (a) Experimental diagrams; (b) Elliptic approximation [49].

There are several mathematical tire models developed in literature with different degrees of accuracy that aim to accurately describe the tire longitudinal and lateral forces generation. The previous discussions of tire forces are based on physical tire models. A semi-empirical model named **Magic Formula** tire model was proposed by Pacejka to describe the steady-state tire force and moment characteristics. It is termed “semi-empirical” because it is based on experimental data but also contains structures that find their origin in physical models [50]. The general expression of the formula is defined as:

$$Y = D \sin[C \tan^{-1}\{B(X + S_H) - E(B(X + S_H) - \tan^{-1} B(X + S_H))\}] + S_V \quad (4.26)$$

Where Y is the output variable (F_x , F_y or M_z); X is the input variable ($\tan \alpha$ or σ); B is the stiffness factor; C is the shape factor; D is the peak value; E is the curvature factor; S_H is the horizontal shift; S_V is the vertical shift. The formula produces a curve represented in **Figure 4.12**.

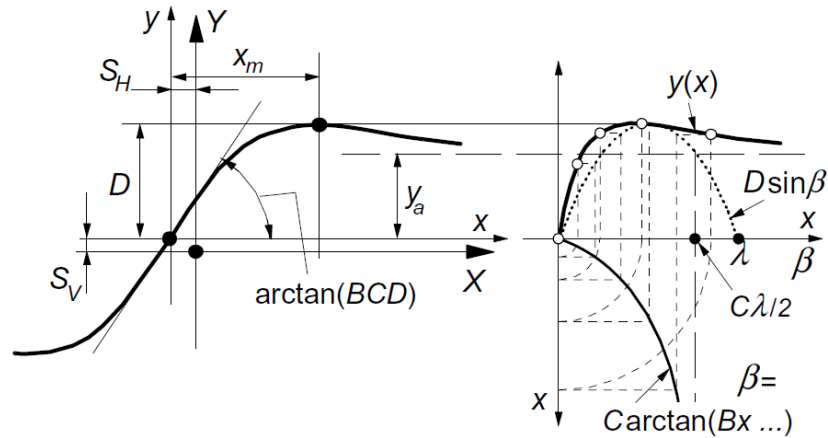


Figure 4.12 Curve produced by the original sine version of Magic Formula [50].

The formula is capable of generating characteristics that closely match the measure curves for F_x , F_y and M_z as function of their relevant slip quantities: longitudinal slip σ and sideslip angle α , considering the effect of F_z and camber angle γ [50]. Starting from the original version, some extensions were further introduced, such as the weighting functions with scaling factors that take into account the interaction between longitudinal and lateral forces in combined slip conditions.

4.4 Handling Diagrams

In order to pass from evaluating mathematical models to characterizing the measured performance of real vehicles, a variety of steady-state directional control tests have been developed by the Society of Automotive Engineers (SAE) and the International Organization for Standardization (ISO). Among all the tests there are two that are the most widely used: the constant radius – variable speed test and the constant speed – variable radius test. These are tests that are typically performed by major carmakers with a set of onboard instrumentations to measure the dedicated signals to be registered [43].

The obtained data are often reduced to response ratios represented by the characteristic angles over the corresponding lateral acceleration expressed in g , with units in deg/g . The most common ones are:

- **Understeer gradient**, from the knowledge of steering wheel angle δ_{sw}
- **Sideslip gradient**, from the knowledge of vehicle sideslip angle β
- **Roll gradient**, from the knowledge of vehicle roll angle φ

These values are usually measured as slopes of the response curves in the linear range of tire performance [43]. An example for obtaining the understeer gradient is shown in **Figure 4.13**. This test is carried out to let the vehicle reach high lateral accelerations, up till the maximum lateral capability where the tire shows nonlinear behaviors. The results are coherent with the mathematical expression of UG in the previous chapter describing lateral dynamics with single-track model.

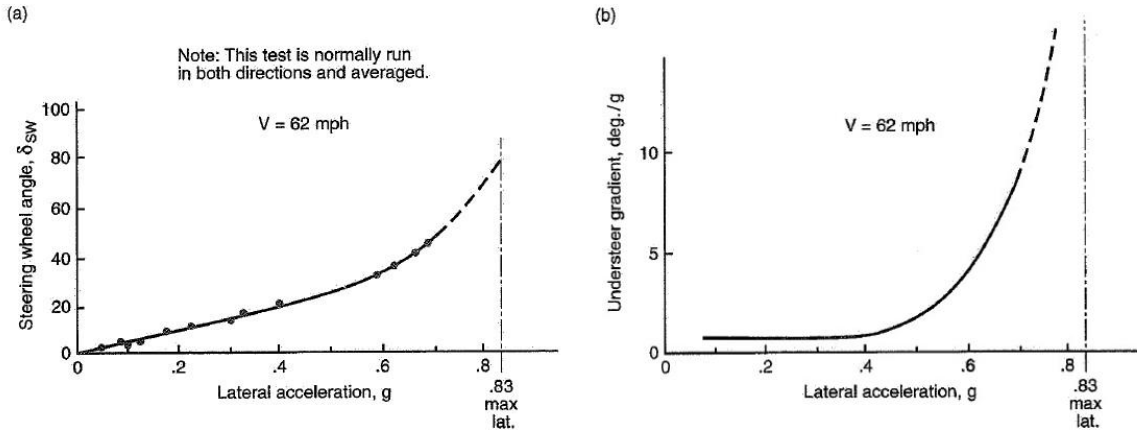


Figure 4.13 Example of steady-state understeer characteristics [43].

Vehicle sideslip angle in dynamic steering condition can be represented, starting from geometrical relationships, as:

$$\beta - \beta_k = -\alpha_r = -\frac{Ml_f}{LC_{\alpha r}} a_y \quad (4.27)$$

Where β_k is the kinematic sideslip angle. From the expression above, the sideslip gradient can be written as:

$$K_\beta = -\frac{Ml_f}{LC_{\alpha r}} \quad (4.28)$$

The sideslip gradient K_β describes how the vehicle's sideslip angle changes according to the lateral acceleration in cornering. In practice it can be obtained as the gradient of the curve in another handling diagram as shown in **Figure 4.14**, where sideslip angle β is plotted against lateral acceleration a_y .

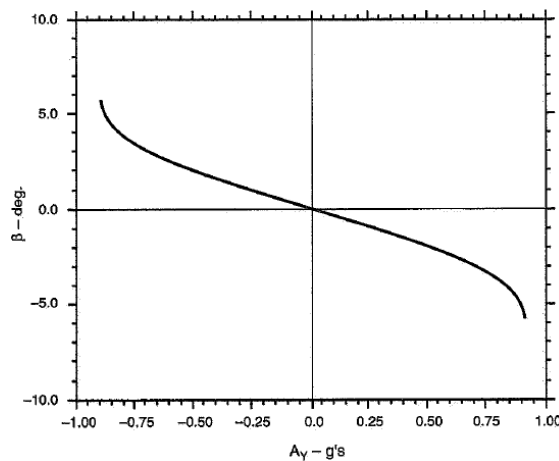


Figure 4.14 Example of steady-state vehicle sideslip angle characteristics [43].

The consideration of vehicle roll motion in the 14 DOF model allows to characterize another handling diagram. In a similar way, the vehicle's roll angle φ can be plotted against the lateral

acceleration a_y , as shown in **Figure 4.15**. The gradient of the curve represents the vehicle's roll gradient which in this case is roughly constant. Note that the vehicle's roll characteristics can be altered by an anti-roll bar that is capable of effectively changing the roll moment on vehicle body.

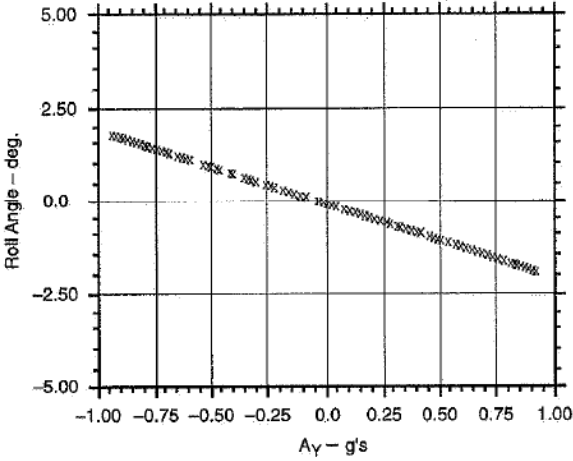


Figure 4.15 Example of steady-state vehicle roll angle characteristics [43].

5. RWS Control Design

After the RWS control literature review and the introduction of relevant vehicle dynamics concepts, in this chapter it is detailed the whole control design process in *MATLAB/Simulink* environment. Firstly, starting from the differential equations that governs the vehicle lateral dynamics, the creation of the vehicle model to be controlled is described. Next, with the goal of improving the vehicle's handling response in mind, a reference model representing the desired cornering dynamics are explained. It essentially generates desired vehicle yaw rate values representing an improved behavior at various speeds and steering inputs. By adopting various control theories, the controlled vehicle strives to follow the reference model minimizing the error between desired and actual yaw rate. Lastly, the proposed control schemes are implemented in *MATLAB/Simulink*.

The overall control scheme is represented in **Figure 5.1** from which three macro blocks are identified: **Vehicle Model with RWS**, **Reference Model**, and **RWS Controller**.

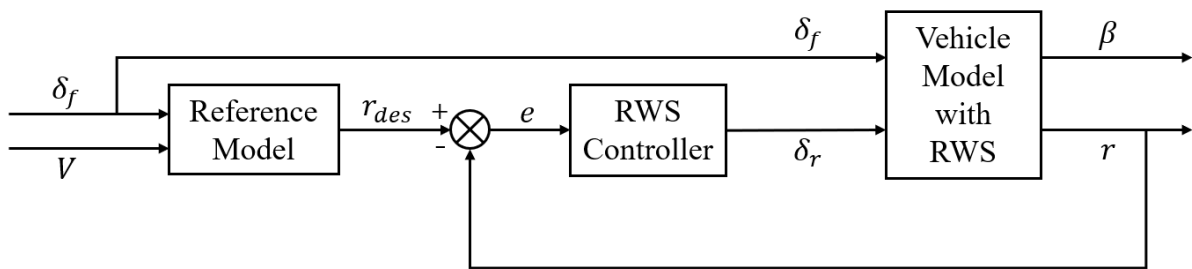


Figure 5.1 RWS overall control scheme.

In the **Vehicle Model with RWS**, a simplified vehicle model with the ability of RWS is constructed in *MATLAB/Simulink* that is capable of representing the essential lateral dynamic characteristics of a vehicle. In particular, two vehicle states important for characterizing a vehicle's lateral behavior are registered, that are the vehicle actual yaw rate r and sideslip angle β

In the **Reference Model**, the desired yaw rate r_{des} is generated based on the imposed front wheel steering angle δ_f and current vehicle forward velocity V . It represents a vehicle model with improved handling behavior that the controlled vehicle is intended to follow.

In the **RWS Controller**, an error e between the desired yaw rate r_{des} and actual yaw rate r is first calculated. Several control methods proposed in literature are adopted for its design with necessary simplifications, among them PI, LQI and MPC. The controller eliminates the error e by exerting the active RWS angle δ_r which then enters the vehicle model as a new model input and alters vehicle's cornering dynamics as desired.

5.1 Vehicle Plant Model Realization

In this section, the generic single-track model equations of motion with RWS capability are illustrated. They are the foundations for the creation of the simplified vehicle plant model used for RWS controller design and validation. All the assumptions considered in the chapter of lateral vehicle dynamics are valid here. The scheme of single-track model of a vehicle with RWS is depicted in **Figure 5.2**.

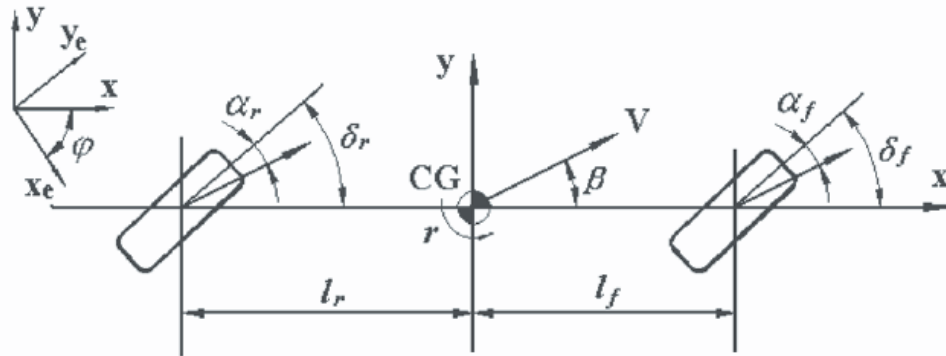


Figure 5.2 Single-track model of a vehicle with RWS [51].

Two reference frames can be identified from the figure:

- 1) Inertial reference frame (x_e, y_e, z_e) : it is fixed on the ground and serves as the reference frame for vehicle motions. Axis z_e is the normal vector of plane (x_e, y_e) and points upwards.
- 2) Vehicle reference frame (x, y, z) : its origin is fixed at vehicle's CG with z axis parallel to z_e and is adopted to describe vehicle motions. Specifically, it is rotated by an angle φ with respect to the inertial frame.

By applying Newton's Second Law, the equations of motion describing the 2 DOF of the model can be derived as follows, starting with lateral direction (all equations are adapted from [51]):

$$MV(\dot{\beta} + r) = F_{yf} \cos \delta_f + F_{yr} \cos \delta_r \quad (5.1)$$

And yaw direction:

$$I_z \dot{r} = l_f F_{yf} \cos \delta_f - l_r F_{yr} \cos \delta_r \quad (5.2)$$

In which M is vehicle mass; V is vehicle's forward velocity; β and r denote the sideslip angle and yaw rate at vehicle's CG; I_z is the vehicle's yaw moment of inertia about its z axis; l_f and l_r are the distances of vehicle's CG between front and rear axles respectively; δ_f and δ_r are front and rear wheels' steering angles; F_{yf} and F_{yr} are the lateral force developed by front and rear axles respectively, with directions perpendicular to wheel's center plane.

Considering small tire sideslip angles α_f and α_r , the linear relationship of tire lateral force and slip angle can be taken. Thus, the expressions of lateral forces are:

$$\begin{cases} F_{yf} = C_f \alpha_f \\ F_{yr} = C_r \alpha_r \end{cases} \quad (5.3)$$

Where C_f and C_r are front and rear equivalent axle cornering stiffness.

Observing **Figure 5.2** and by considering small vehicle sideslip angle β , the expressions of α_f and α_r are obtained:

$$\begin{cases} \alpha_f = \delta_f - \beta - \frac{l_f}{V} r \\ \alpha_r = \delta_r - \beta + \frac{l_r}{V} r \end{cases} \quad (5.4)$$

Further simplifications are made by considering wheel's steering angles δ_f and δ_r small, that leads to:

$$\begin{cases} \cos \delta_f \cong 1 \\ \cos \delta_r \cong 1 \end{cases} \quad (5.5)$$

Finally, the equations of motion are expressed as:

$$MV(\dot{\beta} + r) = -(C_f + C_r)\beta - \frac{(l_f C_f - l_r C_r)}{V} r + C_f \delta_f + C_r \delta_r \quad (5.6)$$

$$I_z \dot{r} = -(l_f C_f - l_r C_r)\beta - \frac{(l_f^2 C_f + l_r^2 C_r)}{V} r + l_f C_f \delta_f - l_r C_r \delta_r \quad (5.7)$$

The model can also be conveniently represented in the following state-space form:

$$\begin{cases} \dot{x} = Ax + Bu \\ y = Cx + Du \end{cases} \quad (5.8)$$

In which the state vector $x = [\beta \ r]^T$, input vector $u = [\delta_f \ \delta_r]^T$, output vector $y = [\beta \ r]^T$ and the coefficient matrices A, B, C, D are:

$$A = \begin{bmatrix} -\frac{(C_f + C_r)}{MV} & -\frac{(l_f C_f - l_r C_r)}{MV^2} - 1 \\ -\frac{(l_f C_f - l_r C_r)}{I_z} & -\frac{(l_f^2 C_f + l_r^2 C_r)}{I_z V} \end{bmatrix}, B = \begin{bmatrix} \frac{C_f}{MV} & \frac{C_r}{MV} \\ \frac{C_f}{I_z} & -\frac{C_r}{I_z} \end{bmatrix}, C = \begin{bmatrix} 1 & 0 \\ 0 & 1 \end{bmatrix}, D = 0$$

In **Table 1** it is summarized the parameters of the vehicle relevant for the model creation. These parameters represent a virtual vehicle based on the company's know-how. In order to take into account the nonlinear behavior of tire's lateral force generation as the lateral acceleration a_y grows towards its maximum value, the real simulation data of C_f and C_r (**Table 2**) obtained from a complete vehicle model having the same parameters as the simplified model are imported. These values decrease as a_y increases till the maximum value. They are stored in dedicated lookup tables in *Simulink* from which the instantaneous C_f and C_r values are approximated based on the imposed breakpoint values of a_y . As a result, their values are updated at run time through the lookup table, which depend on the instantaneous a_y value. The trends of C_f and C_r values against a_y are shown in **Figure 5.3**.

Table 1 Vehicle model parameters

Parameter	Value
Mass M	1850 <i>kg</i>
Wheelbase L	2600 <i>mm</i>
CG height h	490 <i>mm</i>
Weight distribution % front	48 %
Distance front axle to CG l_f	1352 <i>mm</i>
Distance rear axle to CG l_r	1248 <i>mm</i>
Roll moment of inertia I_x	700 <i>kgm</i> ²
Pitch moment of inertia I_y	2600 <i>kgm</i> ²
Yaw moment of inertia I_z	2900 <i>kgm</i> ²
Front axle cornering stiffness C_f	From lookup table
Rear axle cornering stiffness C_r	From lookup table

Table 2 Data of C_f and C_r

a_y [<i>g</i>]	C_f [<i>N/deg</i>]	C_r [<i>N/deg</i>]
0.1	2854.5	6512.9
0.2	2829.2	6377.6
0.3	2779.5	6149.6
0.4	2694.6	5827.3
0.5	2561.7	5408.3
0.6	2366.0	4888.4
0.7	2091.3	4261.3
0.8	1718.9	3515.4
0.9	1221.8	2627.6
1	531.3	1532.3

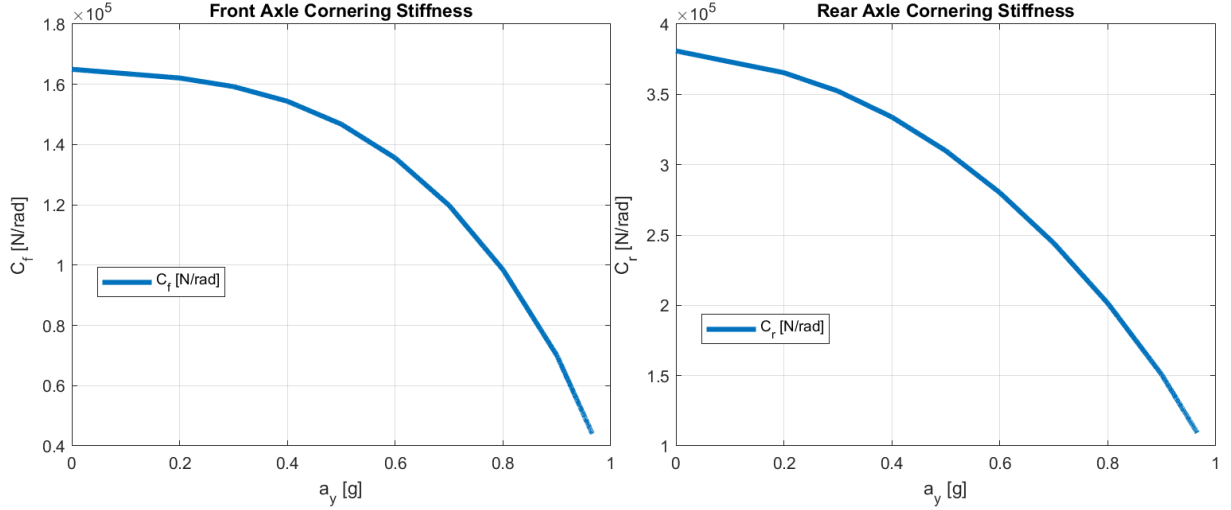


Figure 5.3 $C_f - a_y$ and $C_r - a_y$ relationships.

5.2 Reference Model Realization

To compute the desired yaw rate value r_{des} , a single-track nonlinear static model is utilized by considering nonlinear axle slip – lateral force relationship. This nonlinear relationship can be well represented by the *Magic Formula* of Pacejka previously mentioned.

For every constant speed value V considered in the speed range, it is possible to obtain the analytical expression of the relationship between steady-state lateral acceleration a_y and different values of handwheel angle δ_{sw} through standard steering pad maneuvers, which leads to the handling diagram of steady-state understeer characteristics introduced before (**Figure 4.13**). If this relationship is plotted as a curve, a dual-track characteristic can be noticed: for small a_y values, δ_{sw} grows linearly with increasing a_y establishing the linear tract; while for relatively large a_y values, the relationship between the two values becomes nonlinear establishing the nonlinear tract.

Considering the front wheel steering angle $\delta_f = \delta_{sw}/\tau$ where τ is vehicle's steering ratio, the relationship between δ_f and a_y in the linear tract is (all equations are adapted from [34]):

$$\delta_f = \left(\frac{L}{V^2} + K_{US} \right) a_y \quad (5.10)$$

For the reference model, K_{US} is appropriately changed to modify the vehicle's understeering behavior. In particular, a look-up table is introduced which takes as input every constant speed value V in the speed range considered. Its output is the desired understeer gradient $K_{US,des}$ that varies linearly with V . Specifically, its value should be that $K_{US,des} < K_{US}$ for low-speed range and $K_{US,des} > K_{US}$ for high-speed range. This is decided to make the vehicle more understeering in high-speed (high a_y) maneuvers improving stability while making it less understeering in low-speed (low a_y) maneuvers improving maneuverability. As a result, the desired relationship in the linear tract is:

$$\delta_f = \left(\frac{L}{V^2} + K_{US,des} \right) a_{y,des} \quad \text{for } 0 \leq a_{y,des} \leq a_{y,l} \quad (5.11)$$

Where $a_{y,l}$ is a design parameter, that is the lateral acceleration value representing the upper bound of the linear tract. The desired relationship in the nonlinear tract is:

$$\delta_f = \delta_l - \left(\frac{L}{V^2} + K_{US,des} \right) (\bar{a}_y - a_{y,l}) \ln \left(\frac{\bar{a}_y - a_{y,des}}{\bar{a}_y - a_{y,l}} \right) \quad \text{for } a_{y,l} < a_{y,des} < \bar{a}_y \quad (5.12)$$

Where δ_l is the steering wheel angle corresponding to $a_{y,l}$ at each speed V ; \bar{a}_y is another design parameter which is the vehicle's maximum lateral acceleration. By using the logarithmic relationship, a smooth connection between the linear tract of the curve and the chosen maximum acceleration value \bar{a}_y is realized. It effectively avoids the driver to suddenly feel that the vehicle has reached its cornering limit [34].

Moreover, steady-state condition for the reference generation leads to a direct relationship between yaw rate r and lateral acceleration a_y through constant vehicle speed V :

$$r = \frac{a_y}{V} \quad (5.13)$$

Finally, the complete expressions of desired yaw rate r_{des} as a function of δ_f and V , depending on the design parameters are derived as:

- Linear tract:

$$r_{des} = \frac{V}{L + K_{US,des} V^2} \delta_f \quad \text{for } 0 \leq V r_{des} \leq a_{y,l} \quad (5.14)$$

- Nonlinear tract:

$$r_{des} = \frac{1}{V} \left(\bar{a}_y - e^{\ln(\bar{a}_y - a_{y,l}) + \frac{\delta_l - \delta_f}{\bar{a}_y - a_{y,l}} \frac{L}{V^2 + K_{US,des}}} \right) \quad \text{for } a_{y,l} < V r_{des} < \bar{a}_y \quad (5.15)$$

The values of the design parameters $K_{US,des}$, $a_{y,l}$, \bar{a}_y and τ are chosen as shown in **Table 3**. Here it is supposed that the controller's range of operation is from zero speed to $V = 150 \text{ km/h}$. Subsequently, $K_{US,des}$ varies linearly with V , decreasing or increasing its value with respect to the passive value K_{US} as it is the algorithm of the look-up table adopted. The road is considered to be in nominal condition with friction coefficient $\mu = 1$. For the upper bound of lateral acceleration in the linear range $a_{y,l}$, it is chosen the value $a_{y,l} = 0.4 \mu g$ which is roughly the transition point from linear tire behavior to nonlinear one for most vehicles. For the vehicle's maximum lateral acceleration \bar{a}_y , it represents a physical upper bond for the considered vehicle model, which essentially approximates the maximum lateral acceleration the vehicle can reach.

Table 3 Design parameters of the reference model

Parameter	Value
Desired understeer gradient $K_{US,des}$	$0K_{US} \leq K_{US,des}(V) \leq 2K_{US}$
Road friction coefficient μ	1
Maximum lateral acceleration in linear range $a_{y,l}$	0.4 g
Maximum lateral acceleration \bar{a}_y	1 g
Steering ratio τ	15

The figure that describes the resulting elastic $K_{US,des}$ values which vary with longitudinal velocity V is shown in **Figure 5.4**. In **Figure 5.5** the results of desired and passive vehicle yaw rates r for multiple velocities during a ramp steer maneuver (with steering wheel angle rate $\dot{\delta}_{sw} = 5 \text{ deg/s}$; the steering angle grows from θ till 200 deg at different velocities) is shown. In **Figure 5.6** the desired and passive vehicle steering wheel angles δ_{sw} required to execute the ramp steer maneuver are plotted against various lateral acceleration values $a_{y,des}$ for multiple velocities.

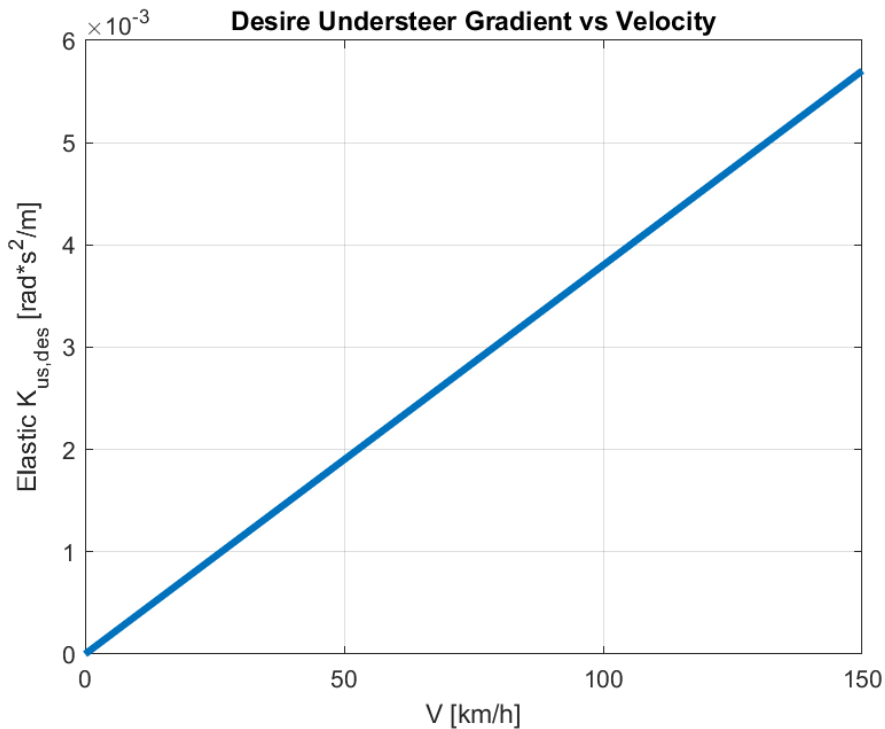


Figure 5.4 Elastic $K_{US,des} - V$.

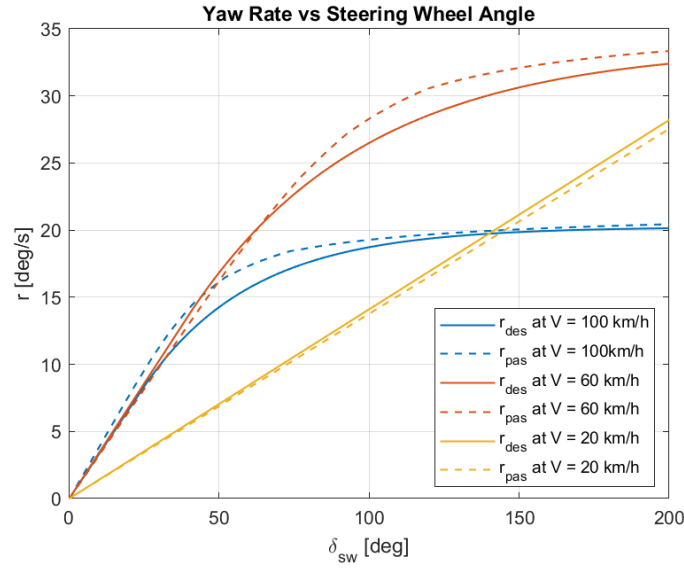


Figure 5.5 $r_{des} - \delta_{sw}$ for different V during ramp steer maneuver.

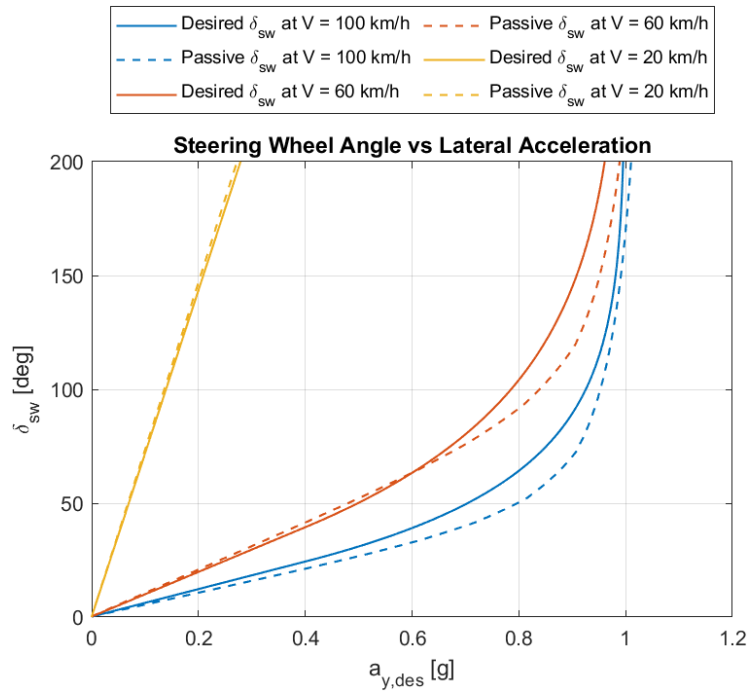


Figure 5.6 $\delta_{sw} - a_{y,des}$ for different V during ramp steer maneuver.

From the figures it can be evidenced how the desired model response differs from the passive vehicle response. In particular, the response in the linear range can be altered as desired by setting the parameters of **Table 3**; while in the nonlinear range the reference model tries to always impose a more understeering behavior for the vehicle. This is advantageous in a safety point of view since the nonlinear tract corresponds to high a_y values. Moreover, it is possible to evidence the nonlinear behavior at high a_y values when the tires enter nonlinear operating region. Furthermore, the dependence of r_{des} on V is noticed: at the beginning, the slope of r_{des}

increases with increasing V , but after entering the nonlinear range, its maximum value decreases with increasing V .

5.3 RWS Controller Design

As anticipated at the beginning of the chapter, the RWS controller produces a RWS angle output δ_r by processing the difference between desired yaw rate r_{des} and actual yaw rate r , which equals the error e :

$$e = |r_{des}| - |r| \quad (5.17)$$

From the value of resulting error, two scenarios are identified:

- $e > 0$: the desired yaw rate response represents a less understeering vehicle. To follow the reference model, the controller output RWS angle δ_r has opposite sense with δ_f , subsequently making the vehicle less understeering, improving maneuverability.
- $e < 0$: the desired yaw rate response represents a more understeering vehicle. To follow the reference model, the controller output RWS angle δ_r has the same sense with δ_f , subsequently making the vehicle more understeering, improving stability.

Following the idea of exploring various controller realization methods, three controllers based on different control theories are created, namely PI, LQI and MPC controllers. The relevant theories behind each controller are detailed in the following sections.

5.3.1 PI Controller

The Proportional-Integral (PI) controller is a simplified form of Proportional-Integral-Derivative (PID) controller, which is a widely used closed-loop compensation technique for SISO systems. It is a very popular feedback compensation method in the industrial process control field due to their robust (insensitive) performance over a wide range of operating conditions including plant uncertainty, parameter variation, and external disturbances [52]. Depending on the performance requirements, different simplified versions can be adopted by removing some terms, such as P and PI controllers.

The basic representation of PI controller equation in time domain is [52]:

$$u(t) = K_p \cdot e(t) + K_I \int_0^t e(\tau) d\tau \quad (5.18)$$

Where $u(t)$ is the controller output; K_p and K_I are the proportional and integral gains. They intervene and modify the system's closed-loop response in different fashions, namely:

- Proportional gain K_p : it multiplies the error e and produces a control output proportional to the error. Although it can effectively reduce the error, zero steady-state error between the state and its reference value usually cannot be guaranteed with this gain alone.

- Integral gain K_I : it multiplies the integral of the error e , which represents the accumulation of past error values. Based on the information of the past, this gain eventually stabilizes the system and also eliminates any steady-state error.

The controller is also conveniently represented in frequency domain by using the corresponding *Laplace Transform* of the constituting terms, leading to the transfer function expression:

$$U(s) = \left(K_P + \frac{K_I}{s} \right) E(s) \quad (5.19)$$

With s the *Laplace operator*. **Figure 5.7** shows the general structure of a PI control loop.

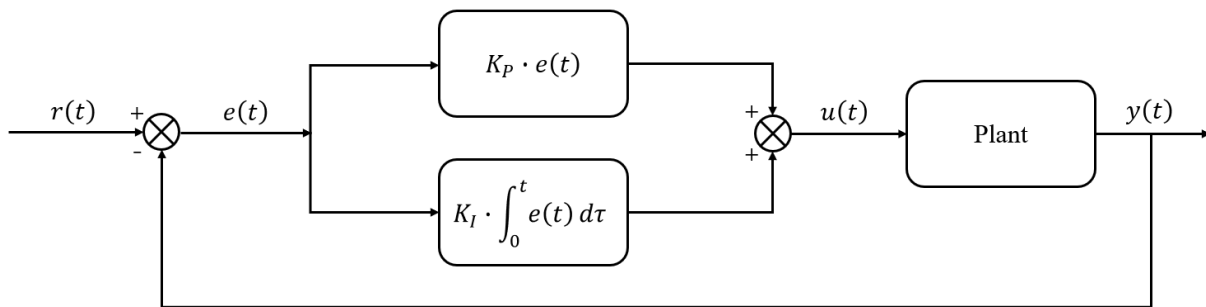


Figure 5.7 General structure of PI control

5.3.2 LQI Controller

The Linear Quadratic Integral (LQI) controller is based on the Linear Quadratic Regulator (LQR) formulation, which is one of the popular optimal control techniques. Comparing to the PI controller, LQR controller involves a lot of mathematical computations to calculate the full state feedback matrix that stabilizes the controlled system [53]. The LQI controller is an extended version of LQR that includes an augmented state in full state feedback represented by the integral of output tracking error e . In the computation process it aims at minimizing a cost function defined by systems equations, thus arriving at an optimized solution. The weights on the states and control input can also be adjusted by changing the coefficients in the relevant matrices in order to vary the value of cost function, according to the desired system response.

Figure 5.8 shows the general structure of LQI control loop.

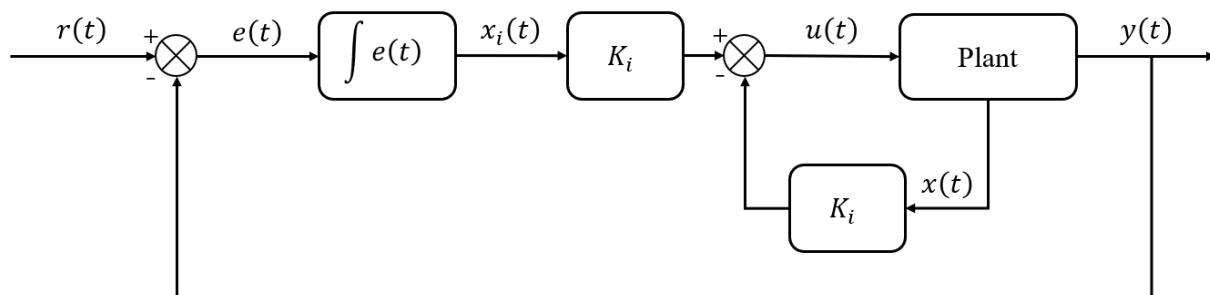


Figure 5.8 General structure of LQI control.

For the vehicle model with RWS, the original system representation in state-space introduced before needs to be modified so that the system control input u is made up of rear steering angle δ_r only, while front steering angle δ_f is considered as a disturbance. Thus, based on the equation of (5.8), the state-space formulation is modified accordingly by splitting the original matrix B :

$$\begin{cases} \dot{x} = Ax + B_r u + B_f w \\ y = Cx \end{cases} \quad (5.20)$$

Where $u = [\delta_r]$; $w = [\delta_f]$; B_r and B_f are the second and first column of matrix B respectively; the states x and the coefficients A, C are the same as before. The additional feedback state is essentially the integral of the tracking error e :

$$x_e = \int e = \int (|r_{des}| - |r|) \quad (5.21)$$

Thus, the state equation is said to be augmented which results as:

$$\dot{x}_a = A_a x + B_{ra} u + B_{fa} w \quad (5.22)$$

In which $x_a = [x; x_e]$ and the coefficient matrices $A_{a(3 \times 3)}, B_{ra(3 \times 1)}, B_{fa(3 \times 1)}$ are:

$$A_a = \begin{bmatrix} A & \text{zeros}(2,1) \\ C(:,2)^T & 0 \end{bmatrix}, B_{ra} = \begin{bmatrix} B_r \\ 0 \end{bmatrix}, B_{fa} = \begin{bmatrix} B_f \\ 0 \end{bmatrix}$$

Note that the term $C(:,2)^T$ in A_a means that only the part related to yaw rate is fed back to compute the integral of its tracking error since the reference model contains only yaw rate.

Then the LQI control problem is generalized as: minimizing the cost function J subject to equation (5.22) by selecting the appropriate Q and R matrices that lead to the feedback gain matrix K . The controller's governing equations are adapted from [54], with modifications made on original subscripts in order to make them coherent with the naming conventions introduced for the RWS vehicle plant in state-space. The cost function J is written as:

$$J = \int_0^{\infty} (x_a^T Q x_a + u^T R u) dt \quad (5.23)$$

Where Q and R are diagonal matrix and a scalar representing the weights assigned to the state parameters and control input parameters respectively. By varying their values, the total value of the cost function can be adjusted according to the desired output [53]. The LQI optimal controller is given by:

$$u = -K x_a = -[K_0 \quad K_e] \begin{bmatrix} x \\ x_e \end{bmatrix} \quad (5.24)$$

Where K_0 are the gains on states x and K_e is the gain on the augmented state x_e . K is given by:

$$K = R^{-1} B_{ra}^T P \quad (5.25)$$

In equation (5.25), P is obtained by solving the following *Algebraic Riccati Equation (ARE)*:

$$A_a^T P + P A_a + Q - P B_{ra} R^{-1} B_{ra}^T P = 0 \quad (5.26)$$

5.3.3 MPC Controller

The Model Predictive Controller (MPC) can be viewed as an advanced version of LQR controller in that although they are both based on optimization principles, MPC presents the concept of prediction and control horizon while in LQR these horizons are considered infinite. MPC comprises the use of an explicit model of the system to predict future trajectory of system states and outputs. From the results of prediction, an optimal control problem can be solved online which effectively minimizes the prediction error and control action over the control horizon, that is the number of sample steps useful for control in the future. The optimal control problem is possibly subject to constraints and weights on inputs, output, and states. From the computed optimal control sequence, it is taken only the first input as the input for the system. Then at the next sample step, the horizon is shifted forward and the whole optimization procedure is repeated. This action is also called Receding Horizon Control (RHC) and it allows to compensate for future disturbance and modeling error [55].

For the RWS control problem, an explicit discrete state-space model is first provided for the MPC controller by modifying equation (5.20) adopted for the LQI control, which serves as the prediction model to predict the system's future output:

$$\begin{cases} x(k+1) = Ax(k) + B_r u(k) + B_f w(k) \\ y(k) = C_r x(k) \end{cases} \quad (5.27)$$

Where k represents the present sampling instant. In this prediction model, the output matrix is modified from C to $C_r = [0 \ 1]$, meaning that it is considered only the second row of matrix C . This is because only the yaw rate output is necessary to be included in the prediction model to realize desired yaw rate tracking with the reference yaw rate model introduced before. The other parameters are the same as used previously in LQI control.

The iterative logic of the RHC (**Figure 5.9**) can be generalized as follows [56]:

1. The current state x is obtained based on the information at sampling instant k .
2. At the current sampling instant k , the MPC strategy calculates a set of M values of the input: $u(k+i-1), i = 1, 2, \dots, M$, consisting of the current input $u(k)$ and $M-1$ future inputs. They are calculated so that a set of P predicted outputs: $\hat{y}(k+i), i = 1, 2, \dots, P$ reaches the set point in an optimal manner.
3. From the above sequence of inputs, only the first element is actually implemented as control action at present sampling instant k .
4. The present sampling instant k moves one step forward reaching the next sampling instant $k+1$, and the same actions repeats from the beginning.

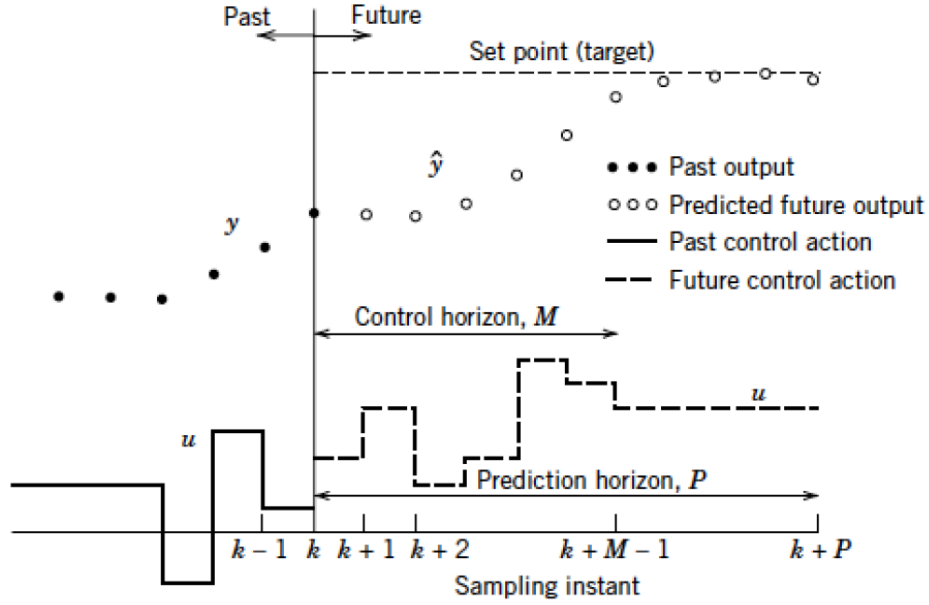


Figure 5.9 RHC logic for MPC [56].

The calculation of the inputs u is based on the formulation of an optimization problem in which the following quadratic cost function J is minimized for each sampling instant k (adapted from [57]):

$$\begin{aligned} \min_u J &= \sum_{j=1}^P \|\hat{y}(k+j|k) - y_{ref}(k+j|k)\| Q + \sum_{j=0}^{M-1} \|u(k+j|k)\| R \\ \text{s.t. } x(k+j+1|k) &= Ax(k+j|k) + B_r u(k+j|k) + B_f w(k+j|k) \\ x(k|k) &= x(k) \\ y(k+j|k) &= C_r x(k+j|k) \\ |u(k+j|k)| &\leq u_{lim} \end{aligned} \quad (5.28)$$

Where Q and R are weights on output prediction error and control energy; $\hat{y}(k+j|k)$ is output's prediction at time step k ; $y_{ref}(k+j|k)$ is the reference value at time step k , which in this case is equal to r_{des} at every time instant k ; $u(k+j|k)$ is the control action at time step k ; P and M are prediction and control horizons respectively. Note that M is generally smaller than P in order to reduce the overall computation time of the solver, i.e., a shorter sequence of inputs is taken into account by the MPC.

The general structure of MPC control loop is presented in **Figure 5.10**.

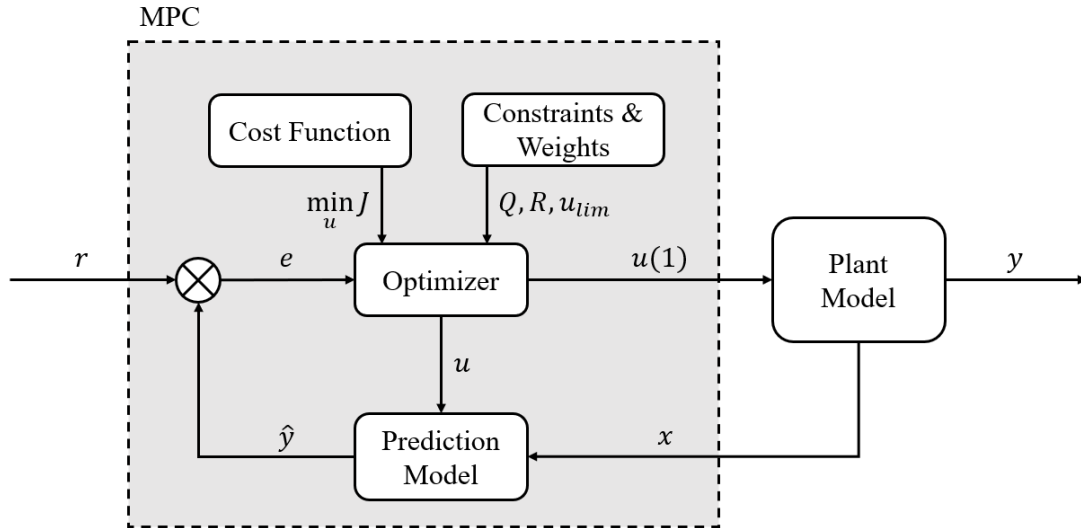


Figure 5.10 General structure of MPC control.

5.4 Control Implementation in MATLAB/Simulink

The vehicle model, yaw rate reference model and various control models with different controller schemes introduced previously are then implemented in *MATLAB/Simulink* to simulate the RWS control loop. First, the overall control scheme is shown in **Figure 5.11**. Then, the functioning of each constituent block is explained in the following subsections.

5.4.1 Vehicle Plant Model

The realization of vehicle plant model in *Simulink* is shown in **Figure 5.12**. It is created based on the single-track model equations with the relevant parameters in **Table 1** that represent the hypothetical vehicle with RWS capability. The model takes the front and rear wheels steering angle δ_f , δ_r and vehicle longitudinal velocity V as inputs, with δ_r the eventual RWS angle decided by one of the RWS controller blocks. It is maintained at $\delta_r = 0$ in the passive vehicle. Several vehicle states such as β , r and a_y are chosen as model outputs. In particular, the actual yaw rate r will be fed back to the input of controller block to complete the feedback action.

The internal details of the vehicle plant model is shown in **Figure 5.13**. In particular, the runtime lateral acceleration values are extracted and feed as inputs to the 1-D lookup table, which consists of the C_f and C_r values from **Figure 5.3** and **Table 2**. These values are then updated at runtime and are provided to the equations of motion, realizing a vehicle model with nonlinear tire lateral force characteristics known *a priori*.

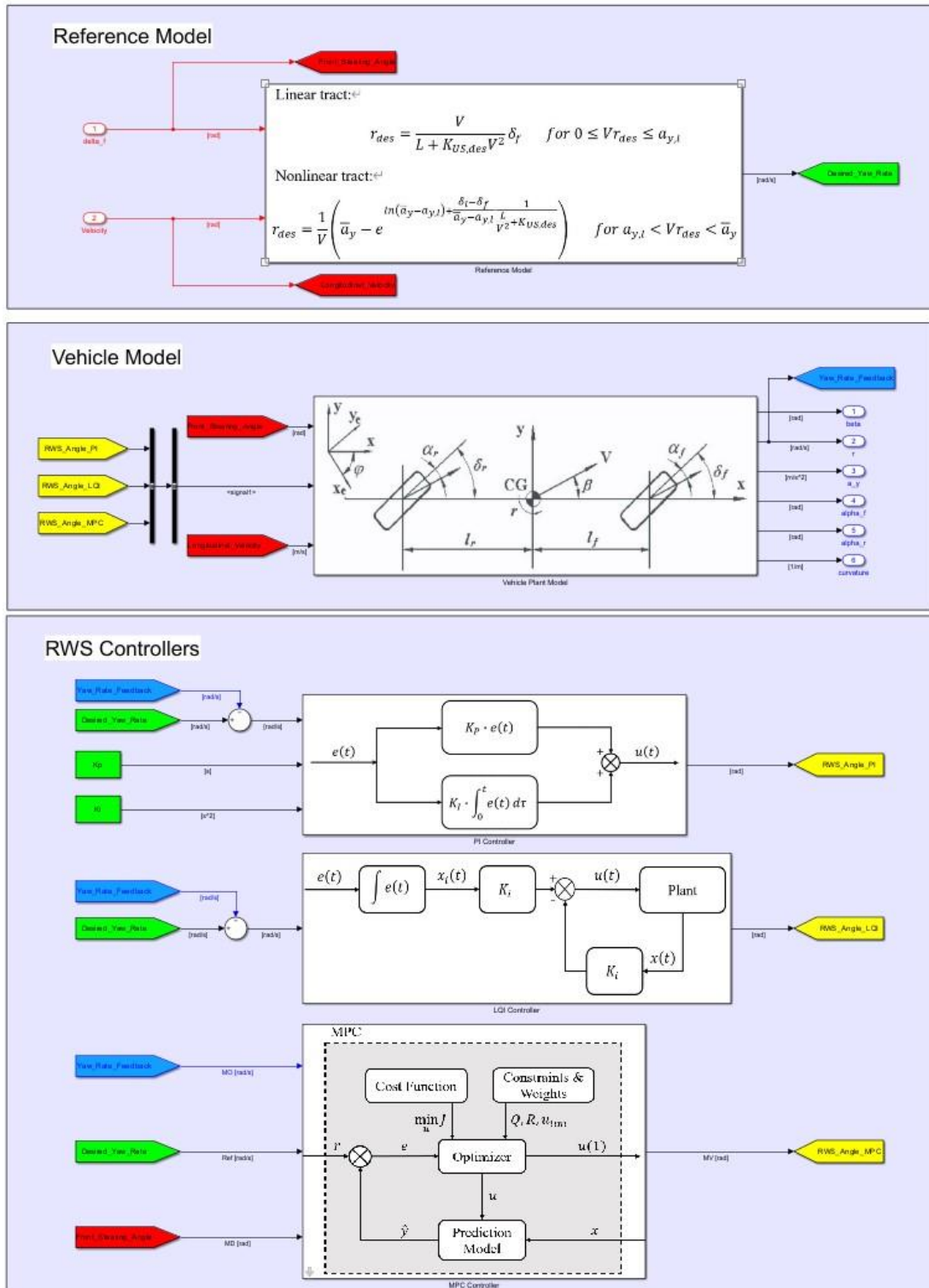


Figure 5.11 RWS control implementation in *Simulink*.

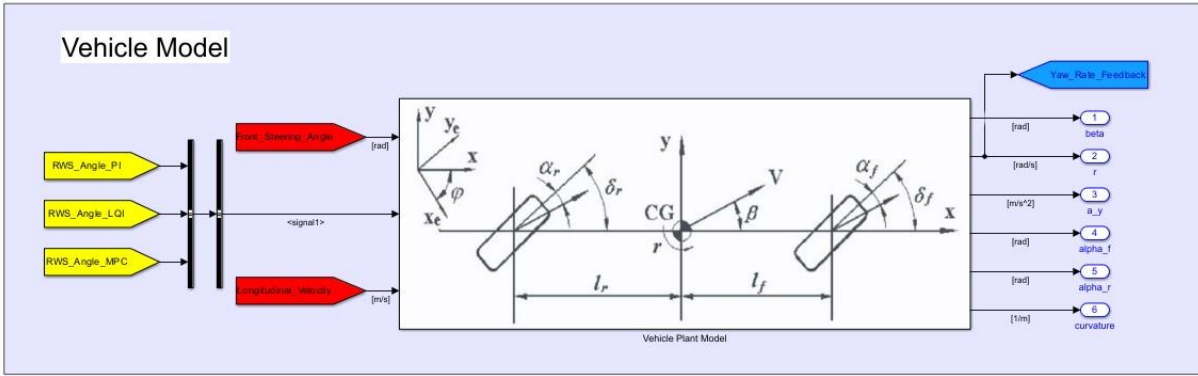


Figure 5.12 Vehicle plant model in *Simulink*.

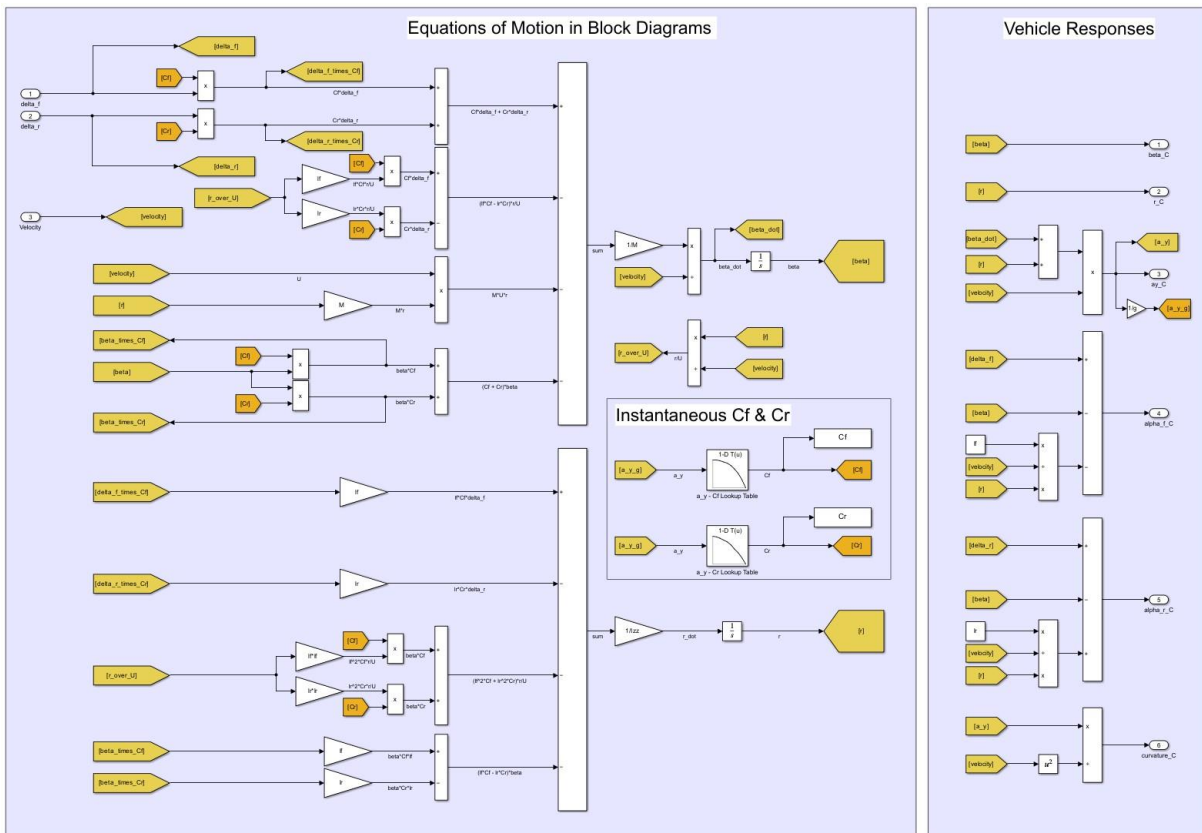


Figure 5.13 Details of vehicle plant model.

5.4.2 Reference Model

The realization of the reference model in *Simulink* is shown in **Figure 5.14**. As is in the vehicle model, this model also takes the front wheel steering angle δ_f and longitudinal velocity V as inputs, since essentially this model could be viewed as a static vehicle model with improved cornering performance. Based on the dual-track equations introduced in **Section 5.2**, the corresponding desired yaw rate r_{des} is obtained. Moreover, a first-order delay transfer function having an appropriate time constant is included in the model after the equations of desired yaw rate r_{des} to get appropriate signals suitable for differentiation and integration.

The internal details of the reference model is shown in **Figure 5.15**. It consists of a “switch” logic which decides when to change from adopting the linear tract equations and the nonlinear ones based on the threshold lateral acceleration dictating linear-nonlinear transition.

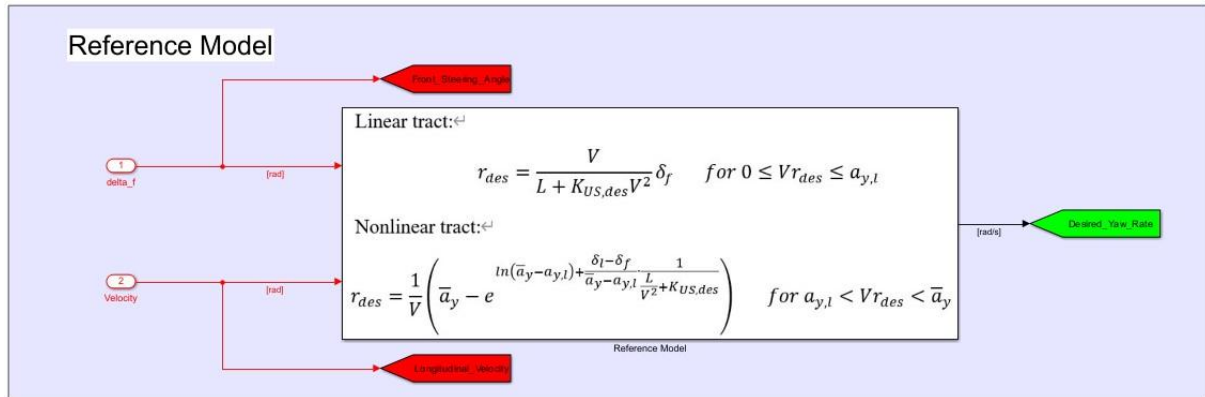


Figure 5.14 Reference model in *Simulink*.

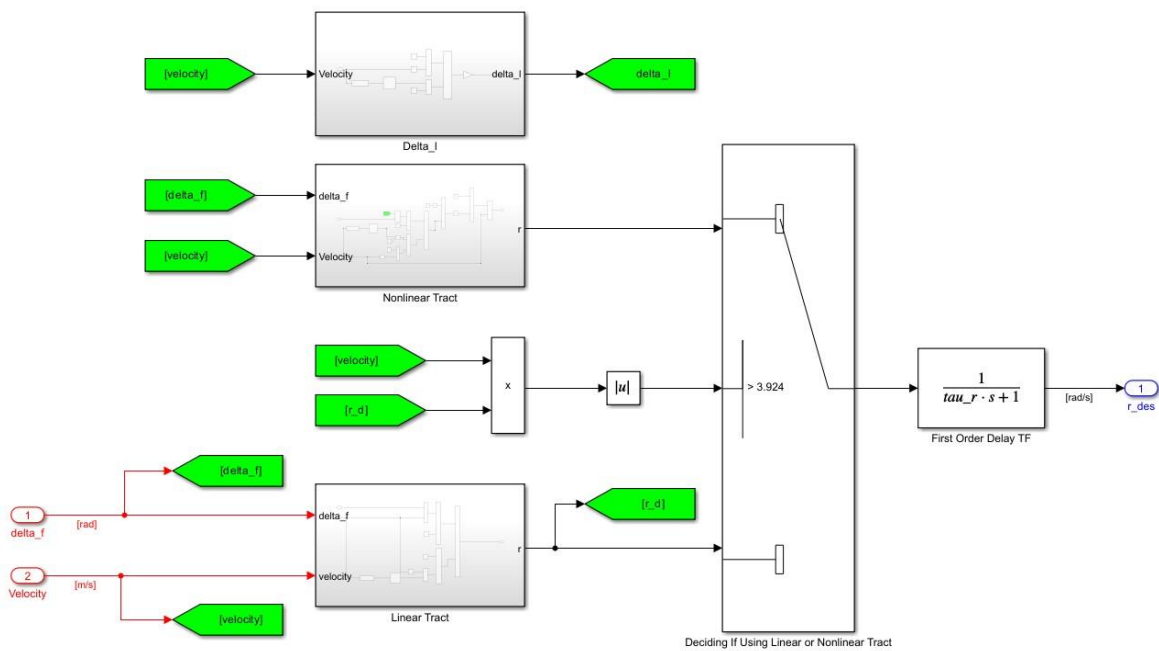


Figure 5.15 Details of reference model.

As anticipated before, $K_{US,des}$ is conveniently implemented in *Simulink* using a 1-D lookup table: for each velocity V in the considered range, a value of $K_{US,des}$ is obtained in between its considered range. The linear relationship between V and $K_{US,des}$ leads to an offline map that correctly reflects the design choices.

5.4.3 RWS Controllers

The various controller models in Simulink are shown in **Figure 5.16**. Several inputs are in common for all three models, namely: the desired yaw rate r_{des} coming from the reference model and the actual yaw rate feedback r exiting the vehicle model block. Each controller model produces a RWS angle output δ_f according to their relevant theories.

Apart from the common ones, in the PI controller the coefficients K_P and K_I are passed as additional inputs, while in the MPC controller the front wheel steering angle δ_f enters as another input. Note that the MPC controller block is taken from *Model Predictive Control Toolbox* in *MATLAB/Simulink* and is realized as a linear MPC controller. Specifically, according to the signal naming conventions, r is the Manipulated Output (MO); r_{des} is the model output Reference value (Ref); δ_f is considered the Measured Disturbance (MD) and δ_r is the Manipulated Variable (MV), i.e., the control action that is sent to vehicle model.

Figure 5.17 and **Figure 5.18** reports the internal details of PI and LQI controller explored.

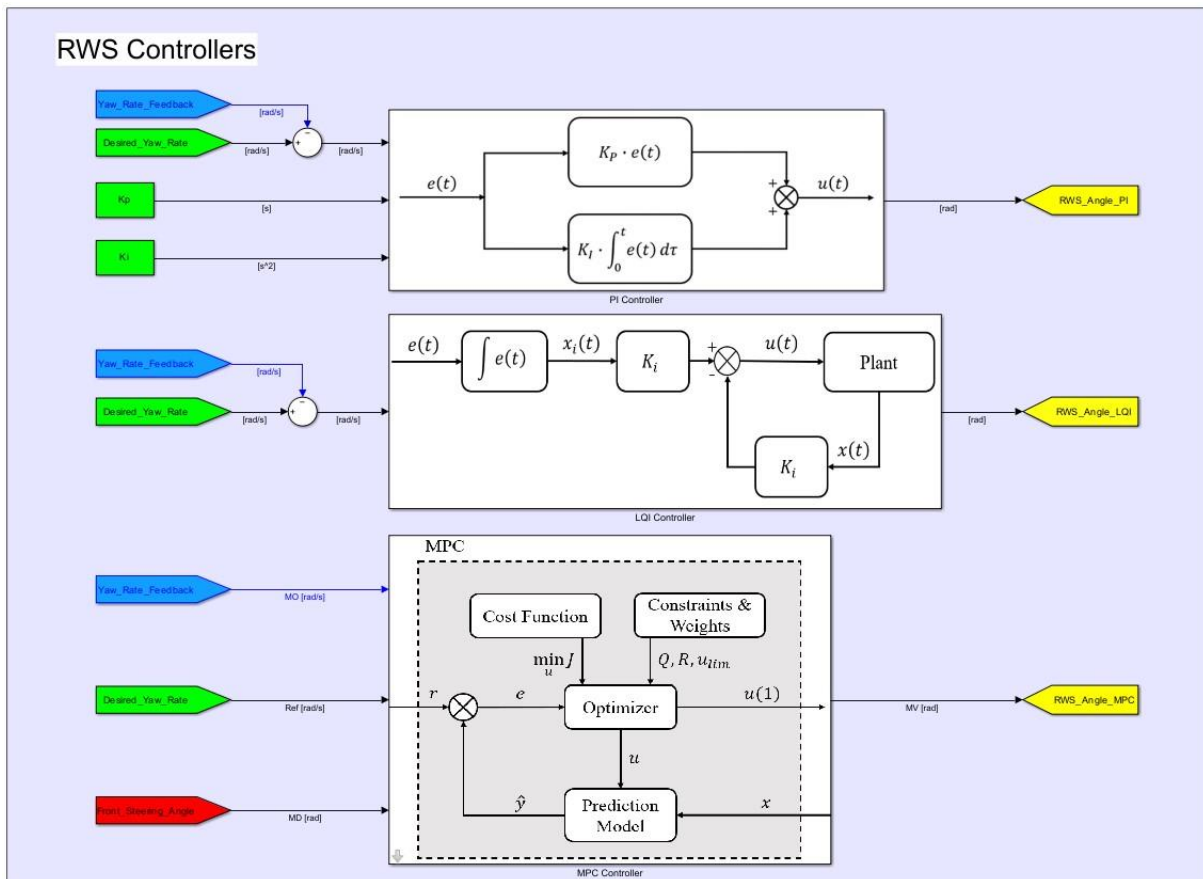


Figure 5.16 RWS controllers in *Simulink*.

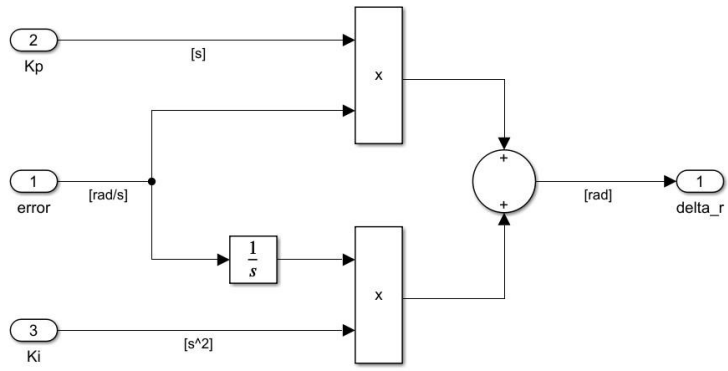


Figure 5.17 Details of PI controller.

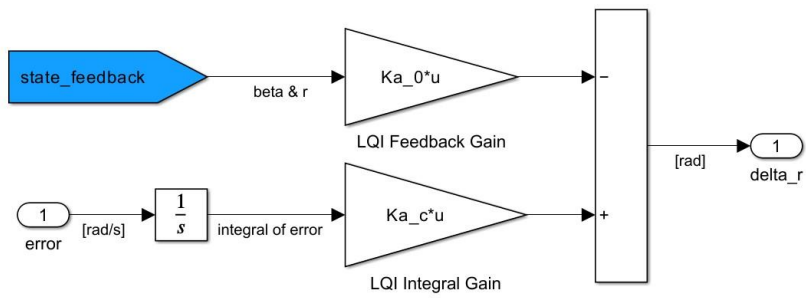


Figure 5.18 Details of LQI controller.

6. Offline Simulation and Results

After having created the complete RWS control loops in *Simulink*, it is necessary to visualize and validate the benefits and improvements that a vehicle with active RWS angle can offer in terms of vehicle handling dynamics. In this chapter, several vehicle handling maneuvers are defined and carried out in *Simulink* with the goal of validating the effectiveness of the various control methods proposed in the previous chapter. These maneuvers intend to help characterize the vehicle's cornering responses, making comparisons between a passive vehicle without RWS angle and the one with RWS control inputs in steady-state and transient conditions. In this way objective feedback is provided, which can be a starting point for any further physical testing and analysis. Controllers tuning is carried out based on the defined maneuvers to guarantee that the controllers perform as desired. Then, the behavior of the controlled vehicle is compared with the one of passive vehicle to observe any improvement of vehicle response.

6.1 Maneuvers Definition

A requirement for the test maneuvers proposed is that they should have an **open-loop** structure. It means that the entire input sequence is created in advance and is then imposed by the driver. After implementation, the driver observes the vehicle's response without intervening and trying to modify the inputs, thus the driver exerts no feedback control on vehicle states. In this way the repeatability of the tests are guaranteed. This structure differs from **closed-loop** structure in which the driver is also included in the control loop and actively changes the inputs to realize control actions, which is beyond the scope of this thesis.

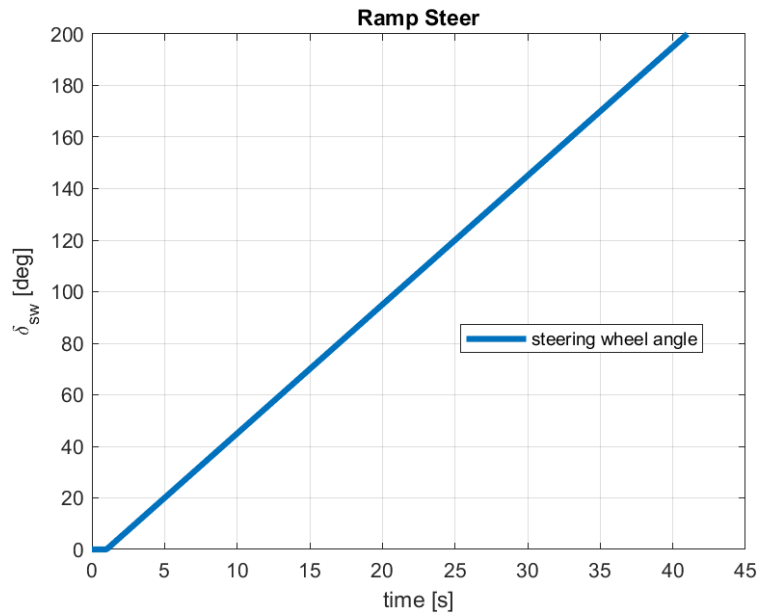
Following the above considerations, a set of maneuvers are defined together with their parameters and are realized in *MATLAB/Simulink*, among them ramp steer, step steer and sine sweep steer that are detailed in the subsequent sections. Note that in each maneuver considered, $\delta_{sw} > 0$ means a left steering action.

6.1.1 Ramp Steer

The ramp steer maneuver is able to characterize the vehicle's steady-state steering response. During this test, the vehicle is first made running in straight line at a fixed longitudinal speed of $V = 100 \text{ km/h}$ with the steering wheel in its on-center position. Next, the steering wheel angle is slowly increased at a rate of $\dot{\delta}_{sw} = 5 \text{ deg/s}$ until it reaches $\delta_{sw,f} = 200 \text{ deg}$. This final value has been chosen such that the vehicle is allowed to have its lateral acceleration a_y slowly increased until reaching its maximum lateral acceleration \bar{a}_y . **Table 4** reports the parameters of ramp steer. The time history of steering wheel angle input in ramp steer is shown in **Figure 6.1**.

Table 4 Ramp steer maneuver parameters

Parameter	Value
Longitudinal velocity V	100 km/h
Steering wheel angle rate $\dot{\delta}_{sw}$	5 deg/s
Final steering wheel angle $\delta_{sw,f}$	200 deg

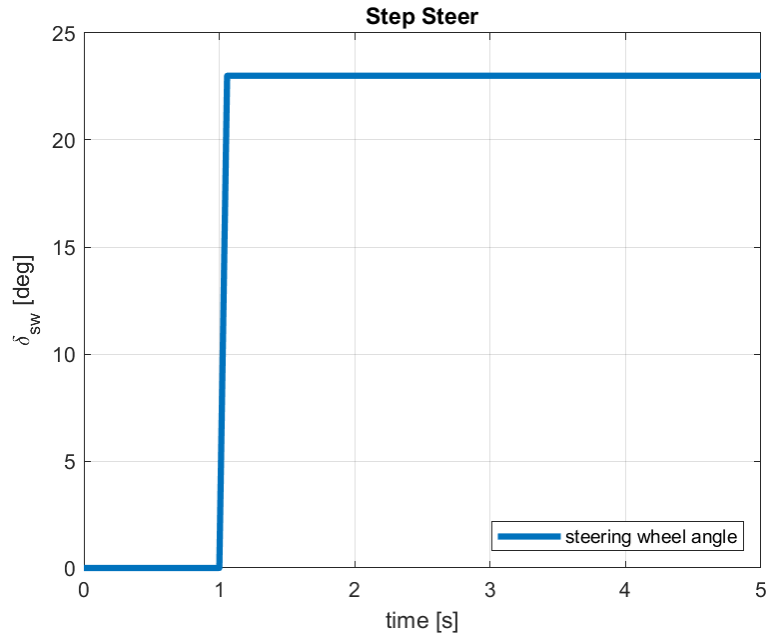
**Figure 6.1** Ramp steer maneuver.

6.1.2 Step Steer

The step steer maneuver is able to characterize the vehicle's transient steering response. During this test, the vehicle is first made running in a straight line at a fixed longitudinal speed of $V = 100 \text{ km/h}$ with the steering wheel in its on-center position. Then, the steering angle is abruptly increased at a rate of $\dot{\delta}_{sw} = 400 \text{ deg/s}$ representing a step input. A suitable final value must be chosen such that the maximum lateral acceleration developed can keep the vehicle operating in its linear tire range. The final value of $\delta_{sw} = 22 \text{ deg}$ is chosen assuming that the threshold of linear range is roughly $a_y = 0.4g$. This value is then maintained for several seconds till the end of simulation to ensure that the transient period fades out and the vehicle reaches steady-state again. **Table 5** reports the parameters of step steer. The time history of steering wheel angle input in ramp steer is shown in **Figure 6.2**.

Table 5 Step steer maneuver parameters

Parameter	Value
Longitudinal velocity V	100 km/h
Steering wheel angle rate $\dot{\delta}_{sw}$	400 deg/s
Final steering wheel angle $\delta_{sw,f}$	22 deg

**Figure 6.2** Step steer maneuver.

6.1.3 Sine Sweep Steer

The sine sweep steer is also able to characterize the vehicle's transient steering response. During this test, the vehicle is first made running in a straight line at a fixed longitudinal speed of $V = 100 \text{ km/h}$ with the steering wheel in its on-center position. Then, multiple periods of sinusoidal steering inputs of different frequencies are applied, starting from an initial frequency $f_i = 0.4 \text{ Hz}$ until a final frequency $f_f = 3 \text{ Hz}$. These inputs all have a fixed steering wheel angle $\delta_{sw} = 22 \text{ deg}$ to guarantee that a_y stays in the linear range within $a_y = 0.4 g$ for the first steering input. The maneuver stop time is chosen such that a frequency increase rate of $f_r = 0.1 \text{ Hz/s}$ is reached. **Table 6** reports the parameters of sine sweep steer. The time history of steering wheel angle input in sine sweep steer is shown in **Figure 6.3**.

Table 6 Sine sweep steer maneuver parameters

Parameter	Value
Longitudinal velocity V	100 km/h
Steering wheel angle δ_{sw}	22 deg
Initial frequency f_i	0.4 Hz

Final frequency f_f	3 Hz
Frequency rate f_r	0.1 Hz/s

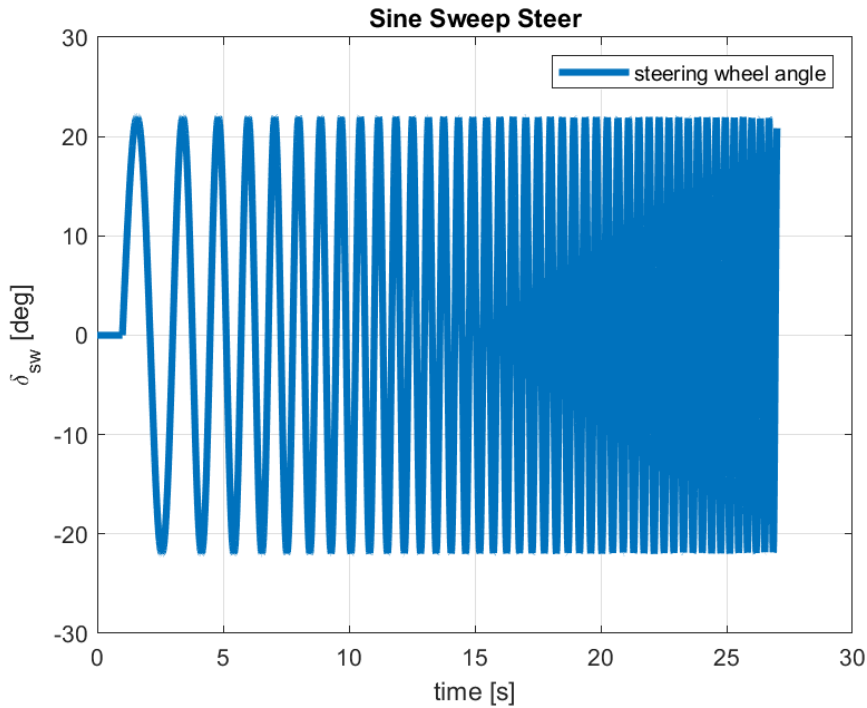


Figure 6.3 Sine sweep steer maneuver.

6.2 Controller Parameters Tuning

After having defined the maneuvers to be performed, the proposed controllers are tuned in an iterative fashion so that the vehicle model's actual yaw rate accurately follows the desired yaw rate at each operating condition. The step steer input is introduced as the basis for controller parameters tuning as it represents a quick direction transition condition that can be experienced in everyday driving scenarios. Depending on the controller type, controller gains or weighting coefficients are modified iteratively until the vehicle's yaw rate response satisfies the requirements in terms of rise time, settling time and overshoots, i.e. the actual vehicle accurately follows the desired yaw rate response by exerting a reasonable active RWS angle. The following sections summarize the tuning processes for each controller and present the eventual controller parameters.

6.2.1 PI Controller

The tuning process for the PI controller consists of iteratively changing the proportional and integral coefficients K_P and K_I and then observing the step steer yaw rate reference tracking performance. Modifying the value of each coefficient independently will lead to different effects, namely [58]:

- Increasing K_P : the rise time and steady-state tracking error will be reduced; however, the overshoot can be potentially increased.

- Increasing K_I : the steady-state tracking error will be eliminated; but also in this case the overshoot can be potentially increased.

These behaviors serve as a guideline for PI controller tuning process. The tuned PI controller parameters are presented in **Table 7**.

Table 7 PI controller parameters

Controller parameter	Value
K_P	-0.4
K_I	-15

6.2.2 LQI Controller

For LQI controller's tuning and simulation, a simplification is made by assuming a vehicle plant model with linear tire properties. This states that the values of C_f and C_r are fixed at values representing the linear tire lateral force behavior. This assumption is in accordance with one of the LQR control's prerequisite, that is: the plant model should be linear. Consequently, only the linear tract of the desired yaw rate r_{des} is imposed in the reference model.

The tuning process for the LQI controller consists of iteratively changing the coefficients in the weighting matrices Q and R . These two matrices are made diagonal by applying appropriate weight values along the diagonal while leaving other values zero. Specifically, weights of Q matrix determine the tracking error allowed in every state and weights of R matrix determine the amount of control effort. Changes made on the two matrices vary the relative importance of the control effort and error respectively in the cost function J . Eventually, the resulting optimal state feedback control gain matrix K is also varied.

Generally, the tuning process starts from an initial choice of diagonal matrices Q and R with [58]:

- $Q_{ii} = 1$ in the presence of requirements on x_i ; $Q_{ii} = 0$ otherwise.
- $R_{ii} = 1$ in the presence of requirements on u_i ; $R_{ii} = 0$ otherwise.

Then, their values are iteratively changed until the requirements are satisfied in simulation. The tuned LQI controller parameters are presented in **Table 8**.

Table 8 LQI controller parameters

Controller parameter	Value
Q	$\begin{bmatrix} 1 & 0 & 0 \\ 0 & 0.1 & 0 \\ 0 & 0 & 5000 \end{bmatrix}$
R	1

6.2.3 MPC Controller

For the sake of simplicity, it is assumed a prediction model with linear axle lateral force relationship for the MPC controller, i.e. the prediction model has fixed parameters: C_f and C_r do not vary with a_y . Their values are chosen to be approximately the ones in the low a_y ranges, i.e. values at the beginning of the curves to improve the controller performance. The tuning process consists of setting the appropriate values for sample time T_s , prediction horizon P , control horizon M , and controller weights. Optionally, constraints on plant outputs and manipulated variables can also be specified which in the case are not considered. The optimal choice of controller parameters should reflect a balance between performance and computational effort. Some general guidelines for choosing the right parameters are summarized as follows [59]:

- Sample time T_s : It is the rate at which the MPC controller executes the control algorithm. The choice reflects how fast the controller can react to setpoint changes. A reasonable choice could be:

$$\frac{T_r}{20} \leq T_s \leq \frac{T_r}{10} \quad (6.1)$$

Where T_r is the rise time of the system's open-loop response, which is the time taken for the response to rise from 10 % to 90 % of the steady-state response. It states that 10 to 20 samples can be fit within T_r .

- Prediction horizon P : the choice of it shows how far the MPC controller can predict into the future. A recommendation is to have 20 to 30 samples covering the open-loop transient system response.
- Control horizon M : It is the number of MV moves to be optimized at control interval k . It is suggested to choose a small M value, since usually only the first couple of control moves have a significant effect on the predicted plant output behavior while the remaining moves only have a minor effect. A rule of thumb is:

$$0.1P \leq M \leq 0.2P \quad (6.2)$$

With M containing minimum 2 to 3 time steps. In this way the complexity of the QP optimization problems is limited.

- Cost function weights: They represent the relative importance assigned to the different plant input and output. Relative weights within input and output groups can be adjusted as well. Generally, a larger weight is assigned to the more important input/output aspect.

The tuned MPC controller parameters are reported in **Table 9**.

Table 9 MPC controller parameters

Controller parameter	Value
Sample time T_s	0.02 s
Prediction horizon P	20 timesteps
Control horizon M	2 timesteps
Weights	1 on both plant input and output

6.3 Simulation Results

In this section, various simulation results obtained on the passive and controlled vehicle with the various maneuvers and controllers setups defined previously are presented. Comparisons of behaviors between passive and controlled vehicles are made for each case, which leads to valuable observations regarding the improvement of vehicle's cornering response with RWS.

6.3.1 Ramp Steer: PI Control

The time history of yaw rate r and yaw rate tracking error e in ramp steer with PI control are shown in **Figure 6.4**.

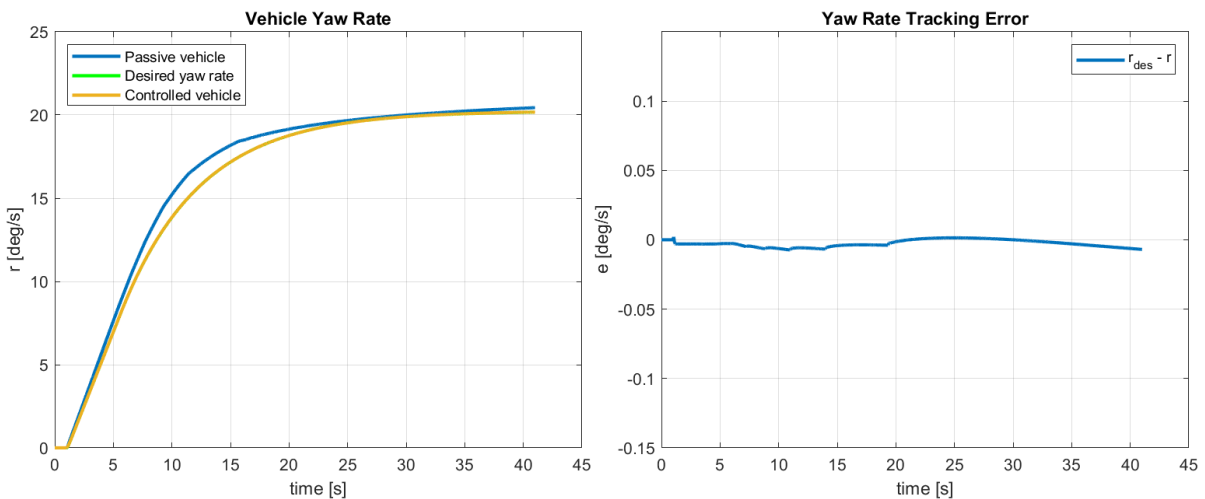


Figure 6.4 PI ramp steer: time history of r and e . The line with green color results “hidden” because the controlled vehicle yaw rate overlaps the desired yaw rate.

From the figures, it is possible to notice the more understeering behavior as imposed by the reference model, since the desired yaw rate curve lies under the passive vehicle yaw rate curve. Moreover, the effectiveness of the controller is evident: the controlled vehicle's yaw rate overlaps the desired one and the resulting yaw rate tracking error always stays in the neighborhood of zero, indicating almost perfect tracking performance.

The resulting handling diagrams of steering wheel angle δ_{sw} and vehicle sideslip angle β as a function of lateral acceleration a_y are shown in **Figure 6.5**. The achievement of more understeering behavior is verified because for the same δ_{sw} input, the controlled vehicle shows a lower a_y value in the operating range. On the other hand, reduction of β is also observed, since for the same a_y the angle β in controlled vehicle is smaller than the one in passive vehicle.

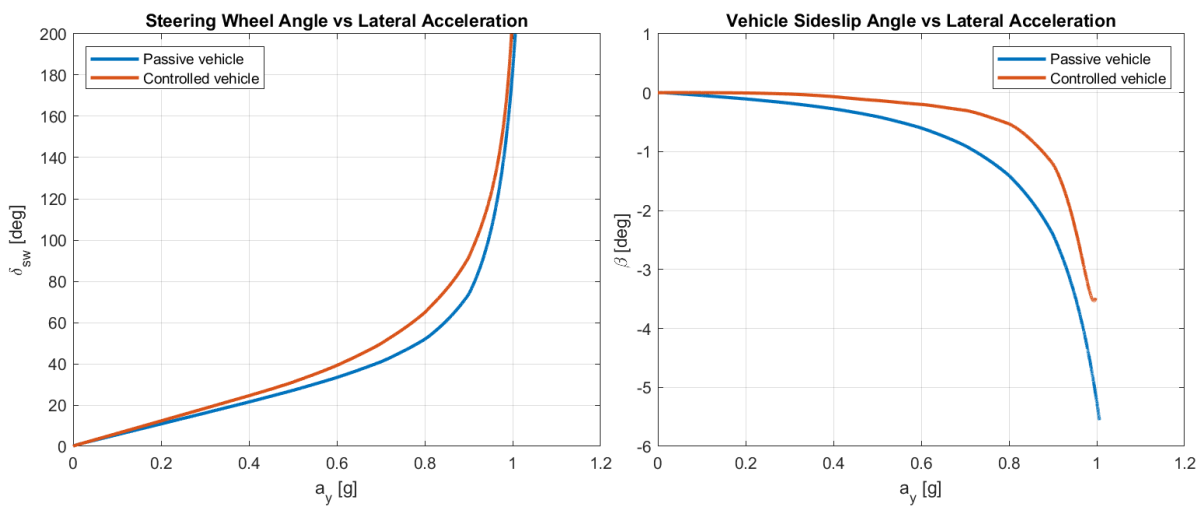


Figure 6.5 PI ramp steer: handling diagrams of $\delta_{sw} - a_y$ and $\beta - a_y$.

The time history of active RWS angle δ_r and the trajectories of the two vehicles are depicted in **Figure 6.6**. The sign of δ_r is always positive and is the same as front steering angle δ_f as in this case in-phase RWS is necessary to help make the vehicle more understeering. Moreover, the values stay in a valid range. Comparing the two vehicle's trajectory clearly shows the improvements in cornering response due to RWS: after the initial straight line driving for 1 s, the controlled vehicle starts to turn on an enlarged circle till the end of maneuver showing more understeering behavior.

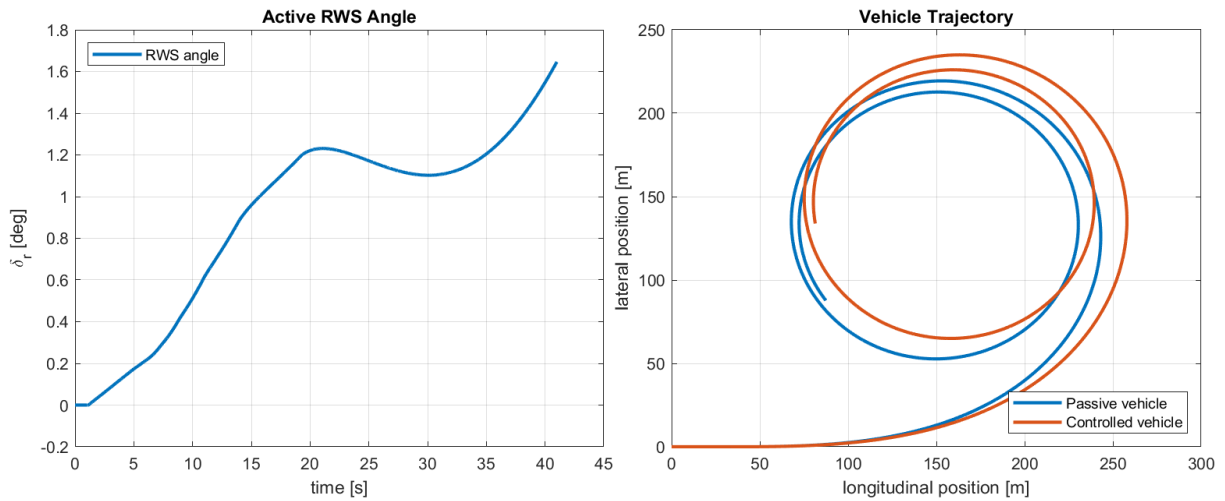


Figure 6.6 PI ramp steer: time history of δ_r and vehicle trajectory comparison.

6.3.2 Ramp Steer: LQI Control

The simulation results with LQI control are obtained on a vehicle plant model with linear axle cornering force relationship, as mentioned at the beginning of **Section 6.2.2**. As a result, this simplification is assumed also for the passive vehicle in order to make valid comparisons. The time history of yaw rate r and yaw rate tracking error e are show in **Figure 6.7**.

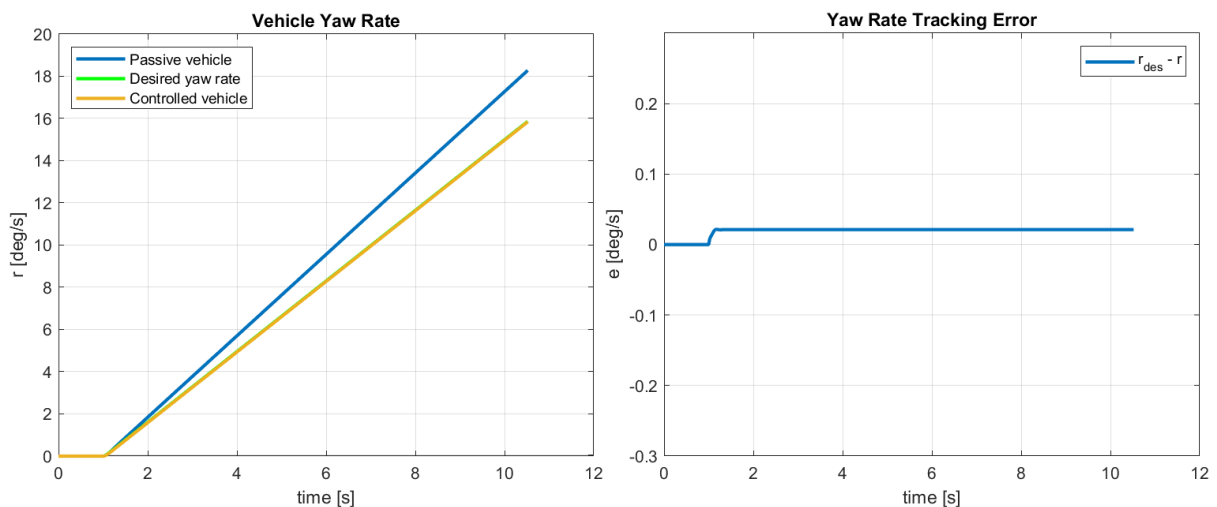


Figure 6.7 LQI ramp steer: time history of r and e .

The simulation is made in a way that it terminates automatically when the lateral acceleration a_y reaches $0.9 g$, which represents the assumed upper bound of linear axle lateral force characteristic. The LQI controller is effective in making the vehicle to track the desired yaw rate represented by a pure straight line, indicating the linear relationship. The two yaw rates are almost overlapping as evidenced also by the tracking error e : it maintains a constant value very close to zero throughout the simulation.

The resulting handling diagram of steering wheel angle δ_{sw} as a function of lateral acceleration a_y is shown in **Figure 6.8**. Results very similar to the ones obtained with PI control truncated in linear range ($a_y \leq 0.4g$) are achieved. Furthermore, with the linear assumption, the understeer gradient is conveniently calculated by taking the gradient of the curves in the handling diagram of $\delta_{sw} - a_y$ (**Figure 6.9**). The improvement in the vehicle's understeering behavior is easily noticed from the resulting steady-state K_{US} values.

The time history of active RWS angle δ_r and trajectories of two vehicles are depicted in **Figure 6.10**. Note that after the short transient at the beginning, the RWS angle grows completely linearly towards the end of simulation. The trajectories are consistent with the initial tract in PI control results.

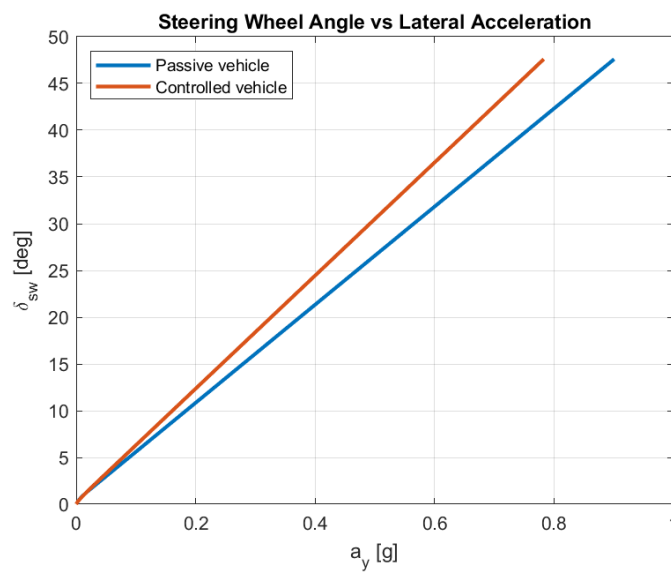


Figure 6.8 LQI ramp steer: handling diagram of $\delta_{sw} - a_y$

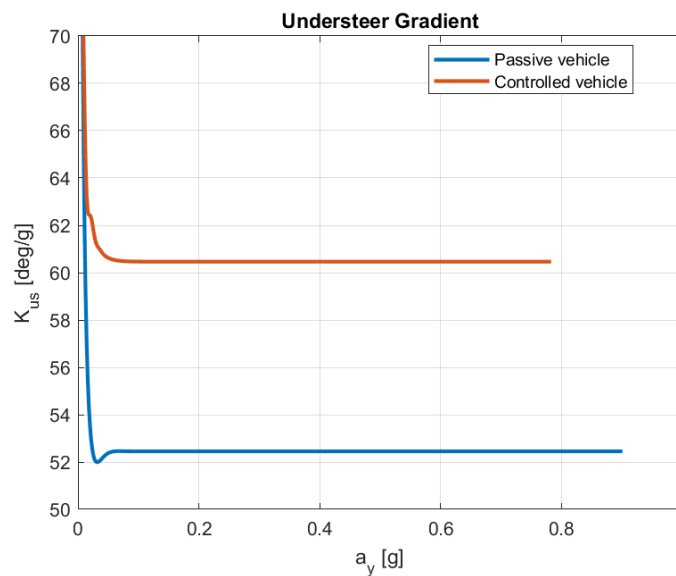


Figure 6.9 LQI ramp steer: understeer gradient K_{US} .

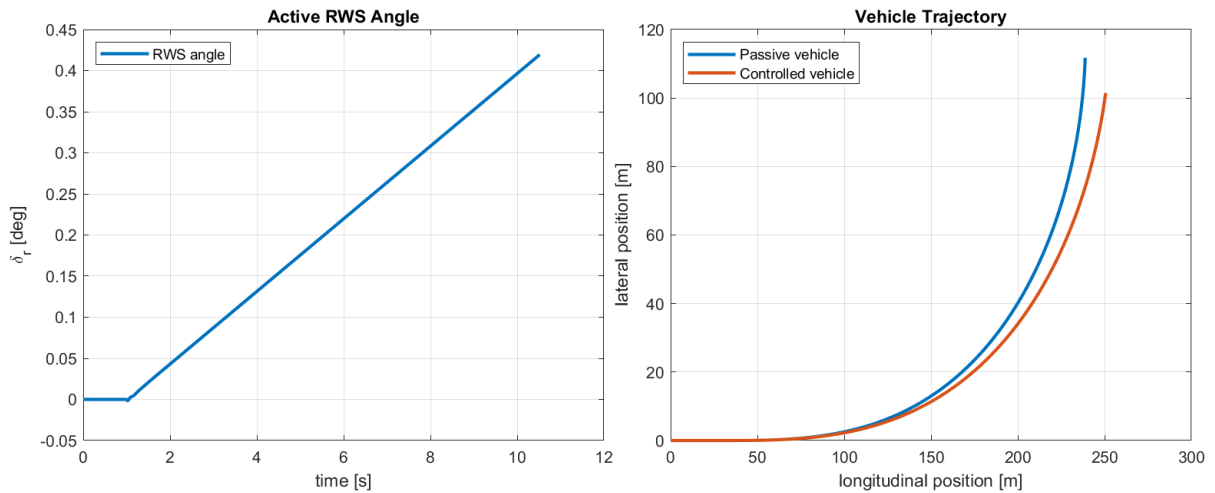


Figure 6.10 LQI ramp steer: time history of δ_r and vehicle trajectory comparison.

6.3.3 Step Steer: PI Control

The time history of yaw rate r and yaw rate tracking error e in step steer with PI control are shown in Figure 6.11. A much improved behavior is observed from the suppression of overshoot during transient. Moreover, after the transient period the vehicle's yaw rate r tracks the desired one well, as evidenced by the null steady-state tracking error e . The controlled steady-state yaw rate value is lower than the passive one which agrees with the design goal.

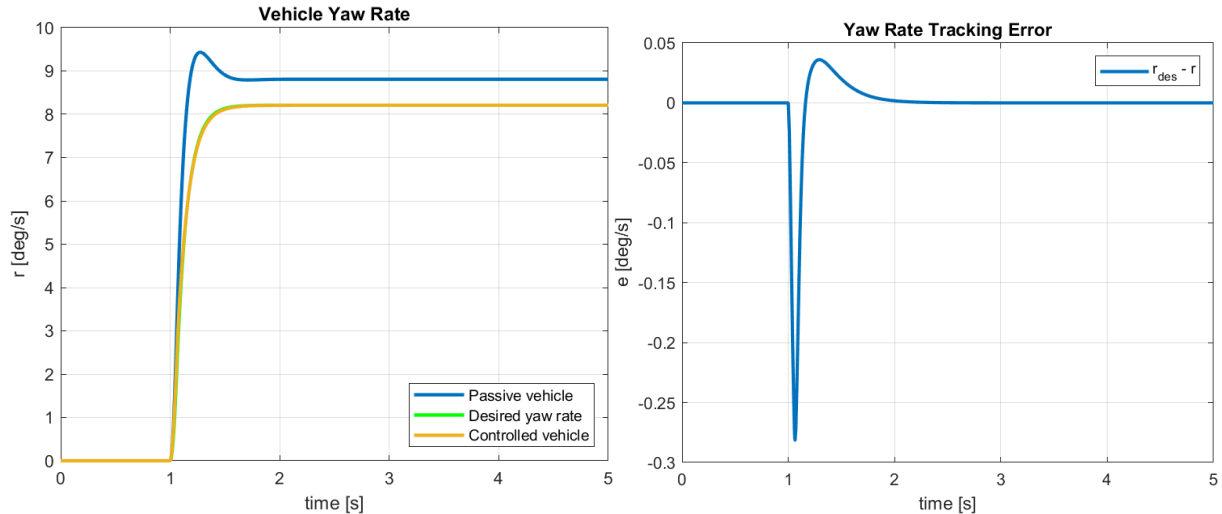


Figure 6.11 PI step steer: time history of r and e .

The time history of active RWS angle δ_r are shown in Figure 6.12. Meanwhile, the controlled vehicle's sideslip angle β shows a more contained overshoot comparing to the passive one. After the transient phase, the controlled vehicle's angle has a reduced absolute steady-state value. The resulting figure suggests an improvement in vehicle's cornering response, even if yaw rate is the only vehicle state actively controlled.

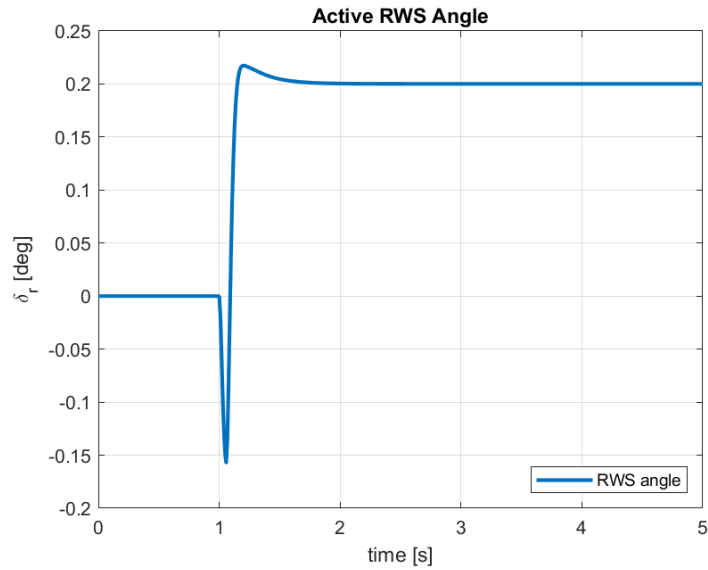


Figure 6.12 PI step steer: time history of δ_r .

6.3.4 Step Steer: LQI Control

The time history of yaw rate r and yaw rate tracking error e in step steer with LQI control are shown in **Figure 6.13**. The results are similar to the ones with PI control, except that with proposed LQI control the tracking error e during transient has opposite sign. It means a relatively slower transient response showing less responsiveness, since the desired yaw rate is always larger than the controlled yaw rate before the error diminishes to zero in steady-state.

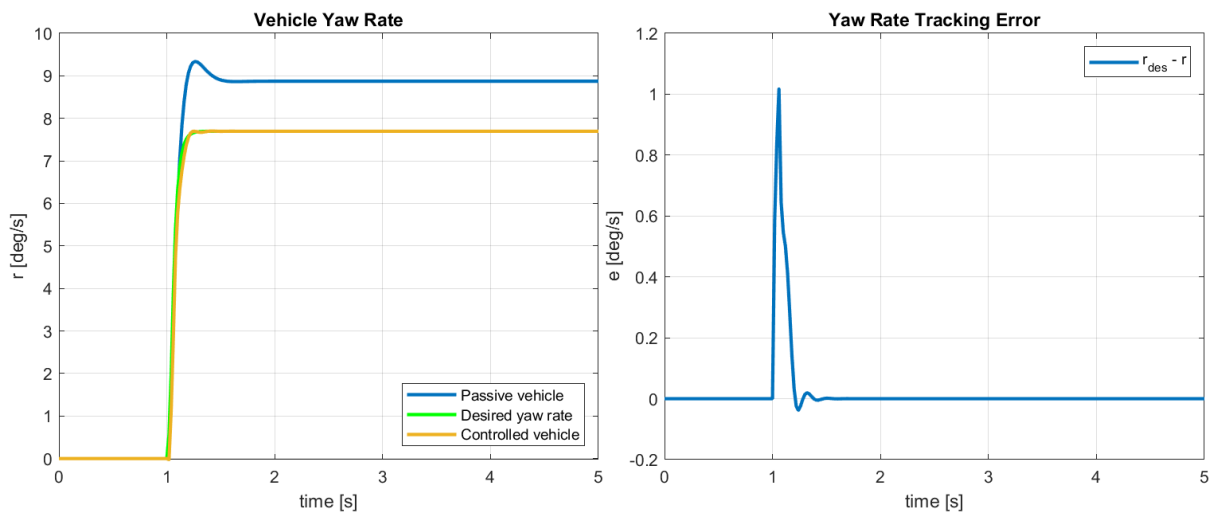


Figure 6.13 LQI step steer: time history of r and e .

The time history of active RWS angle δ_r is shown in **Figure 6.14**. The angle δ_r shows a bit of oscillations in the transient phase before settling to a steady-state value almost identical to the one obtained with PI control. Meanwhile, the sideslip angle β shows a larger overshoot which is also larger than the passive angle. However, after the transient phase, the angle β remains stable near the value of zero.

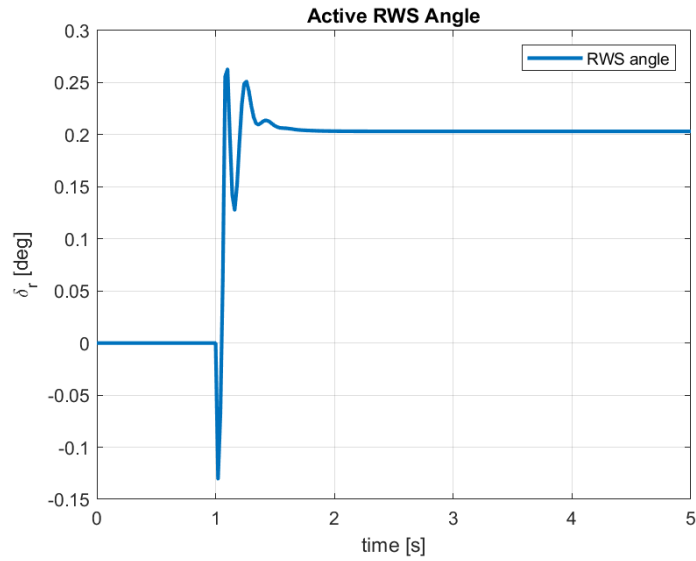


Figure 6.14 LQI step steer: time history of δ_r .

6.3.5 Sine Sweep Steer: PI Control

The time history of yaw rate r and yaw rate tracking error e in sine sweep steer with PI control are shown in **Figure 6.15**. It is obvious that the controller makes the yaw rate value lower in all the frequency ranges. Meanwhile, the controlled vehicle tracks well the curve r_{des} in the low frequency range, but the tracking performance degrades when entering the high frequency ranges as shown by the increasing magnitude of error e .

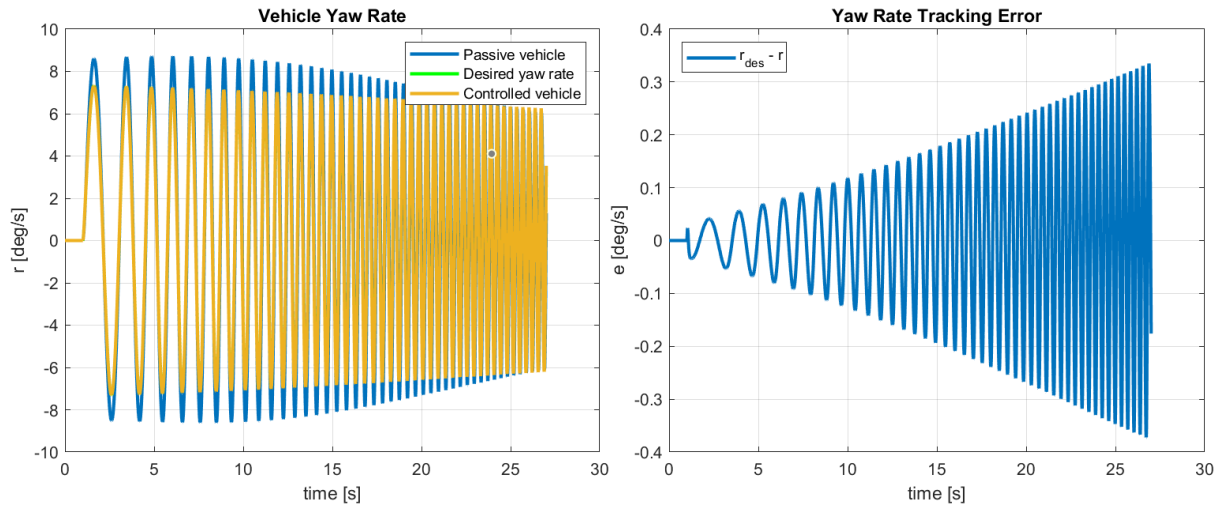


Figure 6.15 PI sine sweep steer: time history of r and e .

The time history of active RWS angle δ_r is shown in **Figure 6.16**. The angle δ_r alters its sign following the sign of δ_{sw} , effectively letting the vehicle track r_{des} with input coming from both directions. At the same time, the controlled vehicle shows a much lower angle β with an almost constant magnitude throughout the frequency range, which is a consequence of the imposed

more understeering behavior by the controller. From the time history of lateral acceleration a_y in **Figure 6.17**, it can be noticed that the control is effective in reducing a_y in the low frequency range. However, its effectiveness drops after around $t = 10$ s when the magnitude of a_y cannot be reduced anymore and it stays above the one of the passive vehicle.

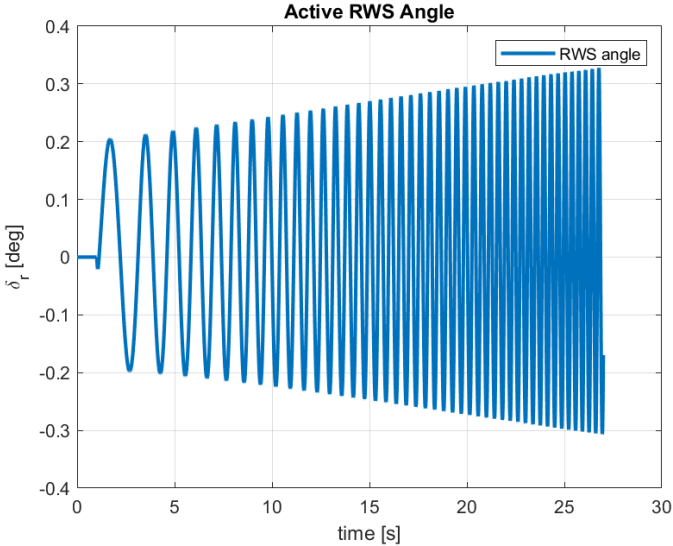


Figure 6.16 PI sine sweep steer: time history of δ_r .

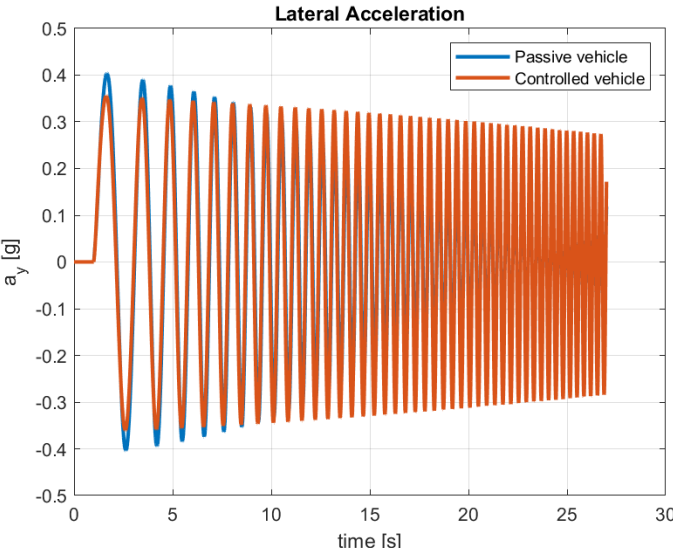


Figure 6.17 PI sine sweep: time history of a_y .

6.3.6 Sine Sweep Steer: LQI Control

The time history of yaw rate r and yaw rate tracking error e in sine sweep steer with PI control are shown in **Figure 6.18**. The yaw rate tracking performance is comparable to the one with PI control in that it is effectively suppressed to almost the same magnitude. However, the tracking error e generally has higher magnitude, especially in the high frequency range where the tracking performance degrades. From the results of the time history of active RWS angle

δ_r (Figure 6.19) it can be noted that with LQI control, δ_r tends to stabilize in high frequency range at a lower magnitude than the one with PI control. Finally, results of the time history of lateral acceleration a_y (Figure 6.20) are comparable with the results of PI control.

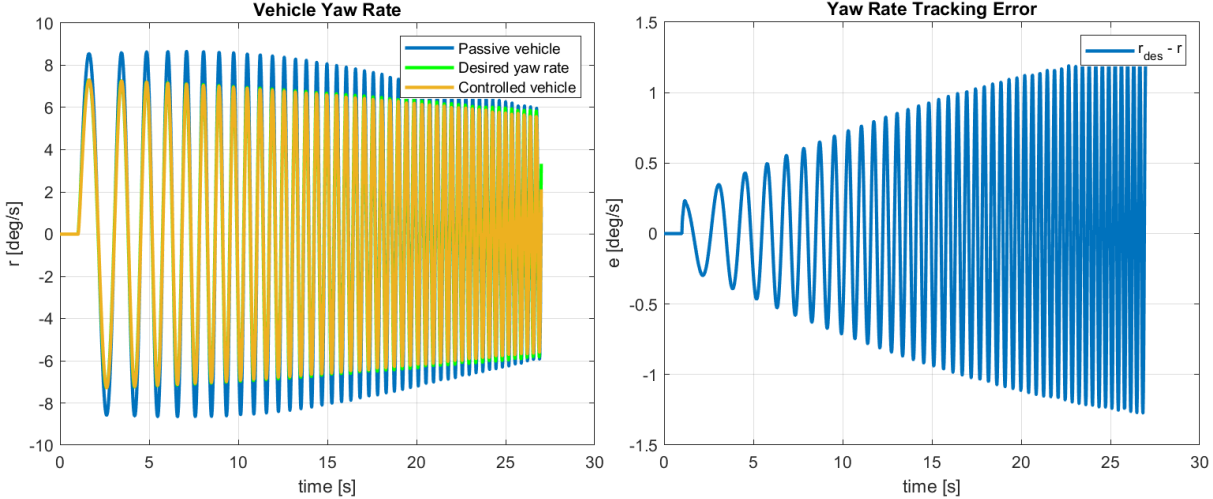


Figure 6.18 LQI sine sweep steer: time history of r and e .

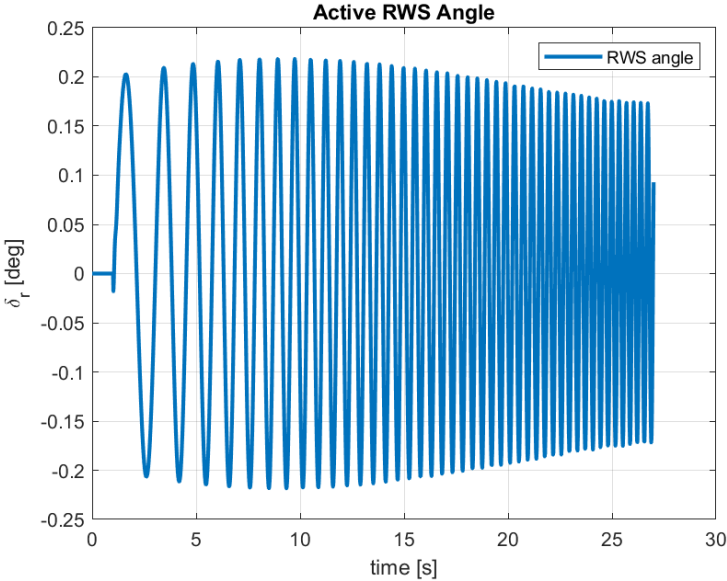


Figure 6.19 LQI sine sweep steer: time history of δ_r .

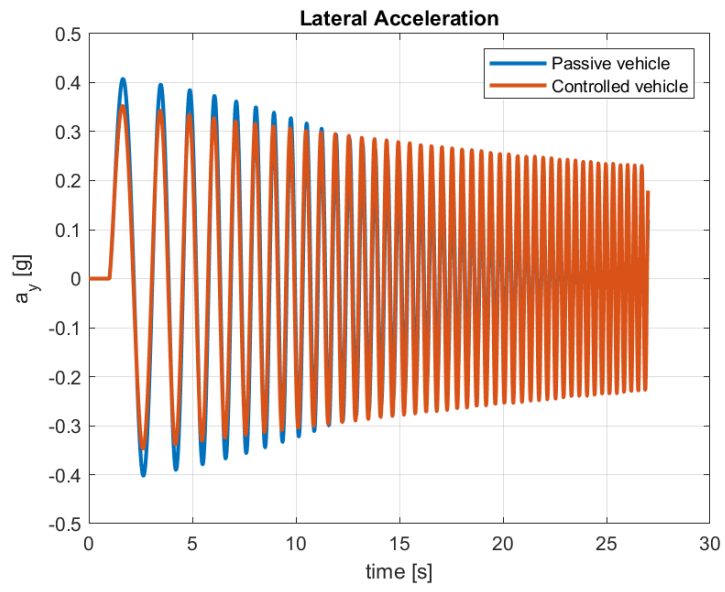


Figure 6.20 LQI sine sweep steer: time history of a_y .

7. Conclusion

The present thesis work deals with the creation of an active RWS control algorithm applied to a virtual vehicle, with the aim of improving a vehicle's lateral dynamic responses. Literature reviews on the RWS systems' application in automotive industry since the last century demonstrated the growing popularity towards RWS systems' research and developments. In view of this, a variety of control methodologies proposed in literature were reviewed and later brought to *MATLAB/Simulink* for RWS controller creation, which aims to influence a vehicle's lateral dynamic responses as desired.

To realize the complete closed-loop RWS control composed of vehicle model, reference model and controller model, it was first developed in *Simulink* a linearized single-track vehicle model with nonlinear axle lateral force characteristics as the vehicle plant model to be controlled. Its parameters were based on the company's know-how. Next, the reference model was defined, which was a key point of the project: in fact, the yaw rate response of this reference model represents the control intention corresponding to a certain understeering behavior different from the one in the passive vehicle. The desired yaw rate r_{des} was established using an analytical expression obtained from the knowledge of current vehicle longitudinal speed V and steering wheel angle δ_{sw} . Some design parameters were identified for the analytical expression, arriving in the end at an improved understeer characteristics in the speed range considered.

The difference in actual and desired yaw rate, i.e. the error signal e was subsequently elaborated by each of the three different controllers, namely PI, LQI and MPC controller. Each of them took the error signal as input and generated an active RWS angle δ_r based on classical and optimal control theories. Some simplifications were made in the vehicle model and prediction model in LQI and MPC control loops respectively.

The effectiveness of the three RWS controllers were evaluated through simulations of several standard open-loop maneuvers in *MATLAB/Simulink*: ramp steer, step steer and sine sweep steer. Simulation results of ramp steer with PI control showed a modified vehicle cornering dynamics behaviors in steady-state as desired; with LQI control subjecting to the linear axle lateral force simplification, a similar change of vehicle's cornering behavior was noticed. Similar trends of modifications of transient cornering response in step steer were noticed from the results of each control, indicating satisfactory performance improvements in overshoot suppression. Similar results were also registered in sine sweep steer for each control proposed, with well suppressed yaw rate in all the frequency ranges.

In conclusion, the proposed active RWS controllers were able to satisfy the control goals, subjecting to the simplifications made in each case. They were all able to bring benefits in terms of vehicle lateral dynamics and active safety, the one created based on LQI formulation were subjected to additional simplification and its computation-intensive computing process turned out to be more complicated; on the other hand, the controller based on PI theory resulted to be the one with the better overall performance regarding reference tracking and computational

effort due to its simplicity in construction and its versatility in producing satisfactory results, extending its validity beyond any further simplifications.

7.1 Future Work

Although the various results obtained in this thesis highlighted the potential improvements in the lateral vehicle dynamics and active safety, several future works could be established based on the current research. This is attributed to the various simplifications made in the thesis and limited availability of time. They are summarized below:

- The controlled vehicle state in this work could be extended: in this work, only the yaw rate feedback was considered and the control goal was imposed on this variable only. A multivariable feedback regime, for example, with combined yaw rate and sideslip angle feedback would generally lead to better control performance.
- The controller design could be improved: the two optimal controllers considered in this thesis both had simplifications related to linear tire lateral force behavior. Designs that could better take the nonlinearities into account could be conceived, such as gain-scheduling LQI control or adaptive MPC control which can better handle the varying nonlinear parameters.
- Some other maneuvers could be carried out: the maneuvers considered in this thesis were all carried out at a fixed predefined longitudinal velocity, which despite its validity as general test procedures, could not fully reflect the reality. Thus, some maneuvers including accelerating and braking in the longitudinal direction could be constructed and tested on a more detailed vehicle model.
- Further design verifications could be made on a more complete vehicle model: in this thesis, only the single-track model was conceived as the vehicle plant model to be controlled. To better demonstrate the promised improvements, the simulation maneuvers could be run on a vehicle model having more DOF with roll/pitch dynamics and load transfer effects which can better represent a real vehicle in the virtual environment.
- Potential driver-in-the-loop simulation and validation on a dynamic simulator (DiM): apart from relying only on objective feedback evaluation in the virtual simulation environment, the controller modelled in *Simulink* could possibly be implemented on a DiM such that subjective feedbacks of steering dynamics modifications could be collected from professional drivers.

Bibliography

- [1] P. Lugner, *Vehicle Dynamics of Modern Passenger Cars*, Springer, 2019.
- [2] "DANISI ENGINEERING – Vehicle Engineering and Prototyping," [Online]. Available: <https://www.danisieng.com/>. [Accessed 13 8 2022].
- [3] Y. Furukawa, S. Sano, H. Takeda, N. Yuhara and Y. Matsushita, "A Review of Four-Wheel Steering Studies from the Viewpoint of Vehicle Dynamics and Control," *Vehicle System Dynamics*, vol. 18, no. 1-3, pp. 151-186, 1 1989.
- [4] "4-Wheel Steering Systems (Pros/Cons and Cars That Have It)," [Online]. Available: <https://oards.com/four-wheel-steering-system-info/>. [Accessed 13 08 2022].
- [5] I. Amdouni, N. Jeddi and L. El Amraoui, "Optimal control approach developed to Four-Wheel Active Steering Vehicles," 2013.
- [6] "AutoZine Technical School," [Online]. Available: https://www.autozine.org/technical_school/traction/Steering_3.html. [Accessed 13 8 2022].
- [7] "what models have hicas??? | Skyline Owners Forum," [Online]. Available: <https://www.skylineowners.com/threads/what-models-have-hicas.161372/>. [Accessed 14 8 2022].
- [8] B. Heissing and M. Ersoy, *Chassis handbook : fundamentals, driving dynamics, components, mechatronics, perspectives*, Vieweg + Teubner, 2011, p. 591.
- [9] "File:Nissan Skyline R31 Sedan GT Passage.jpg - Wikimedia Commons," [Online]. Available: https://commons.wikimedia.org/wiki/File:Nissan_Skyline_R31_Sedan_GT_Passage.jpg. [Accessed 14 8 2022].
- [10] "Honda Global | Steering Angle Sensing Four-Wheel Steering System (4WS) / 1987," [Online]. Available: <https://global.honda/heritage/episodes/19874ws.html>. [Accessed 14 8 2022].
- [11] "Four-wheel steering demystified," [Online]. Available: <https://www.autoweek.com/car-life/a1871191/four-wheel-steering-demystified/>. [Accessed 14 8 2022].
- [12] "File:1991 Honda Prelude Si 4WS coupe (2015-07-24) 01.jpg - Wikimedia Commons," [Online]. Available: [https://commons.wikimedia.org/wiki/File:1991_Honda_Prelude_Si_4WS_coupe_\(2015-07-24\)_01.jpg](https://commons.wikimedia.org/wiki/File:1991_Honda_Prelude_Si_4WS_coupe_(2015-07-24)_01.jpg). [Accessed 14 8 2022].
- [13] "File:MitsubishiGalantVR4Gen6.jpg - Wikipedia," [Online]. Available: <https://en.wikipedia.org/wiki/File:MitsubishiGalantVR4Gen6.jpg>. [Accessed 14 8 2022].

- [14] "Active Rear Axle Kinematics - E31Wiki," [Online]. Available: https://e31wiki.org/wiki/Active_Rear_Axle_Kinematics. [Accessed 14 8 2022].
- [15] "File:BMW 840 Ci 1.jpg - Wikimedia Commons," [Online]. Available: https://commons.wikimedia.org/wiki/File:BMW_840_Ci_1.jpg. [Accessed 14 8 2022].
- [16] "4 wheel steering - whats the deelio? - Page 2 - General Gassing - PistonHeads UK," [Online]. Available: <https://www.pistonheads.com/gassing/topic.asp?h=0&f=23&t=1049307&i=20>. [Accessed 14 8 2022].
- [17] "BMW 7 Series Sedan : Integral Active Steering," [Online]. Available: http://content.bmwusa.com/microsite/7series_2013/com/en/newvehicles/7series/sedan/2012/showroom/dynamics/integral-active-steering.html#t=1. [Accessed 14 8 2022].
- [18] "File:2006 BMW 730d (E65) sedan (2015-07-09) 01.jpg - Wikimedia Commons," [Online]. Available: [https://commons.wikimedia.org/wiki/File:2006_BMW_730d_\(E65\)_sedan_\(2015-07-09\)_01.jpg](https://commons.wikimedia.org/wiki/File:2006_BMW_730d_(E65)_sedan_(2015-07-09)_01.jpg). [Accessed 14 8 2022].
- [19] "Technique : Tout savoir sur les systèmes de 4 roues directrices (Renault 4Control, Honda 4WS...)," [Online]. Available: <https://www.blog-moteur.com/41982/technique-4-roues-directrice-4control-renault.html>. [Accessed 14 8 2022].
- [20] "Ferrari's GTC4Lusso 'Family Car' Steers With All 4 Wheels | WIRED," [Online]. Available: <https://www.wired.com/2016/02/ferrari-gtc4-lusso/>. [Accessed 14 8 2022].
- [21] "File:Ferrari GTC4Lusso IMG 4353.jpg - Wikimedia Commons," [Online]. Available: https://commons.wikimedia.org/wiki/File:Ferrari_GTC4Lusso_IMG_4353.jpg. [Accessed 14 8 2022].
- [22] *The new Lamborghini Urus: The world's first Super Sport Utility Vehicle.*
- [23] "File:2019 Lamborghini Urus V8 Automatic 4.0 Front.jpg - Wikimedia Commons," [Online]. Available: https://commons.wikimedia.org/wiki/File:2019_Lamborghini_Urus_V8_Automatic_4.0_Front.jpg. [Accessed 14 8 2022].
- [24] "Rear-axle steering - Porsche-Fahrwerkentwicklung," [Online]. Available: <https://presskit.porsche.de/specials/it/porsche-fahrwerkentwicklung/topic/rear-axle-steering.html>. [Accessed 14 8 2022].
- [25] "File:Porsche 991 GT3 MkII (37601199836) (cropped).jpg - Wikimedia Commons," [Online]. Available:

- [https://commons.wikimedia.org/wiki/File:Porsche_991_GT3_MkII_\(37601199836\)_\(cropped\).jpg](https://commons.wikimedia.org/wiki/File:Porsche_991_GT3_MkII_(37601199836)_(cropped).jpg). [Accessed 17 8 2022].
- [26] "Mercedes-Benz Revolutionizes Rear-wheel Steering in the 2021 S-Class - autoevolution," [Online]. Available: <https://www.autoevolution.com/news/mercedes-benz-revolutionizes-rear-wheel-steering-in-the-2021-s-class-149535.html>. [Accessed 15 8 2022].
- [27] "File:Mercedes-Benz W223 IMG 3951.jpg - Wikimedia Commons," [Online]. Available: https://commons.wikimedia.org/wiki/File:Mercedes-Benz_W223_IMG_3951.jpg. [Accessed 15 8 2022].
- [28] M. Harrer and P. Pfeffer, *Steering handbook*, Springer International Publishing, 2016, pp. 1-565.
- [29] "HICAS/Super HICAS Active Steering Systems - EHFCV," [Online]. Available: <https://ehfcv.com/active-steering-systems-hicassuper-hicas/>. [Accessed 14 8 2022].
- [30] R. Marino, S. Scalzi and F. Cinili, "Nonlinear PI front and rear steering control in four wheel steering vehicles," *User Modeling and User-Adapted Interaction*, vol. 45, no. 12, pp. 1149-1168, 2007.
- [31] R. Marino, S. Scalzi and F. Cinili, "PI Front Steering and PI Rear Steering Control with Tire Workload Analysis," 2007.
- [32] M. A. Vilaplana, O. Mason, D. J. Leith and W. E. Leithead, "LNCS 3355 - Control of Yaw Rate and Sideslip in 4-Wheel Steering Cars with Actuator Constraints".
- [33] M. Canale and L. Fagiano, "Comparing rear wheel steering and rear active differential approaches to vehicle yaw control," *Vehicle System Dynamics*, vol. 48, no. 5, pp. 529-546, 5 2010.
- [34] M. Canale and L. Fagiano, "Stability control of 4WS vehicles using robust IMC techniques," *Vehicle System Dynamics*, vol. 46, no. 11, pp. 991-1011, 11 2008.
- [35] Z. Zhang, M. Huang, M. Ji and S. Zhu, "Design of the Linear Quadratic Control Strategy and the Closed-Loop System for the Active Four-Wheel-Steering Vehicle," *SAE International Journal of Passenger Cars - Mechanical Systems*, vol. 8, no. 1, pp. 354-363, 5 2015.
- [36] F. Du, J. S. Li, L. Li and D. H. Si, "Robust control study for four-wheel active steering vehicle," *Proceedings - International Conference on Electrical and Control Engineering, ICECE 2010*, pp. 1830-1833, 2010.
- [37] N. Hamzah, Y. M. Sam, H. Selamat, M. K. Aripin and M. F. Ismail, "Yaw stability improvement for four-wheel active steering vehicle using sliding mode control," *Proceedings - 2012 IEEE 8th International Colloquium on Signal Processing and Its Applications, CSPA 2012*, pp. 127-132, 2012.
- [38] A. Lucchini, F. P. Azza, M. Corno, S. Formentin and S. M. Savaresi, "Design and Implementation of a MPC-based Rear-Wheel Steering Controller for Sports Cars,"

- in *2021 IEEE Conference on Control Technology and Applications (CCTA)*, San Diego, California, 2021.
- [39] H. Guo, N. Hao and H. Chen, "Lateral stability controller design for electrical vehicle based on active rear wheel steering," in *12th World Congress on Intelligent Control and Automation (WCICA)*, Guilin, China, 2016.
- [40] D. J. Smith and K. G. Simpson, "Other Industry Sectors," in *The Safety Critical Systems Handbook: A Straight Forward Guide to Functional Safety, IEC 61508 (2010 EDITION) and Related Standards, Including Process IEC 61511 and Machinery IEC 62061 and ISO 13849*, Elsevier, 2016, pp. 187-200.
- [41] "What Is ASIL-D?," [Online]. Available: <https://www.aptiv.com/en/insights/article/what-is-asil-d>. [Accessed 18 8 2022].
- [42] "What is ASIL (Automotive Safety Integrity Level)? – Overview | Synopsys Automotive," [Online]. Available: <https://www.synopsys.com/automotive/what-is-asil.html>. [Accessed 29 8 2022].
- [43] W. F. Milliken and D. L. Milliken, *Race Car Vehicle Dynamics*, Warrendale: SAE, 1995.
- [44] T. D. Gillespie, *Fundamentals of Vehicle Dynamics*, Warrendale: SAE, 1992.
- [45] J. D. Setiawan, M. Safarudin and A. Singh, "Modeling, simulation and validation of 14 DOF full vehicle model," in *International Conference on Instrumentation, Communication, Information Technology, and Biomedical Engineering*, 2009.
- [46] L. Nielsen and U. Kiencke, *Automotive Control Systems: For Engine, Driveline, and Vehicle*, Second Edition, Berlin: Springer, 2005.
- [47] M. H. I. M. Amin, K. Hudha, Z. A. Kadir and N. H. Amer, "Skyhook control for 7 DOF ride model of armored vehicle due to road disturbance," in *2015 10th Asian Control Conference: Emerging Control Techniques for a Sustainable World*, Kota Kinabalu, 2015.
- [48] H. Jamaluddin, E. P. Ping and K. Hudha, "Hardware-in-the-loop simulation of automatic steering control for double lane change and sine steer manoeuvres," *International Journal of Vehicle Autonomous Systems*, vol. 10, no. 1/2, p. 67, 2012.
- [49] G. Genta and L. Morello, *The Automotive Chassis Volume 1: Components Design Second Edition*, Cham: Springer, 2020.
- [50] H. B. Pacejka, *Tyre and Vehicle Dynamics*, Oxford: Elsevier, 2006.
- [51] H. Lv and S. Liu, "Closed-loop handling stability of 4WS vehicle with yaw rate control," *Strojniski Vestnik/Journal of Mechanical Engineering*, vol. 59, no. 10, pp. 595-603, 2013.
- [52] S. M. Shinnars, *Modern Control System Theory and Design 2nd Edition*, New York: John Wiley & Sons, Inc., 1998.

- [53] P. Saraf, M. Gupta and A. Manga Parimi, "A Comparative Study Between a Classical and Optimal Controller for a Quadrotor".
- [54] J. L. Sarmiento and C. Borrás Pinilla, *Modelling, design and analysis of three controllers based on LQR formulation for a non-linear hydraulic uniaxial seismic shake table*, vol. 95, EDP Sciences, 2019.
- [55] A. A. Hassan and A. M. Kassem, *SPEED CONTROL DESIGN OF A PMSM BASED ON FUNCTIONAL MODEL PREDICTIVE APPROACH*, vol. 40, Egypt's Presidential Specialized Council for Education and Scientific Research, 2012, pp. 1121-1135.
- [56] D. E. Seborg, T. F. Edgar and D. A. Mellichamp, *Process Dynamics and Control*, Hoboken: John Wiley & Sons, Inc. , 2004.
- [57] K. Kone, *Lateral and longitudinal control of an autonomous racing vehicle*, Turin: Master thesis of Politenico di Torino, 2018.
- [58] C. Novara, *Lecture Notes of Automatic Control*, 2019.
- [59] "Controller Creation - MATLAB & Simulink - MathWorks Italia," [Online]. Available: <https://it.mathworks.com/help/mpc/controller-creation.html>. [Accessed 13 9 2022].